DRDC Toronto CR 2005-128

Development of a Dynamic Biomechanical Model for Load Carriage: Phase V: Development of the Dynamic Biomechanical Model by Means of the Portable Measurement System

By:

E. L. Morin, J.M. Stevenson, S.A. Reid and J.T. Bryant

Project Managers**:**
E.L. Morin
(613) 533-6562
J.M. Stevenson
(613) 533-6288

PWGSC Contract No. W7711-01-7863/001/TOR
Call-up No. 7863-01

On behalf of
DEPARTMENT OF NATIONAL DEFENCE

as represented by
Defence Research and Development Canada - Toronto
1133 Sheppard Avenue West
Toronto, Ontario, Canada
M3M 3B9

DRDC Scientific Authority
Mr Walter Dyck
(613) 996-9347

May 2005

Abstract

Soldier operational performance is impacted by a number of factors including physiological workload, the biomechanical effects of equipment used in the field, demographics and soldier readiness. The specific objectives of the work reported here are to identify components of a load carriage limit (LCL) equation specifically related to the physiological workload and biomechanical effects, and to further the development of a dynamic biomechanical model (DBM) for load carriage. The ultimate goal of this research program is to develop and fully validate an LCL equation, which includes all relevant factors and which can be used to predict the operational effectiveness of soldiers in the field.

Data were collected in a previous contract (W7711-03-7632-08) on 10 physically fit male subjects. A maximal oxygen consumption test was performed. This was followed by four experimental sessions during which oxygen consumption, accelerations at the sternum and on the framesheet of a loaded backpack, and contact pressures under the backpack were measured during a treadmill test for the conditions of: different backpack loads (0kg, 15 kg, 25 kg, 38 kg); different walking speeds (3.22, 4.83 and 6.44 km/h); and different inclines (0º, 5º, 10º). For the zero load condition, the second accelerometer was mounted on the lumbar spine of the subject, in order to compare the sternum and lumbar locations for predicting energy consumption. It was found that metabolic energy cost increased with increasing load, speed and incline and an interactive effect between load and speed, and load and incline was present. For the zero load tests, it was found that increasing energy cost due to increasing speed was well correlated with the rms magnitude of the acceleration signals (R^2 = 0.96 for both recording locations). Accelerations were less well correlated with energy cost for increasing incline; however, accelerations recorded at the sternum location were better correlated (R^2 = 0.79) than for the lumbar location (R^2 = 0.27). A statistical model using several acceleration parameters was derived for the case in which the subjects carried loaded backpacks during the treadmill tests. An R^2 = 0.60 was obtained for a model involving only acceleration parameters; R^2 = 0.72 was obtained for a model involving acceleration parameters and load.

In the DBM development, a skin layer with appropriate properties was created for the torso model and the modeling of all relevant pack components that form the person-to-pack interface has been completed. Stress analyses, in the equilibrium state, for the skin layer, and the shoulder

strap and waist belt contact regions were done. A library of material properties for biological (skin on the back, skin toughened, skin over bone) and pack materials, both individually and in combination, has been compiled. Completion of the DBM will entail validating the motion and stress response of the DBM against existing test data, improving the user interface, and adding an output format that will provide the biomechanical factor for input into the LCL equation.

Résumé

La performance opérationnelle des soldats dépend d'un certain nombre de facteurs, dont la charge de travail physiologique, les effets biomécaniques de l'équipement utilisé sur le terrain, les caractéristiques de l'effectif et l'état de préparation. Les objectifs particuliers des travaux qui font l'objet du présent rapport consistent à déterminer les composantes d'une équation de limite de transport de charge (LCL) liées particulièrement à la charge de travail physiologique et aux effets biomécaniques, et à perfectionner la mise au point d'un modèle biomécanique dynamique (DBM) pour le transport de charge. L'objectif final de ce programme de recherche consiste à mettre au point et à valider complètement une équation de LCL, qui comprend tous les facteurs pertinents et qui peut être utilisée pour prévoir l'efficacité opérationnelle des soldats en campagne.

Dans le cadre d'un contrat antérieur (W7711-03-7632-08), on a recueilli des données sur 10 sujets mâles en bonne condition physique. Un test de consommation maximale d'oxygène a été effectué. On a ensuite tenu quatre sessions expérimentales au cours desquelles la consommation d'oxygène, les accélérations au niveau du sternum et de l'armature d'un sac à dos chargé ainsi que les pressions de contact sous le sac ont été mesurées durant une épreuve d'effort sur tapis roulant pour différentes charges du sac (0 kg, 15 kg, 25 kg, 38 kg), différentes vitesses de marche (3,22, 4,83 et 6,44 km/h) et différentes pentes (0º, 5º, 10º). Pour la condition de charge nulle, le deuxième accéléromètre était monté sur la colonne lombaire du sujet, pour permettre de comparer la région sternale et la région lombaire du point de vue de la prévision de la consommation d'énergie. On a constaté que la dépense d'énergie métabolique augmentait avec la charge, la vitesse et la pente et qu'il existait un effet interactif entre la charge et la vitesse, et entre la charge et la pente. Pour les essais en condition de charge nulle, on a constaté que l'accroissement de la dépense d'énergie dans le cas d'un accroissement de la vitesse présentait une étroite corrélation avec l'intensité efficace des signaux d'accélération (R^2 = 0,96 pour les deux positions d'enregistrement). Les accélérations présentaient une corrélation moins étroite avec la dépense d'énergie dans le cas d'un accroissement de la pente; cependant, les accélérations enregistrées au niveau du sternum présentaient une meilleure corrélation (R^2 = 0,79) qu'au niveau lombaire (R^2 = 0,27). Un modèle statistique basé sur plusieurs paramètres d'accélération a été établi pour le cas dans lequel les sujets portaient des sacs à dos chargés

durant l'épreuve d'effort sur tapis roulant. Un coefficient de corrélation R^2 de 0,60 a été obtenu pour un modèle basé seulement sur des paramètres d'accélération; une valeur de 0,72 a été obtenue pour un modèle basé sur des paramètres d'accélération et sur la charge.

Dans l'élaboration du DBM, on a créé une couche de peau possédant des propriétés appropriées pour le modèle de torse et on a réalisé la modélisation de tous les composants pertinents du sac qui forment l'interface personne-sac. Des analyses des contraintes, à l'état d'équilibre, pour la couche de peau et les régions de contact des sangles d'épaules et de la ceinture ont été effectuées. On a créé une bibliothèque de propriétés matérielles des tissus biologiques (peau du dos, peau renforcée, peau sur os) et des matériaux du sac, considérés séparément et conjointement. L'achèvement du DBM comprendra la validation de la réponse au mouvement et à l'effort du DBM par rapport aux données d'essai existantes, l'amélioration de l'interface utilisateur et l'ajout d'un format de sortie qui fournira le facteur biomécanique à utiliser dans l'équation de LCL.

Executive Summary

The Defence Research and Development Canada – Toronto (DRDC) with the assistance of the Ergonomics Research Group (ERG) at Queen's University has developed a research program in response to recommendations made at a NATO Research and Technology Organization Specialist Meeting held on 27-29 June 2000. At that meeting it was recommended that further research was needed to understand the impact of factors that affect operational effectiveness of soldiers and to develop predictive models of performance that account for these factors[1]. To this end, the ERG is advancing our understanding of load carriage through the development of a dynamic biomechanical model (DBM) and a load carriage limit (LCL) equation.

To accomplish these objectives, a portable measurement system using the EMBLA® data acquisition system, has been developed. The activity assessment module (AAM) of the portable system incorporates triaxial accelerometers to capture human motion, where it is known that whole body accelerations are related to metabolic energy cost.

The LCL equation, modeled after the NIOSH Lifting Guidelines, is designed to represent the demands of loads carriage based on a starting load constant (SLC) multiplied by the following discount/correction factors: a physiological factor (PF), a biomechanical factor (BF), a demographic factor (DF) and a soldier readiness factor (RF). In this report the AAM will be used for acquisition of the physiological factor (PF) and the DBM will be used to provide the biomechanical factor (BF). Using the same conceptual framework as the NIOSH Lifting Guidelines, the following LCL equation is suggested:

$$\textit{Load Conditions Limit (LCL)} = (SLC * PF * BF * DF * RF) * Time$$

where SLC represents the heaviest load currently used in the field (i.e., 40 - 60 kg).

The overall objectives of this research are to validate independently each component of the LCL equation either through empirical data or based on the scientific literature, and to validate the complete LCL equation in a field trial. This contract was focused on development of the physiological and biomechanical factors. The following milestones were achieved:

[1] Stevenson JM and Bossi LL. (2001). Technical Evaluation Report, *Soldier Mobility: Innovations in Load Carriage System Design and Evaluation* NATO-RTO Meeting Proceedings: MP-056, (Neuilly-sur-Seine: NATO), TER,1-20.

1. *Assessing physiological response to changing load, speed and incline*: The goal was to determine if the variables of load, speed and incline were sufficient to develop a physiological factor (PF) with similar validity to equations developed by Pandolf et al. (1977) and Holewijn et al. (2000). The following equation, relating oxygen consumption, ($\dot{V}O_2$) to load (*L*), speed (*S*) and incline (*I*) was derived:

$$\dot{V}O_2 = 2.559 + 0.107\left(I^2\right) + 0.335\left(S^2\right) + 0.182\left(L\right)$$

   The equation describes 83.3% of the variance in the data, which is sufficient for the PF of the LCL equation.

2. *Validation of accelerometer location*: In previous research on the relationship between whole body accelerations and energy cost, accelerations have been measured at the waist, hips and lumbar spine (e.g. Bouten et al., 1997; Hendelman et al., 2000). Because of pack and tactical assault vest interference, the accelerometer cannot be worn at the waist in field studies involving soldiers. Therefore a sub-study was conducted to validate the sternum location. Results revealed that, for changing speed, accelerations recorded at the sternum were as well correlated with energy cost as accelerations recorded at the lumbar spine. For increasing incline, the correlation between energy cost and acceleration was better for the sternum location; the correlation was poorer, however, than for changing speed.

3. *Predicting energy demand from upper body accelerations*: The purpose of this study was to determine if accelerations recorded at the sternum can be used to predict the energy demand of walking at different speeds and inclines, while carrying different loads. Statistical models were created using the accelerometer data. A model involving only acceleration parameters described 60% of the variance; a model involving acceleration parameters and load described 72% of the variance. Although the accelerometer data did not explain as much of the variance as hoped using a different set of acceleration parameters may increase the predictive power.

4. *Advancement of the DBM*: Under this contract, a skin layer with appropriate properties was created to cover the torso of the DBM, and all relevant pack components that form the person-to-pack interface were modeled. Stress distribution analyses at the shoulder straps, waist belt and back areas were done. A library of material properties for the skin and pack materials, both individually and in combination, has been compiled.

Sommaire

Recherche et développement pour la défense Canada – Toronto (RDDC Toronto), avec l'aide du groupe de recherche en ergonomie (ERG) de l'université Queen's, a élaboré un programme de recherche à la suite des recommandations faites à l'occasion d'une réunion de spécialistes de l'Organisation pour la recherche et la technologie de l'OTAN, tenue du 27 au 29 juin 2000. Lors de cette réunion, on a recommandé d'effectuer d'autres travaux de recherche dans le but de comprendre l'effet de facteurs qui influent sur l'efficacité opérationnelle des soldats et d'élaborer des modèles de prévision de la performance qui tiennent compte de ces facteurs[2]. À cette fin, les travaux de l'ERG nous aident à mieux comprendre le transport de charge par l'élaboration d'un modèle biomécanique dynamique (DBM) et d'une équation de limite de transport de charge (LCL).

Pour atteindre ces objectifs, on a mis au point un système de mesure portatif utilisant le système d'acquisition de données EMBLA®. Le module d'évaluation de l'activité (AAM) du système portatif comprend des accéléromètres triaxiaux pour capter le mouvement de la personne, car on sait qu'il existe un lien entre les accélérations du corps en entier et la dépense d'énergie métabolique.

L'équation de LCL, modélisée à partir des « Lifting Guidelines » (lignes directrices sur le levage) du NIOSH, est destinée à représenter les demandes de transport de charge basées sur une constante de charge de départ (SLC) multipliée par les facteurs de réduction/correction suivants : un facteur physiologique (PF), un facteur biomécanique (BF), un facteur d'effectif (DF) et un facteur d'état de préparation du soldat (RF). Dans le présent rapport, on utilisera le module AAM pour l'acquisition du facteur physiologique (PF) et on utilisera le DBM pour obtenir le facteur biomécanique (BF). En se servant du même cadre conceptuel que dans les « Lifting Guidelines » du NIOSH, on propose l'équation de LCL suivante :

*Limite de transport de charge (LCL) = (SLC * PF * BF * DF * RF) * temps*

où SLC représente la charge la plus lourde utilisée actuellement sur le terrain (c.-à-d. 40 - 60 kg).

[2] Stevenson JM et Bossi LL. (2001). Technical Evaluation Report, *Soldier Mobility: Innovations in Load Carriage System Design and Evaluation* (Rapport d'évaluation technique, *La Mobilité du combattant : innovations dans la conception et l'évaluation des gilets d'intervention*). Procès-verbal de réunion de l'Organisation pour la recherche et la technologie de l'OTAN : MP-056 (Neuilly-sur-Seine : OTAN), TER, 1-20.

Les objectifs globaux de ces travaux de recherche consistent à valider indépendamment chacune des composantes de l'équation de LCL, en se basant soit sur des données empiriques, soit sur la documentation scientifique, et de valider l'équation de LCL au complet par un essai sur le terrain. Le présent contrat porte principalement sur l'établissement des facteurs physiologique et biomécanique. Les étapes suivantes ont été franchies :

Évaluation de la réponse physiologique aux variations de charge, de vitesse et de pente : Le but visé était de déterminer si les variables charge, vitesse et pente étaient suffisantes pour établir un facteur physiologique (PF) de validité comparable à celle des équations établies par Pandolf et coll. (1977) et Holewijn et coll. (2000). L'équation ci-dessous, qui établit une relation entre la consommation d'oxygène ($\dot{V}O_2$), d'une part, et la charge (*L*), la vitesse (*S*) et la pente (*I*), d'autre part, a été établie :

$$\dot{V}O_2 = 2{,}559 + 0{,}107\left(I^2\right) + 0{,}335\left(S^2\right) + 0{,}182\left(L\right)$$

L'équation explique 83,3 % de la variance des données, ce qui est suffisant pour le facteur PF de l'équation de LCL.

Validation de l'emplacement de l'accéléromètre : Dans des travaux de recherche précédents portant sur la relation entre les accélérations du corps entier et la dépense d'énergie, les accélérations ont été mesurées au niveau de la ceinture, des hanches et de la colonne lombaire (p. ex. Bouten et coll., 1997; Hendelman et coll., 2000). En raison des problèmes créés par la présence du sac et de la veste d'assaut tactique, l'accéléromètre ne peut pas être porté à la ceinture par les soldats dans les études effectuées sur le terrain. Par conséquent, on a effectué une sous-étude pour valider le port au niveau du sternum. Les résultats obtenus ont montré que, pour une vitesse variable, la corrélation entre les accélérations enregistrées au niveau du sternum et la dépense d'énergie était aussi bonne que dans le cas des accélérations enregistrées au niveau de la colonne lombaire. Pour un accroissement de la pente, la corrélation entre la dépense d'énergie et l'accélération était supérieure pour le port au niveau du sternum; elle était inférieure, cependant, à la corrélation obtenue dans le cas d'une vitesse variable.

Prévision de la demande d'énergie à partir des accélérations de la partie supérieure du corps : Cette étude visait à déterminer si les accélérations enregistrées au niveau du sternum peuvent être

utilisées pour prévoir la demande d'énergie lorsque le sujet marche à différentes vitesses et suivant différentes pentes, tout en portant différentes charges. Des modèles statistiques ont été créés à l'aide des données des accéléromètres. Un modèle basé seulement sur les paramètres d'accélération expliquait 60 % de la variance; un modèle basé sur les paramètres d'accélération et sur la charge expliquait 72 % de la variance. Même si les données des accéléromètres n'expliquaient pas un pourcentage aussi élevé de la variance qu'on l'espérait, l'utilisation d'un ensemble différent de paramètres d'accélération pourrait accroître l'efficacité de prévision.

Perfectionnement du DBM : Dans le cadre du présent contrat, on a créé une couche de peau possédant des propriétés appropriées pour couvrir le torse utilisé dans le DBM et on a réalisé la modélisation de tous les composants pertinents du sac qui forment l'interface personne-sac. Des analyses de distribution des contraintes au niveau des sangles d'épaules, de la ceinture et du dos ont été effectuées. On a créé une bibliothèque de propriétés matérielles de la peau et des matériaux du sac, considérés séparément et conjointement.

Table of Contents

List of Figures

List of Tables

1 Introduction

At a NATO Research and Technology Organization Specialist Meeting held on 27-29 June 2000, it was recommended that further research be done to understand the impact of factors that affect the operational effectiveness of soldiers in the field and to develop predictive models of performance that account for these factors[3]. To this end, Defence Research and Development Canada – Toronto (DRDC) has supported Queen's University in a research and development program to advance our understanding of load carriage through the development of a dynamic biomechanical model (DBM) and the determination of a load carriage limit (LCL) equation. To accomplish these objectives, it is necessary to have an appropriate input source to gather the human motion data during field operations. Field unit system development began with the selection of a sophisticated data logger – the EMBLA® data recorder[4] – and the construction of appropriate electronic interfaces to specific sensors. Various input sensors that promised to be appropriate for field measures (i.e., Shapetape®, elgons, in-sole pressure sensors, and accelerometers) have been evaluated. Of these possibilities, triaxial accelerometers have been selected as the best choice to capture human motion in the field.

This phase of the research program has specific objectives to reach our ultimate goals of a Load Carriage Limit equation and a Dynamic Biomechanical Model. The milestones, which were stated in the original contract were:

1) to assess whether upper body accelerations measured at the sternum can be used to predict energy expenditure with the same accuracy as those measured at a lumbar recording location
2) to assess the effects of changing load, speed and incline on energy cost and determine whether upper body accelerations are sensitive to these effects
3) to advance the dynamic biomechanical model through the development of a outer layer on the torso that has the response characteristics of human skin and underlying tissues
4) to develop a transfer function that will permit validation of the contact forces and pressures on the DBM resulting from the load under different conditions.

[3] Stevenson JM and Bossi LL. (2001). Technical Evaluation Report, *Soldier Mobility: Innovations in Load Carriage System Design and Evaluation* NATO-RTO Meeting Proceedings: MP-056, (Neuilly-sur-Seine: NATO), TER,1-20.
[4] The Embla data logger is manufactured by Flaga, Re Iceland and its capabilities have been reported in a previous contract report.

Since there were unexpected technical difficulties with the pressure measurement technology, we altered milestone 4 and added a milestone to develop an additional aspect of the Load Carriage Limit equation. Hence the revised milestones are:

4) *(revised)* to develop a transfer function based on the differences in pack-person motion that could be used in the Dynamic Biomechanical Model over different load conditions, and
5) to develop a physiological factor for the Load Carriage Limit equation based on the measures of load, speed and incline.

1.1 The Load Carriage Limit (LCL) Equation

A detailed description of the Load Carriage Limit (LCL) Equation was described by Stevenson et al. (2001) and in an additional supplement proposal (Dyck: May 21, 2003). In essence, the LCL uses the proven approach of the NIOSH Lifting Guidelines as its model (Waters et al, 1993). Without delving into details of the NIOSH 1991 Lifting Guideline, it is hypothesized that a multiplicative model can be used to represent the demands of load carriage based on a starting load constant (SLC) multiplied by discounting/correction factors: the physiological factor (PF), biomechanical factor (BF), demographic factor (DF) and soldier readiness factor (RF). Using the same conceptual framework as for the NIOSH Lifting Guidelines, the following NATO Load Carriage Guideline is proposed:

LCL = (SLC * DF * PF * BF * RF) * Time

Where:

- SLC represents the heaviest load currently used in the field (i.e., 40 kg to 60 kg)
- DF includes body size, gender and age
- PF is derived from physiological factors, principally metabolic energy cost
- BF includes shoulder and hip reaction forces, pack motions and contact pressures
- RF includes soldier readiness, fitness, injury factors and acceptance factors[5]
- Time represents the mission expectations in terms of time and distance to be traveled.

[5] Soldier Readiness Factor (RF) is used to capture those variables not easily acquired without subjective input.

The purpose for a valid LCL would be to provide operations personnel and commanders with a quick and effective tool to predict soldier performance in the field. The formula would allow a user to determine the dominant components affecting how much weight could be loaded in a backpack, with no appreciable decrement in performance, and to assist operations personnel with making the necessary pre-mission adjustments.

To develop the LCL equation, each of the proposed terms in the equation must be validated either empirically or based on the scientific literature. This involves two steps, 1) developing a valid factor for each component of the equation and 2) testing the validity of the LCL equation in a field setting. The work done in this contract has focused on the first step, namely developing valid equations for the physiological and biomechanical factors. Although only the biomechanical factor was named as a deliverable in this contract, our experiments were set up to collect physiological as well as biomechanical data, where the physiological information can be used to determine the physiological factor.

1.1.1 Developing the Physiological Factor

To develop the physiological factor (PF), it is necessary to establish the most important variables that will affect the PF and then determine a method to measure them in the field. In the equations for PF reported by Pandolf et al. (1977) and Holewijn et al. (1992), body weight, load mass and velocity are common parameters, which affect metabolic energy cost. Other variables may be suggested in the scientific literature. After identifying the variables to be included in the PF equation, they must be validated against an accepted measure of metabolic energy cost, e.g. indirect calorimetry.

1.1.2 Developing the Biomechanical Factor

Biomechanical variables and human perceptions have been proven to be the best measures for design evaluation, based on a literature review and our research. For example, the magnitude of shoulder and lumbar reaction forces and contact pressures are related to soldier discomfort scores (Stevenson et al., 1995; 1998, Bryant et al., 2001). Hence, the ability of soldiers to carry various loads over long marches and perform skills, such as accurate marksmanship, is governed by the design of the load carriage system (based on biomechanical factors) was well as other

factors in the LCL equation. Hence the overall goal is to develop a valid dynamic biomechanical model (DBM) for load carriage (LC) systems in order to predict soldier responses to LC system designs, to develop a field measurement tool to acquire these measures and to provide a tool that can be used during new design iterations.

The Queen's Ergonomics Research Group has developed several iterations of a static biomechanical model to calculate shoulder, lumbar and waist-belt forces (Stevenson et al., 1995; MacNeil, 1996; Rigby, 1999; Pelot et al., 2001; Hadcock et al. 2002). However, the indeterminacy, due to the number of straps and contact points, makes it difficult, if not impossible, to use direct measurement approaches. Therefore, a dynamic biomechanical modeling (DBM) approach that uses the resultant motions of the pack and person to determine the contact forces and pressures has been undertaken. Previous DRDC contracts have been devoted to various sub-components of the DBM development, including: inputting the pack and person coordinates, driving the model from the forcing function of the Load Carriage Simulator (LCSim) or measured human motion, measuring and inputting the stiffness characteristics of specific materials for backpack straps, setting the restraints on the model due to boundary conditions such as strap length and waist belt tension and creating separate upper and lower body segments.

The purpose of this phase of the model development was to add a 3-5 mm outer layer with the mechanical properties of skin and underlying tissues. This phase is important to predict the actual contact forces under various conditions when carrying a load carriage system.

To validate the model's outputs for contact forces and pressures, it is necessary to have an accurate system to measure contact pressures. In previous work, using the LCSim, TekScan® Fscan 9811 sensors were used to measure contact pressures under various backpack elements. In a previous contract (Morin et al., 1998), the FScan sensors were tested on a human subject and their performance was found to be unacceptable. In previous contracts[6], two additional systems were tested (F.S.A. and Xsensor) in hopes of finding a system that was suitable for human measurements. Based on preliminary standardized calibrations, we selected Xsensor® as a system that may give us the accuracy, resolution and compliance we need for human measurements. With the support of Xsensor Technology Corporation, we were provided with an industrial sensor system that had the required range (0-133 kPa) for measuring contact pressures

[6] W7711-0-7632 (6) (7)

under the shoulder straps and framesheet of a backpack loaded with between 10kg and 50kg. This system was used for our original testing in the PWGSC contract # W7711-0-7632 (08) in the summer of 2003. It was also used it to collect contact pressure data for a range of loads on the LC Simulator. Unfortunately, despite support from Xsensor Technology Corporation, the pressure measurements for the new industrial range pad were not accurate and therefore cannot be used as a gold standard for the DBM pack-person interface pressures and forces. The revised calibration for previously collected data and subsequent Matlab cell-by-cell correction algorithms still yielded poor results and consumed considerable time and energy. Nonetheless, we have proceeded with an alternate plan that should take us some distance toward validation of the DBM model.

Based on previous research, the pack-person motion between the LCSim (or person) and the pack is an important indicator of load control and comfort (Stevenson et al., 1997; Bryant et al., 2001). Thus milestone 4) was revised to examine the relationship between accelerations recorded from the pack and from the manikin of the LCSim, and extend this analysis to the relationship between accelerations recorded from the pack and the person in human trials. The hypothesis is that the change in relative motion due to pack load, speed and incline is systematic and useful in describing the forces and pressures experienced by the LCSim and eventually the person. If the transfer function is proven to be valid, then the DBM will receive its input from a triaxial accelerometer in the pack and second triaxial accelerometer on the person.

1.1.3 Field Measurement of Physiological and Biomechanical Variables

Once the PF equation and DBM have been established, it will be necessary to measure the relevant variables in the field. A portable system module, which provides measures of physiological parameters (heart rate and skin surface temperature) and biomechanical parameters (body acceleration and backpack strap tensions) has been developed[7]. This module was used in a major human performance study done in December 2001, which is reported in Morin et al. (2003). Subjects completed an activity circuit while carrying a backpack with a light (15.7 kg), medium (24.455 kg) or heavy (34.3 kg) load. Two Crossbow[8] model #CXL10LP1 accelerometers were used to measure the acceleration of the upper body and the backpack. The

[7] This work was done under DRDC Contract no. 7711-0-7632/01-TOR; Call-up no. 7632-04
[8] Crossbow Technology Inc., 41 Daggett Dr., San Jose, CA, USA. www.xbow.com

body accelerometer was mounted over the sternum and fixed firmly in place using *Skin bond*®; the pack accelerometer was fixed to the centre of the framesheet inside the pack. It was found that the upper body acceleration patterns were specific to the task performed, which included walking, traversing a balance beam, a boulder hop[9], going over and under barriers, ascending and descending a ramp, doing a slalom run and traversing a sidehill ramp. As well, it was noted that the activities could be ranked by the rms magnitude of the upper body accelerations: the rms magnitudes for the balance beam, the shuttle run and the sidehill ramp were consistently lower than those for walking, and the rms magnitudes for the up-down ramp, the over-under barriers and the boulder hop were consistently higher.

It has been reported in several studies, that whole body acceleration is correlated to metabolic energy cost (e.g. Bouten et al., 1997a; Hendelman et al., 2000). While Bouten et al. found a significant correlation between accelerometer output and energy expenditure (r = 0.89), they noted that the system underestimated energy cost for some intensive activities (e.g. stepping or carrying loads) and overestimated energy cost for sedentary activities (e.g. sitting, lying and desk work). Hendelman et al. noted that the relationship between whole body acceleration and energy cost was dependent on the type of activity performed, and reported that the accelerometer did not detect increased energy cost from upper body movements, load carriage or changes in surface terrain. In the first study (Bouten et al. 1997a), the subjects wore a triaxial accelerometer at the level of the 2nd lumbar vertebra and in the second study (Hendelman et al., 2000) both a uniaxial and a triaxial accelerometer unit was worn at the level of the hips. Bouten et al. (1997b) also reported that although the accelerometer placement did affect acceleration amplitude[10], there was little effect on the correlation between body acceleration and energy cost. In this study, however, the only activity performed was walking on a treadmill (at 3, 4, 5, 6 and 7 km/h) and whole body accelerations were only measured with an accelerometer at the lower lumbar spine. Accelerations of other body segments, including a segment comprising the head and trunk, were estimated from the body movements recorded on video. Thus, it may be possible that metabolic energy cost for movements other than walking, can be better predicted from accelerations measured at other body locations.

[9] In this case, boulders were represented by a series of round markers on the floor. These markers were not raised to reduce the possibility of injury when landing.

Other experimenters have reported that other performance measures can be estimated from body accelerations. Schutz et al (2002) measured anteroposterior accelerations at the waist during treadmill walking, walking on a standardized urban circuit and under free-living conditions. They reported that walking speed, and the pattern, intensity and duration of daily walking could be estimated from the measured accelerations. They did not include the effect of incline, however, and noted that speed prediction is not accurate for variable slopes. Herren et al (1999) used a neural network to predict speed and incline from triaxial accelerations measured at the lumbar spine and the anteroposterior acceleration of the heel. The root mean square error (RMSE) between the measured and predicted speed was 0.12 m/s, for speeds ranging between 2.6 and 5.8 m/s; the RMSE between the measured and predicted incline was 0.014 rad, for inclines varying between –0.109 rad to +0.109 rad. The variance of the four accelerations measured had the highest correlation with speed, indicating that there is a general increase in the amplitude of body accelerations with speed. The parameter which showed the highest correlation with incline was the median value of vertical acceleration, indicating that vertical accelerations, measured at the lumbar spine, are affected by a change in slope.

1.2 Objectives

The specific objectives of the work reported here are:

- to define and validate the relevant parameters for the PF equation
- to assess whether upper body accelerations measured at the sternum can be used to predict energy expenditure with the same accuracy as those measured at a lumbar recording location
- to assess the effects of changing load, speed and incline on energy cost and determine whether upper body accelerations are sensitive to these effects
- to continue the development of a DBM capable of providing accurate estimates of biomechanical load factors as well as pack-person interface information

[10] The measured accelerations were low-pass filtered at 20 Hz, rectified and integrated over the recording period to obtain the integral of the modulus of body acceleration (IMA). This parameter was used in the correlation analysis, between energy cost and body acceleration.

2 Metabolic Energy Expenditure During Treadmill Walking with Loads

2.1 Experimental Set-up and Data Collection

An experimental study, involving human subjects, was designed to measure body accelerations and energy cost while carrying a loaded backpack and walking at different speeds and inclines on a treadmill. Fit male subjects were recruited for the study. During the initial experimental session, subjects were asked to fill out a Par-Q questionnaire, to ensure no contra-indications to exercise were present, and to sign an informed consent form (included in Appendix A). The experimental protocol was outlined in detail in a Letter of Information, and subjects were encouraged to ask any questions before commencing the study. The subjects were then asked to complete a $\dot{V}O_{2\max}$ test (described in detail in Appendix B) to determine their maximum aerobic capacity. Subjects were required to have a minimum $\dot{V}O_{2\max}$ of 44.5 ml/kg/min, so that the measured energy cost during the experimental study would not be confounded due to fatigue. For this cut-off value, subjects are in the top 40% fitness level for the 20-39 year age range (ACLS, 1998).

Those subjects accepted for the study were asked to return for four data collection sessions. Sessions were done on separate days, with adequate rest between trials. In each session, subjects completed one of four test batteries, (summarized in Table I), which comprised two 18 minute treadmill walks, while subjects carried one of two loads in a Canadian CTS backpack. Either speed or incline was varied in six minute intervals – this duration was chosen, so that subjects would be in steady state oxygen consumption for at least the last half of the interval.

Table I: Test batteries for data collection.

BATTERY	TEST	LOAD (kg)	SPEED (km/h)			INCLINE (deg)		
A	A1	0	3.22	4.83	6.44	0		
	A2	38.7	3.22	4.83	6.44	0		
B	B1	0	4.83			0	5	10
	B2	38.7	4.83			0	5	10
C	C1	16.6	3.22	4.83	6.44	0		
	C2	25.9	3.22	4.83	6.44	0		
D	D1	16.6	4.83			0	5	10
	D2	25.9	4.83			0	5	10

At the beginning of each session, each subject was outfitted with required measurement sensors and an appropriately sized CTS backpack[11]. One Crossbow triaxial accelerometer (model #CXL10LP1) was affixed to the subject's sternum using Skin-Bond® (accelerometer #1) and a second accelerometer was mounted onto the centre of the framesheet of the backpack (accelerometer #2). The zero-g offset voltage and sensitivity of the accelerometers is summarized in Appendix B. The accelerometers were oriented such that the *y*-axis was vertical, the *z*-axis was in the anteroposterior direction, and the *x*-axis was in the mediolateral direction. The pack accelerometer was rotated 180° about the *y*-axis with respect to the body accelerometer. In the zero load condition (test A1 and B1), the second accelerometer was mounted on the lumbar spine of the subject, using Skin-Bond®. The accelerometer outputs were sampled at 100 Hz and stored using the Embla data recorder[12], which is part of the portable human performance assessment module. For the load bearing tests, the CTS backpack was loaded such that the load mass was concentrated in the centre of the backpack. The packing protocol is described in Appendix B. The total load carried was 16.6, 25.9 or 38.7 kg. The backpack was outfitted with load cells, which were attached in-line at the lower left shoulder strap, the waist belt, the lower hip stabilizer and the load lifter strap. The load cell outputs were sampled at 10 Hz and stored using the Embla recorder. The acceleration and load cell data were subsequently copied onto a PC for off-line analysis. The subject was also outfitted with a mask that covered his mouth and nose and which was connected to airflow tubes by a high flow pneumotach and plugged into the TEEM 100 metabolic cart. Oxygen consumption ($\dot{V}O_2$) and CO_2 production were recorded at 20s intervals by the TEEM 100. These data were also transferred to a PC for off-line analysis.

Eight subjects completed the four test batteries. The mean age of the subjects was 23.6 years (range 21 – 26 years), mean height was 1.77 m (range: 1.689 – 1.848 m) and mean body weight was 78.24 kg (range: 65.4 – 97.07 kg). Full $\dot{V}O_2$ records were obtained from the subject group.

[11] Subject chest circumference, waist circumference, buttock circumference, biacromial breadth and waist-back length were measured to determine the proper shoulder strap, waist belt and pack size, where medium and large sizes of each were available. Fitted backpack sizes are summarized in Appendix B.

However, accelerations were not successfully recorded from both accelerometers for all tests completed by the subjects, due to instrumentation problems. A summary of the acceleration records for each subject is given in Appendix B.

2.2 Relationship between Metabolic Energy Cost and Load, Speed and Incline

2.2.1 Objective

The objective is to derive the physiological factor of the LCL equation based on the correlation between the measured metabolic energy cost ($\dot{V}O_2$) and speed, incline and load carried.

2.2.2 Analysis of metabolic energy cost data

Oxygen uptake data were collected using a TEEM 100 metabolic cart, which was calibrated before and after each test on room air composition. The data were recorded at 20 s intervals for the duration of each test. At the conclusion of each test, the data were downloaded to a PC using Aerosport v.10 software. The reported data were converted to units of ml/min and divided by body weight to give normalized $\dot{V}O_2$ in ml/min/kg.

A plot of $\dot{V}O_2$ vs time for the eight tests for a single subject is shown in Figure 1. It can be seen that, in most cases, when the speed or incline is increased, there is a transient rise in $\dot{V}O_2$, but the subject quickly levels off to a steady state O_2 consumption. Subsequent data analysis was done using data measured during the steady state periods.

The $\dot{V}O_2$ data were analyzed to determine if load, speed and incline significantly affect metabolic energy cost and if there are interactions between load and speed and load and incline. This was done using two-way ANOVA with repeated measures tests on load and speed and on load and incline.

[12] The Embla recorder accepts input voltages in the range ±250 mV; the output voltage of the Crossbow accelerometers is 0-5 V. The accelerometer voltages were attenuated by a factor of 0.0447 before being sampled by the Embla recorder. See Morin and Reid (2003).

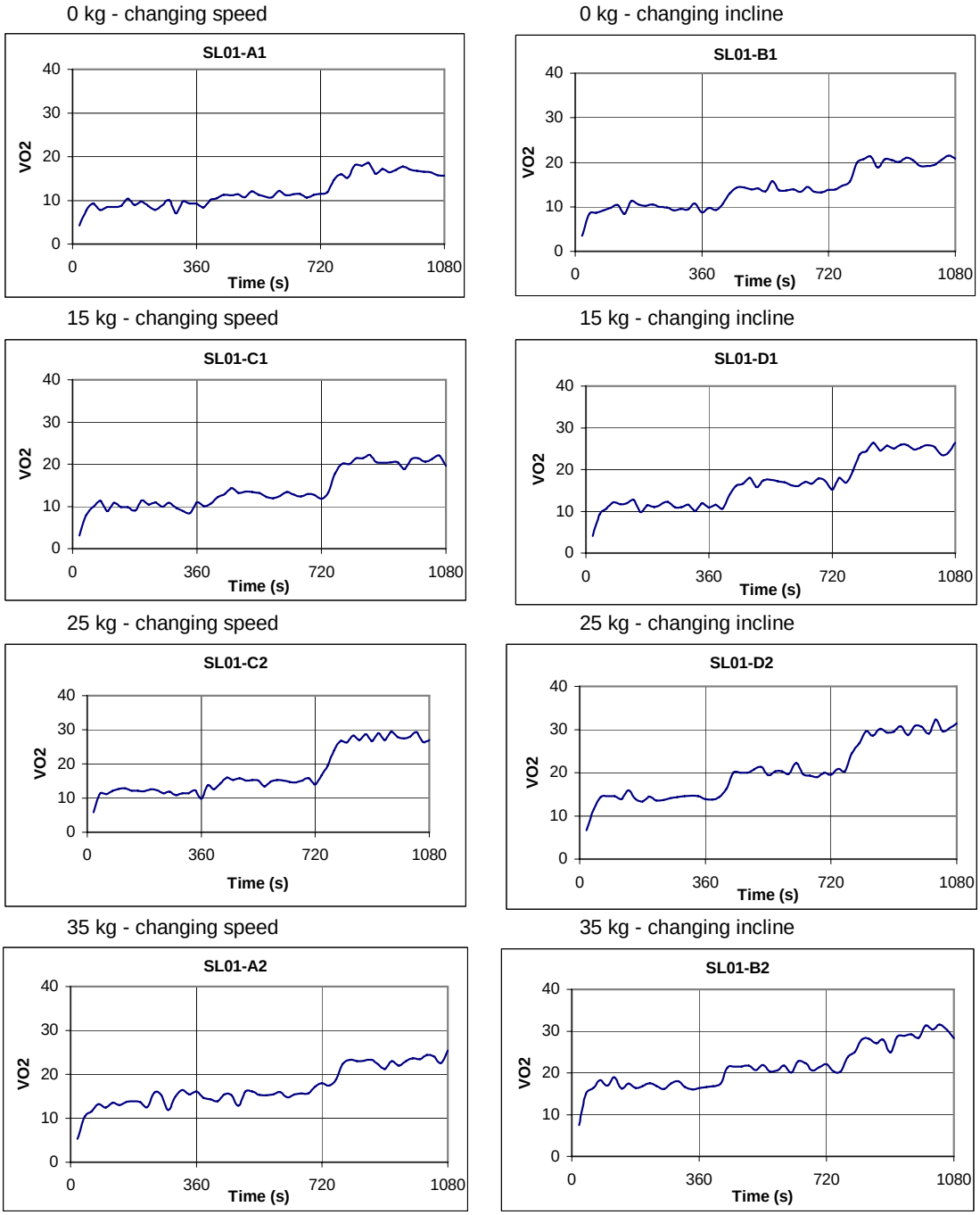

Figure 1: Measured $\dot{V}O_2$ over time for each 18 minute test performed by one subject (SL01). The test condition (speed or incline) changes after 6 minutes (360 s) and after 12 minutes (720 s). In most cases, there is a transient rise in $\dot{V}O_2$ immediately following the change in speed or incline. There is also a general trend of increasing $\dot{V}O_2$ with increasing load.

2.2.3 Results

The results of the first two-way ANOVA with repeated measures indicated that increasing load and increasing speed each resulted in significant increases in $\dot{V}O_2$ ($p<.01$), as shown in Figure 2. An interaction between load and speed was also established ($p<.01$), such that when speed is increased, an additional metabolic cost is added when load is also increased.

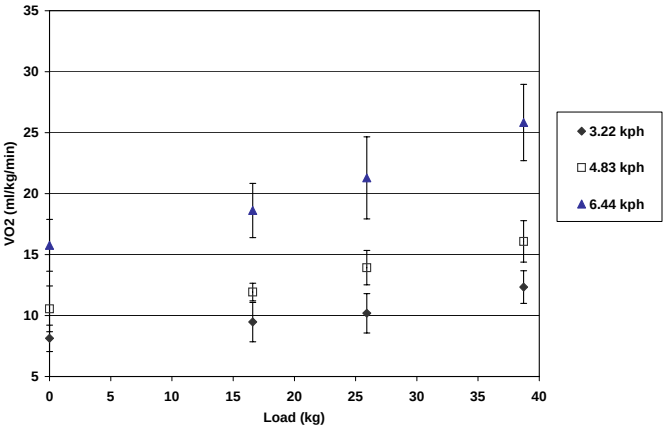

Figure 2: Increasing $\dot{V}O_2$ due to increasing load for the three speeds tested.
It is apparent that $\dot{V}O_2$ also increases with increasing speed.

The results of the second two-way ANOVA with repeated measures indicated that there was a significant increase in $\dot{V}O_2$ with increased load ($p<0.01$), and with increased incline ($p<0.01$), as shown in Figure 3. An interaction was also established between load and incline ($p<0.05$), such that when load is increased, there is an additional metabolic cost when the incline is greater than 0°.

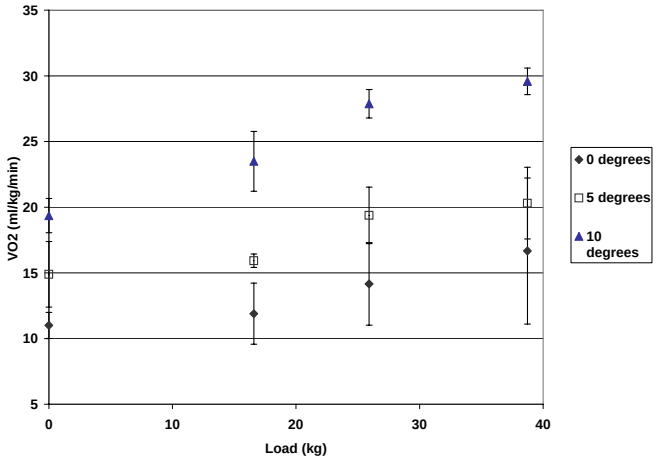

Figure 3: Increasing $\dot{V}O_2$ due to increasing load for the three inclines tested.
It is apparent that $\dot{V}O_2$ also increases with increasing incline.

2.2.4 Predicting VO_2

A linear multiple stepwise regression test was performed using SPSS. The following regression equation was derived to model oxygen uptake using the variables, load carried (*L*), speed (*S*) and incline (*I*): $\dot{V}O_2 = 2.559 + 0.107(I^2) + 0.335(S^2) + 0.182(L)$ EQ 1

This model has an $R^2 = 0.833$, meaning the factors of load, incline squared and speed squared account for 83.3% of the variance.

Using the load, speed and incline data from the human trial, estimated $\dot{V}O_2$ was determined from the above equation. The estimated values were plotted against the measured $\dot{V}O_2$ values as shown in Figure 4. This resulted in a logarithmic regression equation, $\dot{V}O_{2\,pred} = 14.248\ln(\dot{V}O_{2meas}) - 22.399$ with an $R^2 = 0.86$, which explains 86% of the variance.

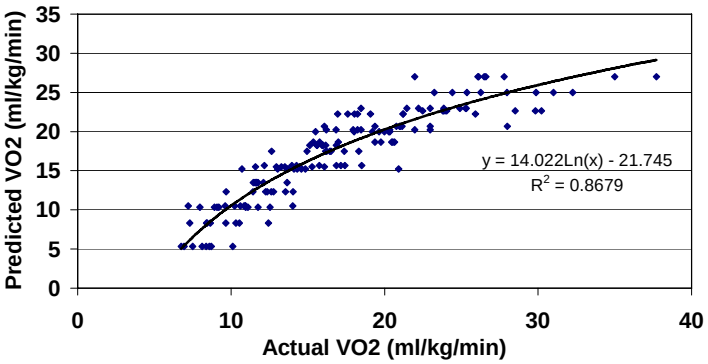

Figure 4: Actual $\dot{V}O_2$ vs $\dot{V}O_2$ predicted using the EQ 1.

2.3 Prediction of Metabolic Energy Cost from Upper Body Accelerations

2.3.1 Objective

The analysis in this section has been done to determine the correlation between the recorded upper body accelerations and measured $\dot{V}O_2$ during the treadmill exercises, and to determine if the upper body accelerations are sensitive to the effects of load, speed and incline on energy expenditure. The ultimate goal is to use upper body accelerations to predict energy expenditure and the physiological factor of the LCL equation.

2.3.2 Analysis of Acceleration Data

The accelerometer and $\dot{V}O_2$ data for analysis were taken from minutes 3-5, 9-11 and 15-17 of each test, when the subject is in steady-state oxygen consumption for each test condition, i.e. walking at 3.22 km/h, 4.83 km/h or 6.44 km/h with a 0° incline; or walking at 4.82 km/h at a 0°, 5° or 10° incline. Sample recorded accelerations for each condition are shown in Appendix C. The $\dot{V}O_2$ data were processed as described in the previous section.

The recorded voltages from the accelerometers were converted to g's of acceleration using the equation given in Appendix B. Any remaining offset in the data records was due to gravity and was removed by averaging over the duration of the extracted record (2 min.) and subtracting the average value from the data values[13]. These averaged values were recorded as the mean values on each accelerometer axis for each test: $mean_x$, $mean_y$, and $mean_z$. With the offset removed, the mean rms values for each axis were computed for the 2 min. interval – m_rms_x, m_rms_y and m_rms_z respectively[14]. The mean rms magnitude was computed using:

$$m\_rms_{mag} = \sqrt{m\_rms_x + m\_rms_y + m\_rms_z}$$

[13] To a first approximation, the average values of the accelerations on each axis allow the tilt angle of the accelerometer to be calculated, since the gravity vector is oriented strictly downward. For the data analysis reported here, the effect of the tilt angle was assumed to be negligible. A discussion of the tilt angle effect is included in Appendix D.

[14] Because taking the rms value involves squaring the data and averaging the squared values, it is not necessary to rotate the position of accelerometer #2 relative to accelerometer #1. The *x*- and *z*-axes of accelerometer #2 are rotated 180°, effectively inverting the data, with respect to accelerometer #1.

The resulting values for each subject and each test are included on a separate CD-Rom as part of Appendix C.

The same acceleration records were used for a spectral analysis of the data. For each record the power spectral density (PSD) was computed in Matlab®. Because the recorded accelerations are essentially periodic, each PSD exhibits a distinct peak at the fundamental frequency and peaks at harmonic frequencies. The fundamental peak is related to the step frequency; the harmonics are present because the recorded accelerations are not strictly sinusoidal. Total signal power for each record was computed by integrating the PSD's.

2.3.3 Results

Mean rms values of the acceleration signals were plotted versus load for the different speeds and inclines as shown in Figure 5. There is no consistent pattern of increasing rms value with load, indicating that upper body accelerations do not change in a predictable way for increasing load carried. The rms values on all axes clearly increase with increasing speed; the rms value on the *z*-axis shows a consistent increase with increasing incline.

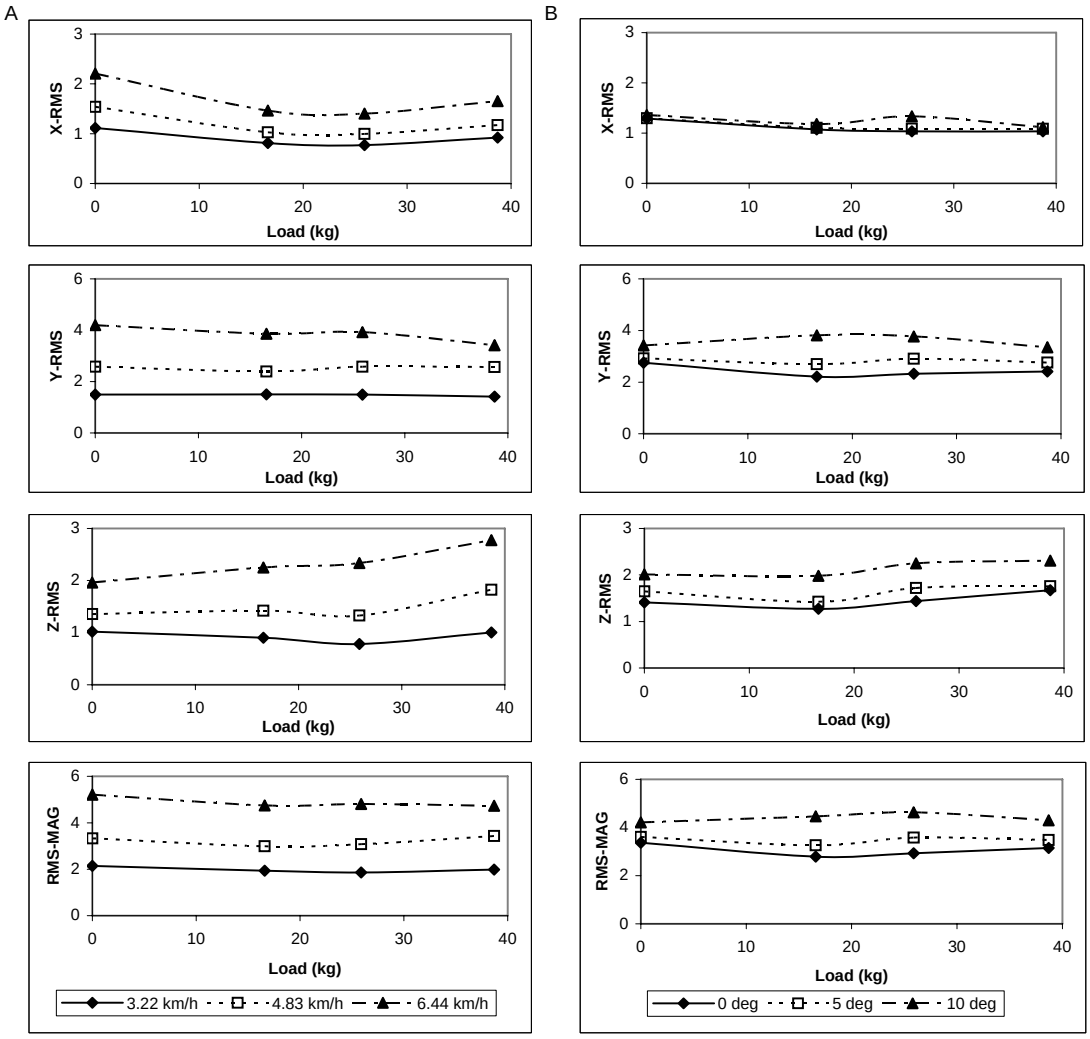

Figure 5: Mean rms values for each axis and mean rms magnitude, across all subjects, for the sternum accelerometer.

Column A is mean RMS and mean RMS magnitude vs load and speed

Column B is mean RMS and mean RMS magnitude vs load and incline

Average values and standard deviations are given in Appendix C.

The averaged spectral power for accelerations recorded at the sternum on each axis and the fundamental frequency of the *y*-axis accelerations are shown in Figure 6.

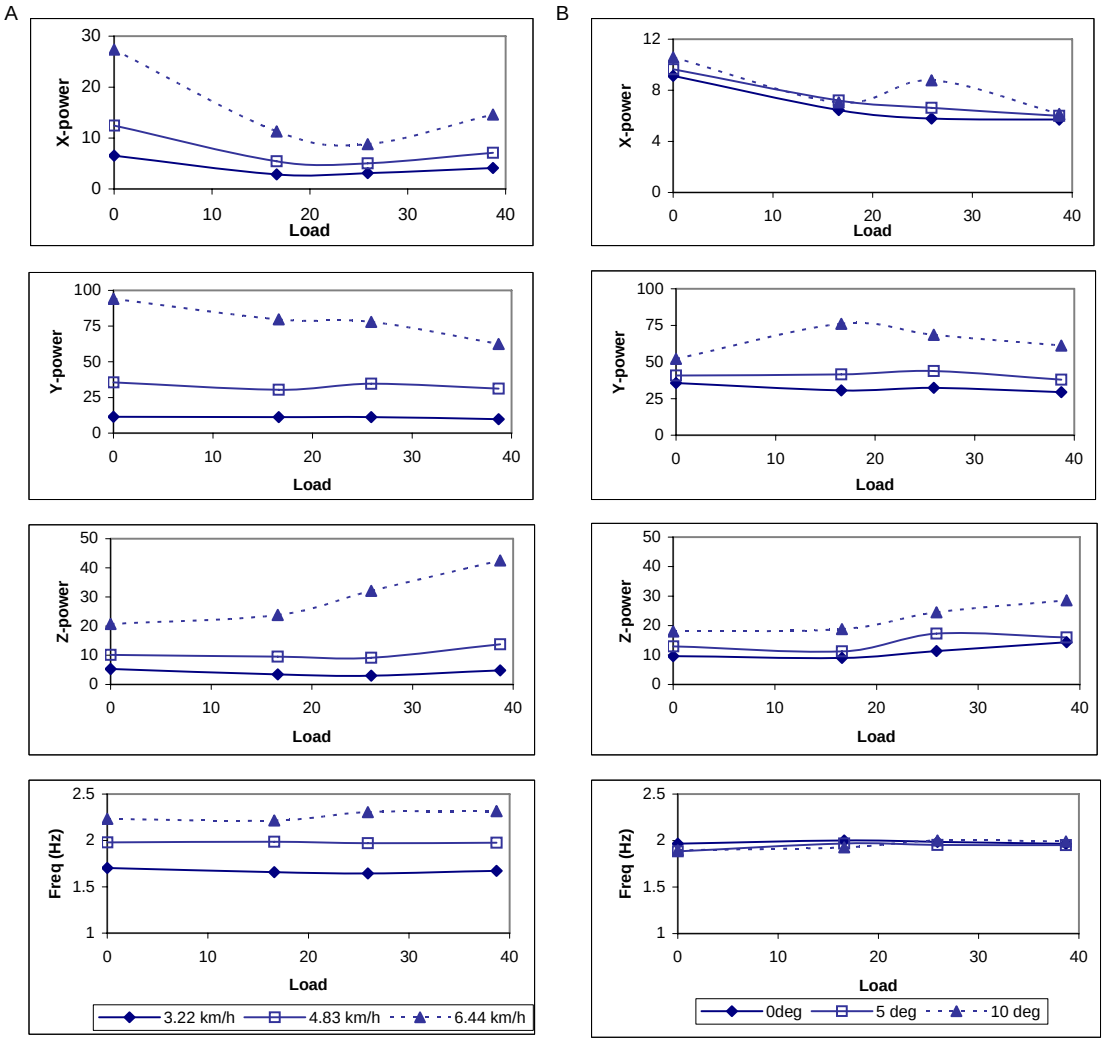

Figure 6: Spectral power on each accelerometer axis and fundamental frequency on Y axis
Column A is spectral power versus load and increasing speed
Column B is spectral power versus load and increasing incline.

As with the average rms values, the spectral power on each axis exhibits no consistent pattern of change with increasing load carried. The spectral power on all axes increases with increasing load carried; spectral power on the *y*- and *z*-axes shows an increasing trend with increasing incline, but this is not as clear as for increasing speed. The fundamental frequency of the *y*-axis spectra increases with increasing speed but not with increasing incline. This is to be expected, since this frequency represents the subject's step rate, and one means by which the speed of walking can be increased is to increase step rate. The subjects were walking at the same speed

for the changing incline tests, and their step rates remained essentially constant over the four tests.

2.3.4 Case 1: Zero Load with Changing Speed and Incline

In the zero load condition, accelerations were recorded from the sternum and lumbar spine. A correlation analysis between the accelerometer *m_rms* values, from both accelerometer #1 and accelerometer #2, and the measured $\dot{V}O_2$ was performed in Excel. The correlation coefficient, R, was calculated as the ratio of the covariance of the *m_rms* and $\dot{V}O_2$ values divided by the product of their standard deviations.

For test A1 - accelerometer #1, the number of data points in each correlation was 18; for test A1 - accelerometer #2, the number of data points in each correlation was 17. For these tests, the data values for subject WW08 were not included in the analysis, because the average acceleration on the *z*-axis was very high, indicating that the results might be affected by the tilt of the accelerometer. For test B1 - accelerometer #1 and accelerometer #2, the number of data points in each correlation was 16. For these tests, the data values for subject JD06 were not included in the analysis, because the average acceleration on the *z*-axis of accelerometer #2 was very high. The R values for both tests are summarized in Table II.

Table II: Correlation coefficients (R values) between measured $\dot{V}O_2$ and rms accelerations for the sternum (#1) and lumbar (#2) recording locations

Test A1 – Accelerometer #1				**Test A1 – Accelerometer #2**			
m_rms_x	m_rms_y	m_rms_z	m_rms_{mag}	m_rms_x	m_rms_y	m_rms_z	M_rms_{mag}
0.8089	0.9312	0.8981	0.9550	0.8688	0.9571	0.9465	0.9562
Test B1 – Accelerometer #1				**Test B1 – Accelerometer #2**			
m_rms-x	*m_rms-y*	*m_rms-z*	*m_rms-mag*	*m_rms-x*	*m_rms-y*	*m_rms-z*	*M_rms-mag*
0.1646	0.7199	0.7904	0.7938	-0.2606	0.4787	0.2707	0.2741

It can be seen that the correlation coefficients are close to 1 for both accelerometers for test A1, in particular for m_rms_y and m_rms_{mag}. This indicates that increased energy expenditure due to increased speed can be well predicted from the measured vertical accelerations or the magnitude of the accelerations of the body. However, for the case of increasing energy consumption due to increasing incline, the correlation between whole body acceleration,

measured at the lumbar spine and energy expenditure is very poor. The correlation is better for accelerations recorded from the sternum, indicating that upper body accelerations better reflect the change in energy cost due to changing incline. A plot of the mean rms magnitudes versus the average measured $\dot{V}O_2$ values is shown in Figure 7.

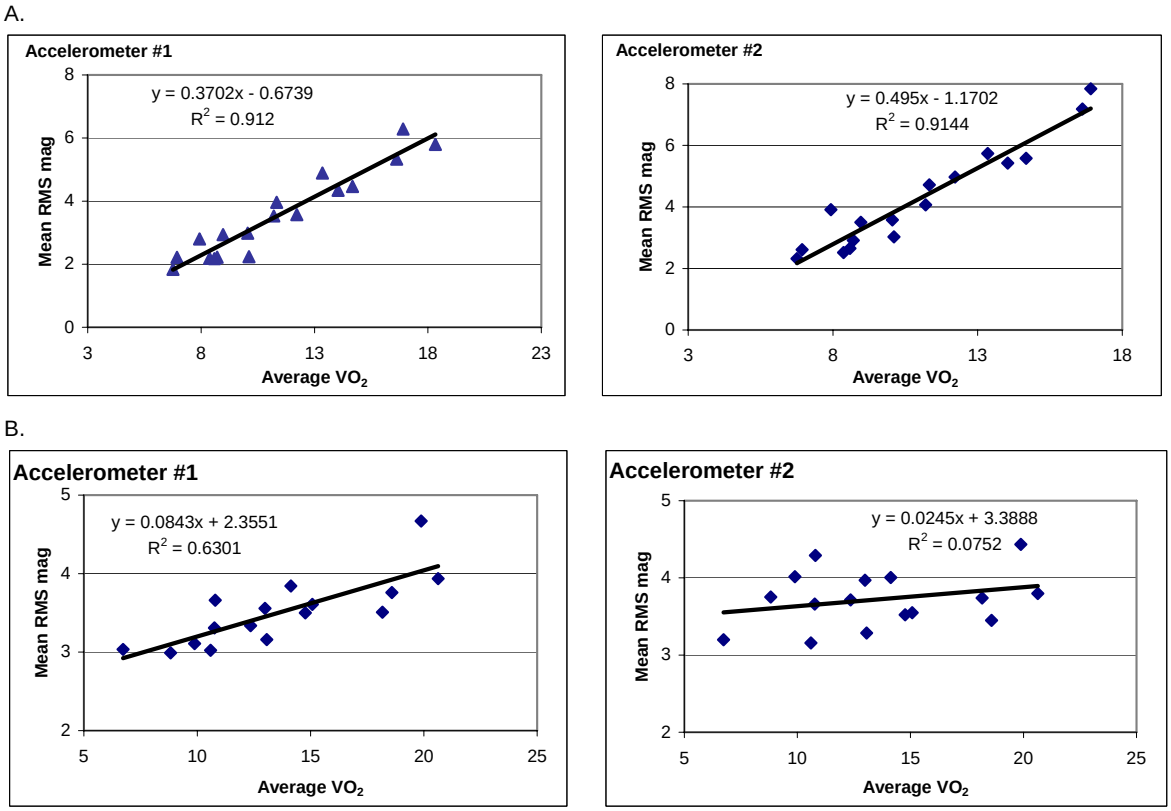

Figure 7: Mean accelerometer rms vs average $\dot{V}O_2$ sternum (A1) and lumbar (A2) locations.
Column A increasing speed,
Column B increasing incline. Data from six subjects are included.

The results indicate that the sternum recording location is as good as, or better than, the lumbar recording location in terms of predicting the metabolic energy cost of specific activities. Given this result, the analysis of upper body accelerations versus measured $\dot{V}O_2$ for the conditions of carrying different loads in a backpack and walking at different speeds and inclines is warranted.

2.3.5 Case 2: Light, Medium or Heavy Load with Changing Speed and Incline

In six out of eight tests, subjects carried a loaded backpack while walking on the treadmill at increasing speed or increasing incline. Multiple regression analyses were performed where measured $\dot{V}O_2$ is the dependent variable and the independent variables are: load, speed, incline, and the following parameters from accelerometer #1: m_rms_x, m_rms_y, m_rms_z, m_rms_{mag}, $mean_x$, $mean_y$, $mean_z$, $mean\_mag$, sp_peak_x, sp_peak_y, sp_peak_z, (the peak frequencies of the *x*-, *y*- and *z*-axis accelerations respectively), $power_x$, $power_y$, $power_z$ and $power_{mag}$ (the spectral power for the *x*-, *y*- and *z*-axis accelerations and the magnitude of the spectral power).

In the first analysis, a statistical model using only load, speed and incline as independent variables was derived as the baseline model for prediction of $\dot{V}O_2$. Results of the analysis are given in Table III.

Table III: Results of statistical model using load, speed and incline as independent variables

Model	R^2	Std Error of the Estimate (SEE)
Incline	0.371	4.96
Incline, Speed^2	0.625	3.84
Incline, Speed^2, Load	0.796	2.84

The model equation is:

$$\dot{V}O_2 = 4.222 + 1.363(I) + 0.765(S^2) + 0.2(L) \qquad \text{EQ 2}$$

and it explains 89.2% of the variation in the results.

In the second analysis, only the following acceleration parameters were used as the independent variables: m_rms_{mag}, $power_x$, $power_y$, $power_z$, sp_peak_y, and sp_peak_z. These parameters represent the amplitude and frequency content of the measured accelerations. In this case the resultant model is given in Table IV.

Table IV: Results for statistical model using accelerometer parameters.

Model	R2	SEE
$Power_z$	0.487	4.63
$Power_z$, $Power_y$	0.552	4.31
$Power_z$, $Power_y$, $Power_x$	0.567	4.23
$Power_z$, $Power_y$, $Power_x$, $(m\_rmsmag)^2$	0.583	4.16
$Power_z$, $Power_x$, $(m\_rmsmag)^2$, sp_peak_y	0.585	4.15
$Power_z$, $Power_y$, $Power_x$, $(m\_rmsmag)^2$, sp_peak_y	0.594	4.11
$Power_z$, $Power_y$, $Power_x$, $(m\_rmsmag)^2$, sp_peak_y, sp_peak_z	0.604	4.05

The resulting polynomial equation is:

$$\dot{V}O_2 = 1.438 + 0.146(P_z) - 0.251(P_x) + 0.448(m\_rms_{mag})^2 + 5.733(sp\_peak_y) - 1.105(sp\_peak_z) \quad \text{EQ 4.}$$

This equation, EQ 4, explains 60.4% of the variance in the data. Note that $power_y$ was dropped out of the equation after $(m\_rms_{mag})^2$ was added. This is not surprising. $(m\_rms_{mag})^2$ is the mean squared magnitude of the acceleration signal; the largest contribution to the mean squared magnitude would come from the *y*-axis accelerations, which have the highest amplitude. Thus $(m\_rms_{mag})^2$ and $power_y$ are correlated and provide redundant information to the model.

If the load carried is included with the accelerometer parameters as an independent variable, the model R^2 value increases to 0.723 as shown in Table V.

Table V: Results for statistical model using load and accelerometer parameters.

Model	R^2	SEE
$Power_z$	0.487	4.63
$Power_z$, Load	0.582	4.20
$Power_z$, Load, $(m\_rms_{mag})^2$	0.706	3.53
$Power_z$, Load, $(m\_rms_{mag})^2$, $Power_x$	0.723	3.44

The resulting polynomial equation is:

$$\dot{V}O_2 = 5.35 + 0.068(P_z) + 0.191(L) + 0.578(m\_rms_{mag})^2 - 0.148(P_x) \quad \text{EQ 5}$$

and this equation explains 72.3% of the variance in the data.

2.4 Conclusions and Future Work

Analysis of measured $\dot{V}O_2$ for conditions of increasing load carried in a backpack, increasing speed of locomotion and increasing incline verified that each of these factors results in increased energy cost and that $\dot{V}O_2$ can be reliably predicted if all of these factors are known. This is easily

accomplished in a laboratory setting. However for field studies or during military training exercises, it is not possible to determine the speed of locomotion and the characteristics of the terrain, and the energy costs of the tasks performed must be estimated using other information.

In the study reported here, the use of upper body accelerations to predict $\dot{V}O_2$ for different walking speeds, inclines and loads carried was evaluated. With no load carried, the rms magnitude of upper body accelerations is highly correlated to $\dot{V}O_2$ for increasing speed, but less well correlated for increasing incline. The rms values and spectral power of the accelerations do not increase with increasing load, and thus do not follow the increase in $\dot{V}O_2$. A predictive equation involving acceleration parameters and load carried was derived and found to explain 72.3% of the variance in the data. The ultimate goal is to replace speed and incline (and possibly load) with acceleration parameters in the equation to predict $\dot{V}O_2$. Although the equation derived here explains a reasonable amount of the variation in the data, other acceleration signal parameters may produce better results.

3 Transfer Function Between the Body and Pack Accelerations

3.1 Objective

The objective of this study is to determine whether the relative motion of a backpack with respect to the body can be accurately estimated using accelerations recorded from the upper body and the pack. This will be done initially for the LCSim and then extended to humans. This is a revised objective, where the original objective was to determine the transfer function between the relative acceleration of the body and the pack, and the contact pressures under the pack. As will be explained later, we do not have confidence in our pressure recordings at this time. Thus, the first part of the analysis – identifying the relationship between the pack and body accelerations – will be completed.

3.2 Data Collection

Using the LCSim, body and pack acceleration and contact pressure data were collected for four backpack loads. The LCSim manikin was outfitted with a military shirt and helmet. One

triaxial accelerometer was mounted on the manikin's upper chest (analogous to the sternum location in human subjects) and the second was fixed to the framesheet of the pack. In both cases, the positive *y*-axis of the accelerometer was oriented vertically. An Xsensor pressure pad was attached to the underside of a CTS backpack (the side which makes contact with the dorsal surface of the manikin) and under the left shoulder strap to measure the contact pressures due to the loaded pack. The Embla® portable data recorder was used to sample and store data from the accelerometers and load cells, which were attached in-line to the shoulder strap, waist belt, upper hip stabilizer and lower hip stabilizer of the backpack, such that they carried all of the strap tension. The data from the Xsensor pressure system were recorded separately using dedicated software and hardware. All of the data were downloaded onto a PC after each trial.

Four sets of data were collected for total pack loads of 16.6 kg, 25.9 kg, 38.7 kg and 50 kg. The manikin was set to move at a pace of 5.6 km/hr (1.6 m/s). The LCSim is driven by computer controlled pneumatic activators that are programmed to create a vertical displacement pattern of ±2.54 cm amplitude and 1.8 Hz frequency, where the motion is defined by a sine wave. Ten independent trials were done for each of the four loads. Prior to each trial, the backpack was removed and placed back on the manikin and the tensions in the shoulder straps and waist belt were adjusted to be within the following values: shoulder strap: 60 ±5 N; waist belt: 50 ±5 N; upper hip stabilizer strap: 65 ±5N and lower hip stabilizer strap: 65 ±5 N. At the start of each session (for the four different loads), the tilt of the manikin was adjusted such that the anterior-posterior moment at the hips was zero. This moment is measured using a load cell located at the level of the manikin's hips.

Both acceleration and pressure data were recorded for all trials. Each trial was repeated, since pressures from the two Xsensor pads could not be recorded simultaneously, thus a pressure recording was taken for the shoulder and a second recording was taken for the back. The accelerations of the pack and manikin were also recorded, for the two repetitions. In total for each load ten pressure recordings for the shoulder, ten pressure recordings for the back and twenty acceleration recordings for the upper chest and the pack were obtained. The only exception is for the 25kg load, which was tested first. In some of the ten trials, only one acceleration recording was done.

3.3 Results

The data analysis includes computing the forward lean angle of the manikin, correcting the accelerometer data for this lean angle, determining the relationship between the body and pack accelerations, and identifying the transfer function between body accelerations and pack accelerations.

3.3.1 Forward Lean Angles

The tilt of the manikin can be determined from the accelerations measured in the static position for each load. The manikin is an anthropometrically correct 50^{th} percentile male, and the upper chest is tilted with respect to vertical as shown below in Figure 8. Because the accelerometer registers the gravity vector, this can be considered to be the global vertical, and the tilt angle of the chest can be computed from the vector projection onto the vertical and anterior-posterior axes of the accelerometer[15]. The backward tilt angle of the chest is defined as positive. When a pack is placed on the manikin, it is rotated forward to zero the moments at the hip and the tilt angle will decrease, and eventually become negative. The tilt angle of the backpack can be found in the same way, using the accelerations measured by the accelerometer mounted on the framesheet.

During dynamic movement, the gravity vector is present as a non-zero offset, after removal of the zero-g offset of the accelerometers. Thus, the tilt angle can also be determined using the overall mean value of the accelerations on each axis. Tilt angles for the four LCSim loads were computed both from static manikin positions and from the dynamic data and are summarized in Table VI.

[15] Care was taken to insure that the mediolateral axis was horizontal so that there was no (or only a very small) component of the gravity vector on this axis.

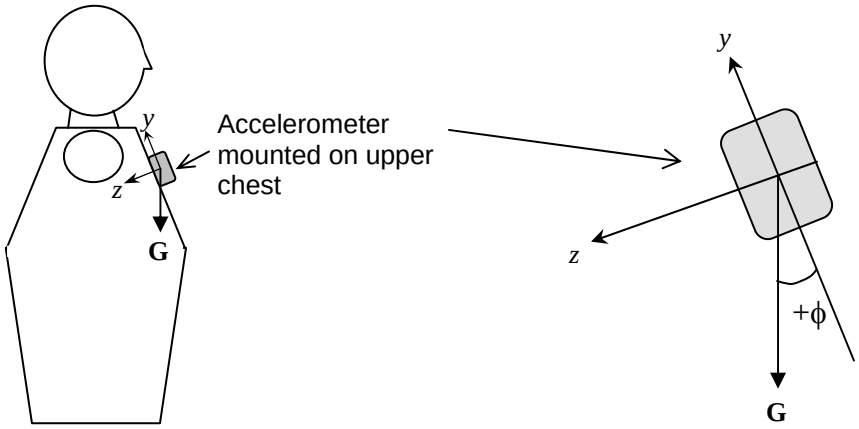

Figure 8: Schematic diagram of the LCSim manikin showing accelerometer.
Accelerometer position and angle of the accelerometer mounted on the centre of the upper chest is analogous to the sternum location in human subjects. The detail view of the accelerometer shows the tilt angle, ϕ, which is defined as a positive angle for the upright manikin position (zero load).

Table VI: Tilt angles for the LCSim manikin and backpack, determined from accelerations. Accelerations recorded during static positioning and during dynamic testing.

Load (kg)	Static		Dynamic			
	Manikin tilt angle	Pack tilt angle	Average manikin tilt angle*	Standard deviation	Average pack tilt angle*	Standard deviation
0	22.56	N/A				
16.6	16.8	8.26	14.4033	0.1956	1.2522	0.7145
25.9	13.21	1.38	12.4564	0.0956	4.0245	1.4424
38.7	9.29	0.84	9.4625	0.94	2.0095	1.2349
50.0	0.78	Not available	5.2667	0.9196	3.7361	2.4561

* Averaged over the ten trials for each load.

It is apparent that the pack lean angle does not necessarily follow the body lean angle as load is increased. This may be partly due to a counter-rotation of the pack, which increases as the load increases. As well, the pack loading protocol was designed such that the load is positioned at the pack's centre of volume; however, load position may differ slightly from load to load, resulting in slight offsets from the centre of volume. The other observation is that the manikin lean angles, computed from the static data, do not exactly follow those computed from the dynamic data. This difference is shown in Figure 9.

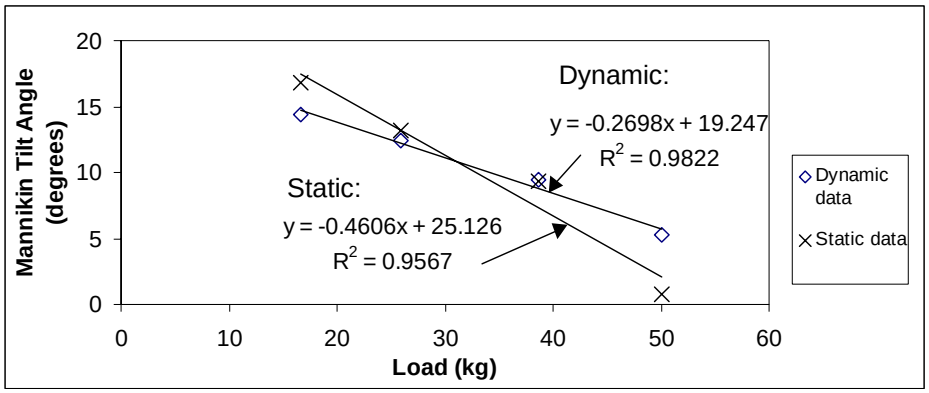

Figure 9: Manikin tilt angles computed during static position and dynamic testing. Linear regression equations for both data sets are given.

Figure 9 shows that the change in lean angle from load to load is different when computed from the static versus the dynamic case. One explanation for this difference is that the manikin lean angle may differ slightly between its base position and its raised position, and it is possible that the base plate is not exactly level, causing an "average" angle to be computed. It may also be that there are accelerations present which are not related to the vertical displacement of the manikin, e.g. vibrations or wobbles, which introduce an additional offset to the acceleration data. In humans, high accelerations due to the ground contact force during gait, may contribute to altering the total offset, thereby shifting the estimated lean angle. Computed lean angles for the human subjects and a discussion of the effect of lean angle on the measured accelerations is included in Appendix D.

3.3.2 Relative accelerations between manikin & pack

In order to compare the acceleration of the manikin with respect to the pack, it is necessary to rotate the accelerometer vectors so that they are aligned. In this case the tilt angles were used with a 2-D rotation matrix to align both the manikin and the pack accelerometer vectors with gravity. A schematic of the alignment is shown in Figure 10; mathematical details are included in Appendix D.

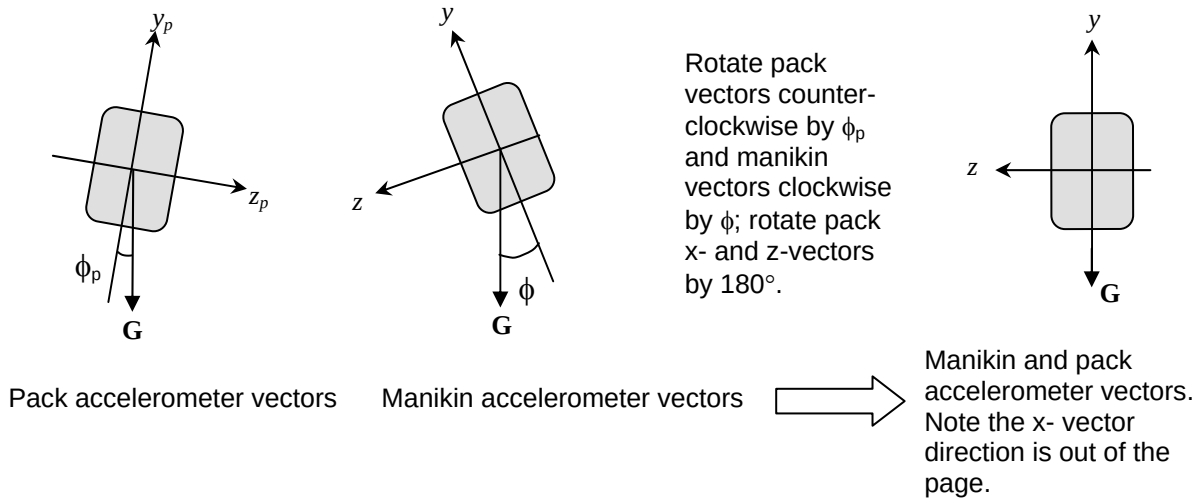

Figure 10: Rotation of manikin and pack vectors into global coordinate system. Rotation is based on aligning the gravity vector, **G**.

The proper rotation matrix was applied to the accelerometer data so that off-axis accelerations due to the tilt were removed. A comparison of the resulting vertical (*y*) and anterior-posterior (*z*) accelerations for the four loads is shown in Figure 11.

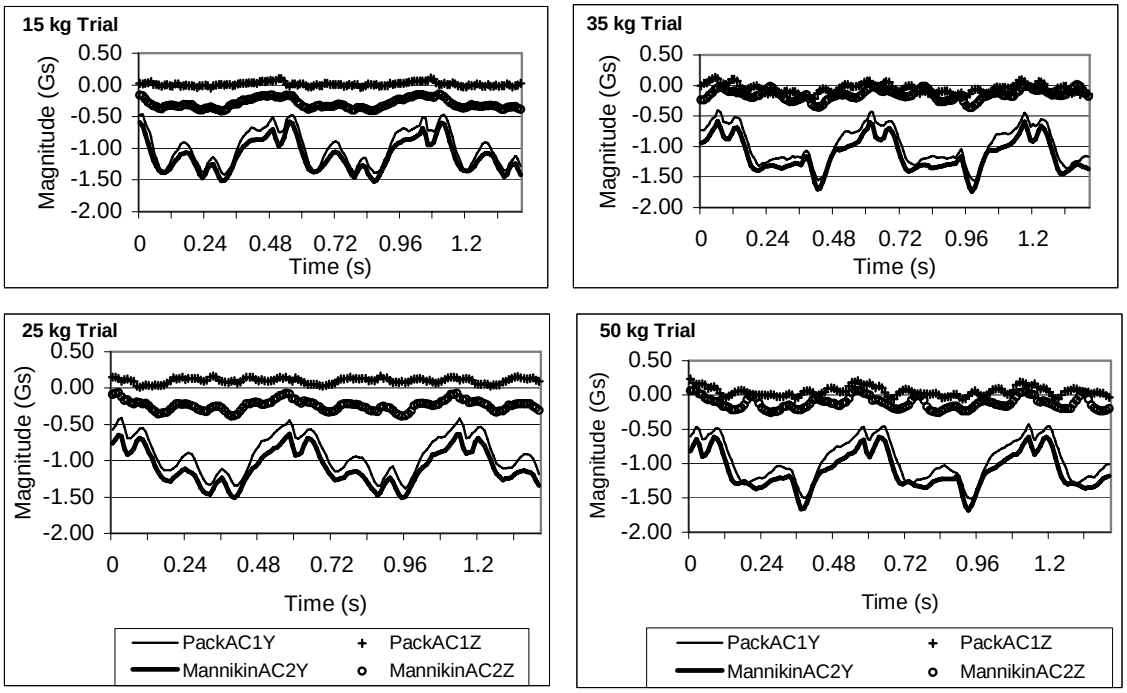

Figure 11: Manikin and pack accelerations on the vertical (*y*) and anterior-posterior (*z*) axes.

The LCSim manikin is displaced vertically to simulate the vertical motion of walking. Because of the tilt of the accelerometers, this vertical motion results in acceleration components on the vertical (*y*) and anteroposterior (*z*) axes (assuming that there is negligible tilt on the mediolateral (*x*) axis). Aligning the accelerometer vectors with the gravity vector should remove the acceleration components on the *z*-axes and all acceleration should appear on the *y*-axes of the manikin and pack accelerometers. From Figure 11, it is apparent that the rotated accelerations are primarily on the *y*-axes, which have an offset of −1g, or acceleration due to gravity. There is some residual acceleration on the *z*-axes, which again may be due to manikin accelerations unrelated to the vertical displacement pattern.

Close examination of Figure 11 reveals that there are distinctive differences in the vertical acceleration patterns of the manikin versus the pack accelerometer. There is an upward shift in the pack accelerations, and as load increases, there is an increasing delay in the pack accelerations with respect to the manikin accelerations. There are also differences in the acceleration slopes – primarily on the upward slopes – indicating that there is a relative difference in the manikin and pack velocities. Mathematical identification of the relationship between the pack and manikin accelerations is being done as part of a Master's thesis project[16].

4 Dynamic Biomechanical Model V3

4.1 Introduction

This section summarizes the progress made in the development of the 3-D Dynamic Biomechanical Model (DBM) project, which was previously described in Reid et al., (2002). The DBM is being developed in support of the creation of a Load Carriage Limit equation that would take into account key factors that effect the load a soldier could carry based on task conditions (especially time and/or distance travelled). As part of the supporting work for the development of the biomechanical factor, a dynamic biomechanical model of a soldier and his equipment is

[16] Anita Lee, Royal Military College of Canada. The thesis work will be completed by Aug. 2004.

being developed to generate a number of estimates for biomechanical pack and human load carriage variables[17] (Reid et al., 2002).

4.2 Objectives for the DBM

The purpose of this work is to develop a dynamic biomechanical model capable of providing accurate estimates of biomechanical load factors as well as pack-person interface information when provided with activity, load carried, generalized pack geometry and material property inputs.

4.3 DBM Model Developments

The previous version of the model, V2, consisted of a 3D human torso model separated into an upper and lower torso coupled with a rigid joint. The pack model was a parallelepiped with custom inertial properties determined during human trials (Morin and Reid, 2003). Shoulder straps were modeled as a Voigt-Kelvin visco-elastic material with a stiff linear spring in series with a linear damper to reproduce the combined effect of a compliant shoulder pad and stiff webbing material. Motion of the model is controlled by providing an initial position and an integrated 3D acceleration time history which was developed from data recorded with the portable system (Morin and Reid, 2003). In Version 2, reaction forces and moments on the lumbar spine and the total shoulder reaction force were estimated. The distribution of force to the upper and lower torso and the total contact force were also calculated. Development of DBM Version 3 has concentrated on adding detailed models of all pack components forming the contact interface and on creating a skin surface on the torso.

4.3.1 Creation of Skin Layer

The human torso model was created by scanning the surface of the 50 percentile LCSim manikin. This cloud of data points was read into a computer aided design (CAD) program and a 3 dimensional solid was generated using these data points. The resulting geometric body (ACIS, STL or SAT format) cannot be modified within VisualNastran 4D (VN4D). VN4D has a very

[17] The "body" used in the DBM is a computerized version of the 50th percentile male manikin. In future it can be extended to use a female body.

limited geometry creation facility; instead it provides built-in integration routines, compatible with most mid level CAD programs. All modification to CAD created bodies must be done in the CAD environment. No mid level CAD program proved capable of capturing the 3D surface torso and creating a separate layer lying immediately on the underlying surface. Fortunately, Queen's University Mechanical Engineering department is a licensed user of the fully functional UNIGraphics CAE software that was capable of performing this task.

4.3.2 Skin Geometry

Graphics programs interpret surface geometry of a solid body as a series of discrete patches. Organization and shape of these entities is determined during the initial grouping of the scanned data points into a solid body. The size and shape of these patches determines what can be detected as a separate entity and subsequently modified by the CAD package. Typically this process is highly automated and only expert operators can control this process in detail. Using Unigraphics V18, a layer of skin was developed by copying the surface geometry of all patches forming the torso surface and then thickening these to 5 mm. The completed layer of skin is shown below in Figure 12 and consists of 49 separate patches. Details of the skin layer and it's thickness can be seen in the close up of the shoulder area in Figure 13.

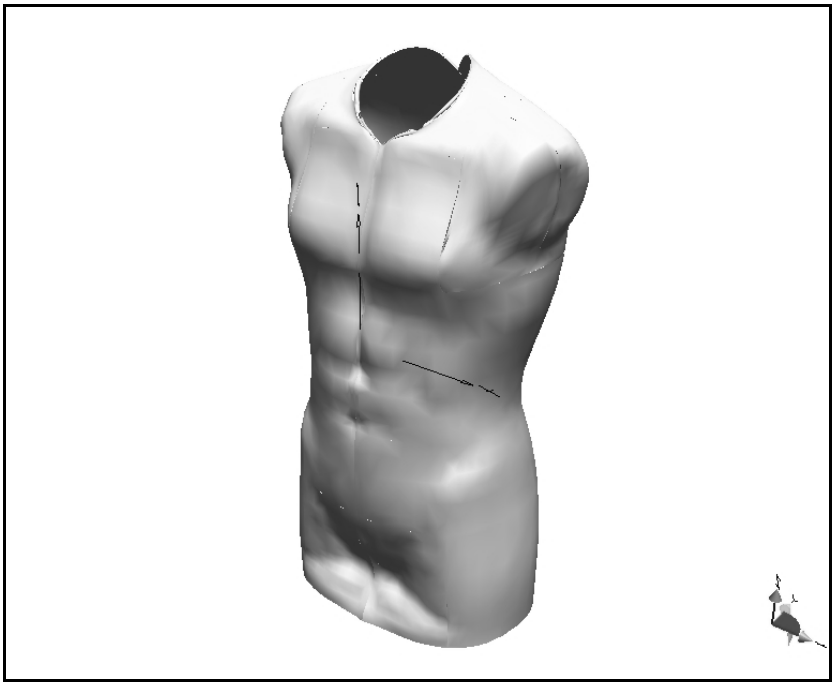

Figure 12: Skin Layer of DBM

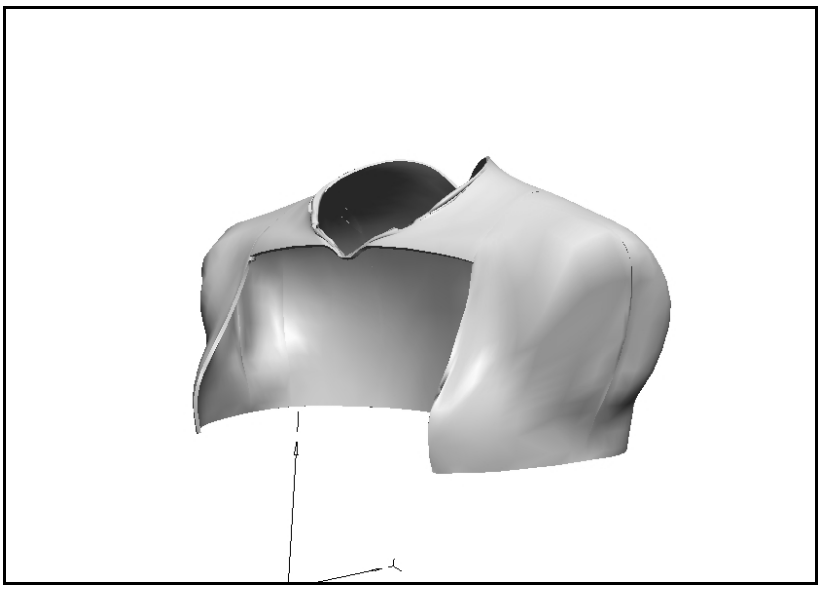

Figure 13: Skin Layer, Shoulder Detail

4.3.3 Skin Material Property Definitions

The behaviour of most soft tissue, including skin, is typically represented by the response shown in Figure 14. This response pattern is normally broken into three regions, the initial very low stiffness – high elongation region, a transition region with a constantly increasingly rate of stiffness and a third region of approximately linear high stiffness response. Material properties of human skin vary by body region, age, thickness and gender (Ridge, 1965). For skin, the initial region of low stiffness extends for 40 to 75% elongation depending on body region. Values for the elastic modulus and density for skin on the back and shoulder regions, 1.10e+5 Pa and 1.07e+3 kg/m^3 were taken from Duck (1990). This reference was also used to create materials reflecting toughened skin, based on the soles of the feet and skin over bone. Sanders et al. (1998) measured the coefficient of friction (COF) of skin with socks to be 0.75±0.09 while Naylor (1955) reported a range of values depending on the level of moisture on the skin; dry skin at 0.6 and wet skin at 1.00. The pack and torso were defined with a COF of 0.9, which is consistent with damp skin.

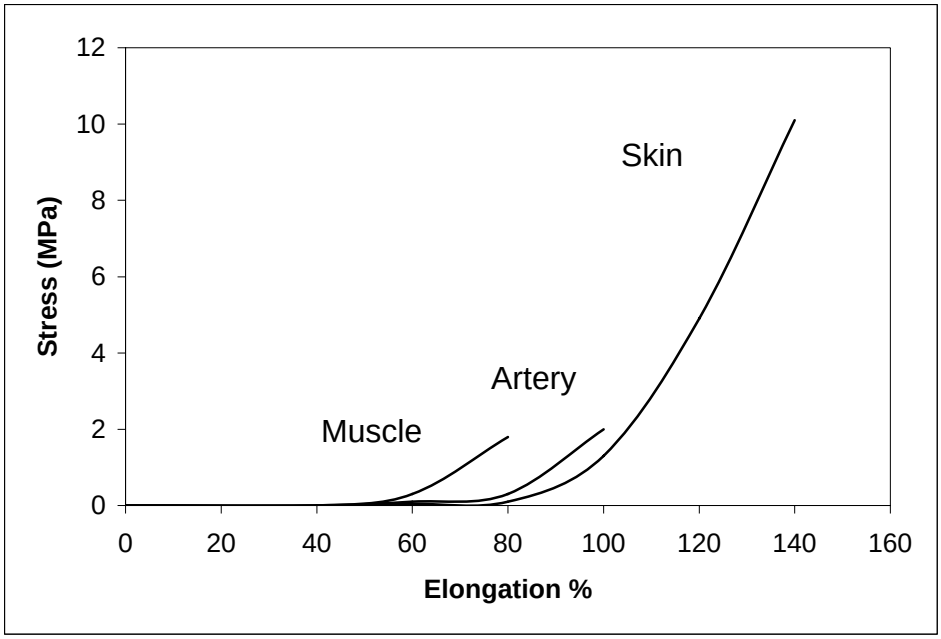

Figure 14: Generalized variation in longitudinal strain of soft tissue.
Values are for muscle, artery and skin. Graph reproduced from Chapter 5 of Duck, (1990).

4.3.4 Skin Constraint

Each skin patch was constrained to the underlying body shape with a rigid constraint so that VN4Dl can distribute the contact forces over the entire contact surface of the skin patch[18].

4.4 Shoulder Straps

4.4.1 Shoulder Strap Geometry

Initially, shoulder straps were created in a mid level CAD program (Mechanical Desktop 2002) that approximated the shape of the shoulder pads. Motion trials indicated that the program was having great difficulty solving the initial static equilibrium condition. Gaps between the shoulder strap model and the shoulder caused wide variations in the location and magnitude of contact force during each iteration, leading to instability in the numerical solution. Again, the process described in Section 2.1 was used to extract the surface geometry of the skin and this surface became the contacting surface of the shoulder straps. Figure 15 shows the complex 3D surface that forms the shoulder strap to person contact interface.

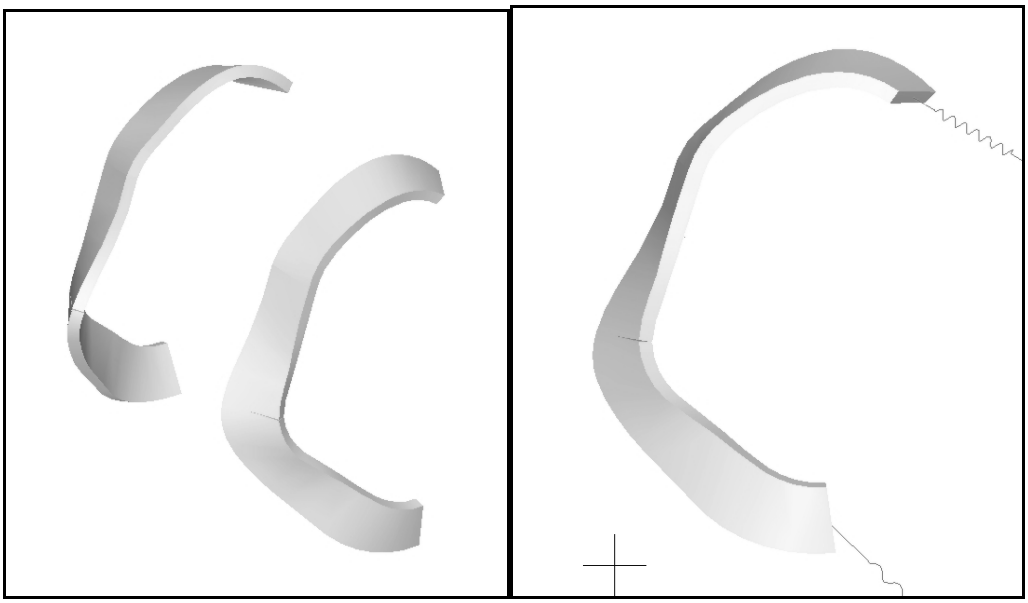

Figure 15: Shoulder Strap contours (left) and detail (right). Shoulder strap width 5cm and thickness 0.6 cm

4.4.2 Shoulder Strap Material Properties

The material properties of the shoulder strap pads separated into two portions, the pads were given an elastic modulus of 290 kPa, and a density of 32 kg/m^3. These values were the average test values of Evacote® (EVA) and Volara® measured during the 1.8 Hz dynamic compression testing performed during the previous phase of DBM development (Reid et al., 2002). The strap material modeled by the springs shown in Figure 4b, were given stiffness based on the effective stiffness of the complete shoulder suspension system (combined webbing straps and shoulder pads) tested dynamically at 1.8 Hz. Material definitions are summarized in Table VII.

Table VII: Material property definitions for DBM shoulder straps.

	Modulus Elasticity kPa		
Component	1.8 Hz	3.2 Hz	Density
Shoulder pad	290 kPa	353 kPa	32 kg/m^3
Strapping	723 kPa	906 kPa	10 kg/m^3

[18] Reference: email communication, Bernard Chan, Technical Support desk MSC.Software, vndesktop.support@mscsoftware.com

4.5 Waist Belt development

4.5.1 Waist Belt Geometry

Attempts were made at using the same methodology of extracting the lower torso surface shape to construct the waist belt on but this effort failed to import into VN4D properly. Instead, the individual padded segments of the hip belt were modeled as half cylinders, each with a separate flat backing plate. A rounded rectangular lumbar pad and a shoulder pad were also added to the basic pack model. Figure 16 shows an overhead view of the resulting articulating waist belt. One distinct advantage of this approach is the ability to vary the material properties of the different pads as required. As well, segments of the waist belt are joined with user definable constraints, permitting the user/designer to control the degrees of freedom and stiffness of the linkage between adjacent segments.

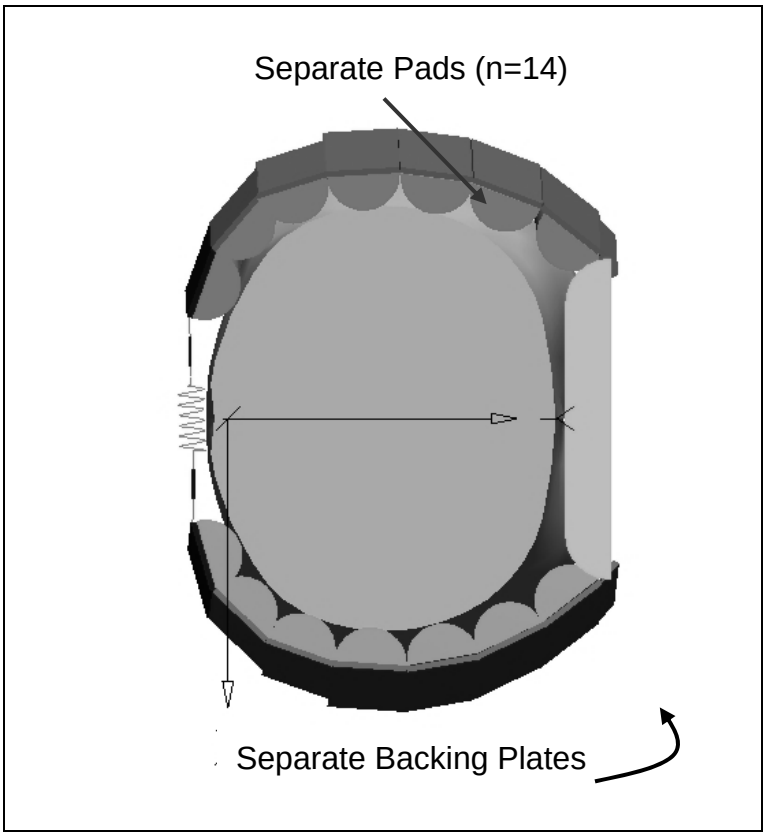

Figure 16: Top View of Waist Belt

4.5.2 Waist Belt Material Properties

Initially, the hip padding, lumbar and back pads have been given the same material values as those used for the shoulder strap padding, elastic modulus 290 kPa, and density of 32 kg/m^3.

4.6 Waist Belt Constraints

4.6.1 Revolute Constraints between Hip Pads

The waist belt has 16 revolute constraints between adjacent pad segments. In Figure 17, revolute constraints appear as circles. These constraints act like a door hinge and allow the belt segments to rotate, permitting the hip belt to follow the curve of the body around the hips of the model. This ability to conform is shown in Figure 18, where the waist belt has been “tightened” into place by applying a horizontal closing force to the open two ends of the belt. All backing plates are attached to the underlying pads with rigid joints, which appear in Figure 17 as squares. Rigid joints permit VN4D to treat the two bodies as a single object during motion solution, but allow the pad and backing plate to have differing material properties for the purposes of stress analysis.

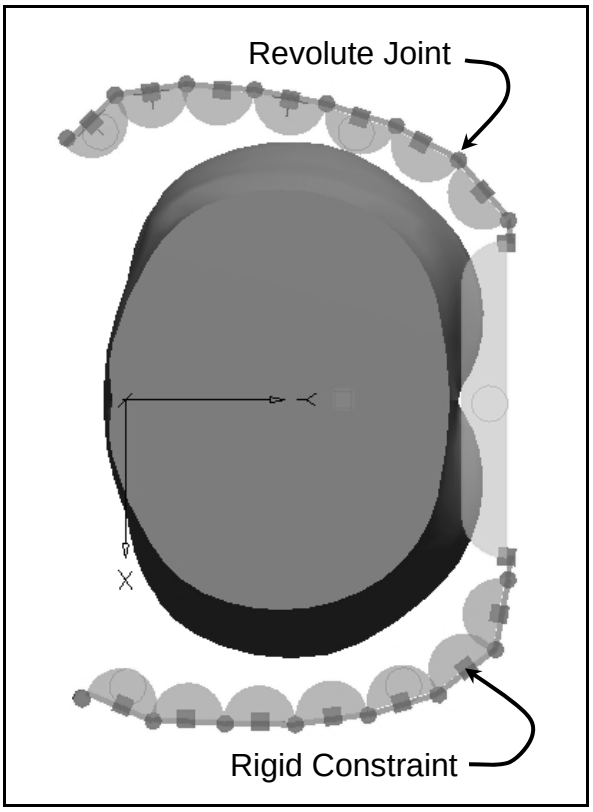

Figure 17: Waist belt constraint – belt shown open

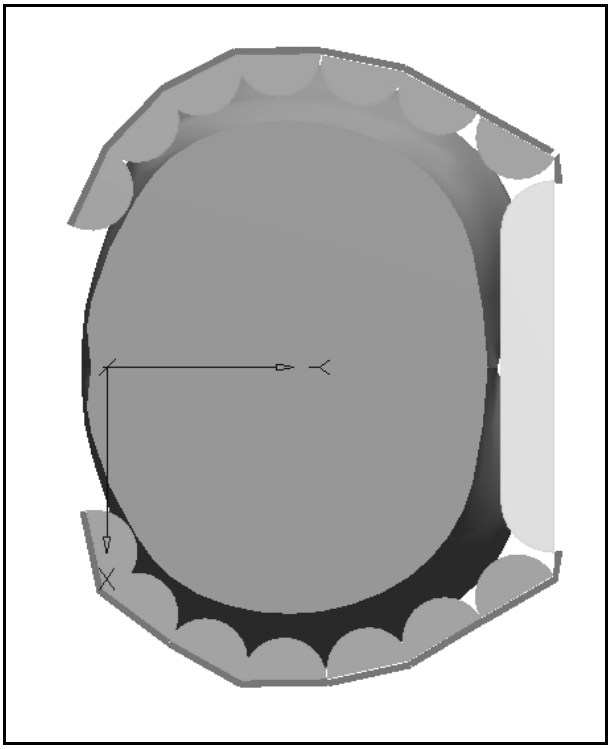

Figure 18: Waist belt shown tightened into position.

4.6.2 Constraints Between Lumbar Pad and Hip Belt Sections of Waist Belt

Two spherical joints connect the lumbar pad to the right and left hip belt section of the waist belt assembly. Spherical joints act as a pin joint, they free the lumbar pad and hip belt sections to rotate about all axes independently. This was done to allow the lumbar pad to align itself to the body, independent of the orientation of the hip belt portions. Results of this freedom of motion are apparent in Figure 19, showing the hip sections aligned with the shape of the body.

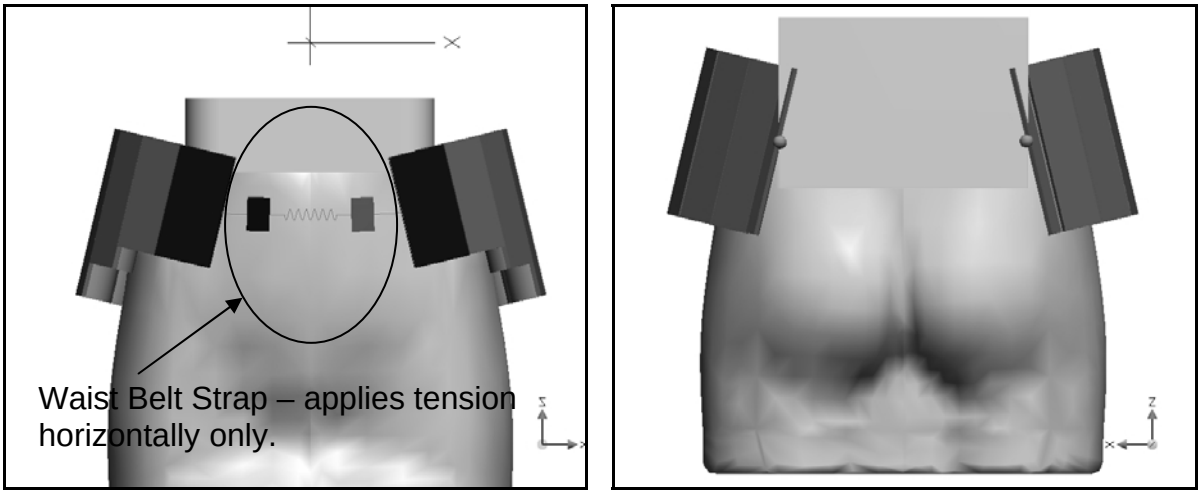

Figure 19: Spherical constraints – effect on ability of belt to conform.
Front view (left) and back view (right). Hip pads are allowed to penetrate lumbar pad to ensure good fit.

4.6.3 Tensioning Of Waist Belt

The waist belt strap is shown in detail in Figure 20 and consists of three linked constraints. The centre element is a spring element with variable stiffness and the two outer constraints are ropes. The rope elements prevent any force from being applied if the belt is slack, the spring provides the tension when the belt is tightened into place.

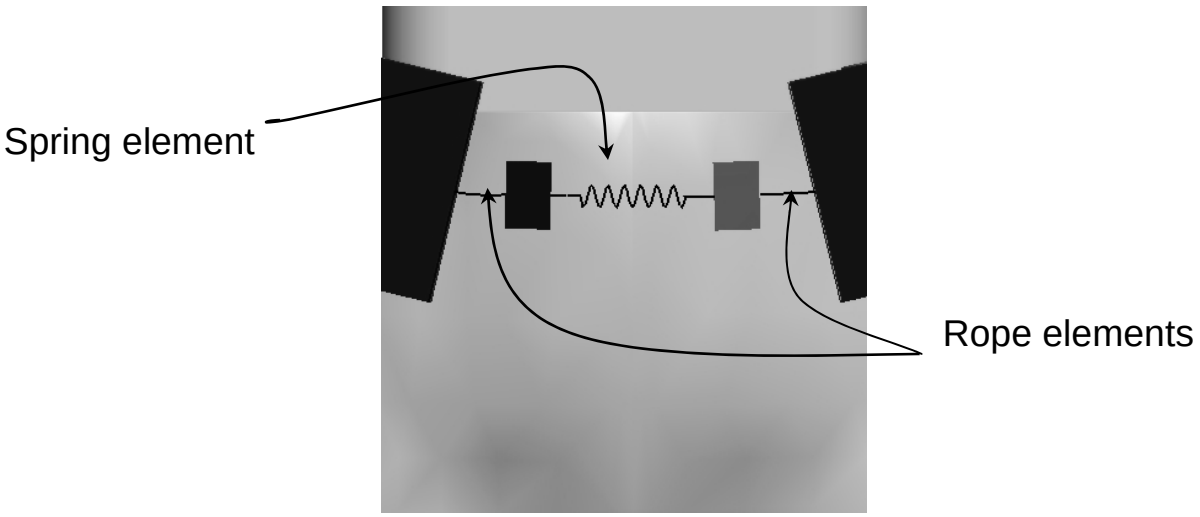

Figure 20: Detail of waist belt strap model

4.7 Constraints - Effect on Solution Procedures

The dynamic relationships for all components of a model must be correctly defined to permit the formulation of the equations of motion. A motion solution typically advances in steps; the first step is to simply allow elements of a model to come to rest in equilibrium. This permits the equations of motion to resolve small geometric and force imbalances arising from model assembly. Once the model is in equilibrium, and all components have settled in place, typically this solution is saved and becomes the new starting position for subsequent motion solutions.

4.8 Stress Distributions – Static Solutions

In addition to defining dynamic relationships for all components, interaction forces must be correctly assigned to components in a manner consistent with physics for the program to properly evaluate a body's internal stress state. The stress distribution for the equilibrium state of the model has been evaluated and the results are presented here.

4.8.1 Stress in the Skin Layer

Although a skin layer was successfully created and brought into the model, a number of difficulties then arose with the model. Numerous system crashes spontaneously occurred and the program began to freeze during execution. When the components were meshed and stress analysed, it was found that a number of these components had internal stresses even when

unloaded. The cause of this was unclear but thought to be a result of geometric interference of the thickness dimension during creation of the skin patches. These skin components were recreated and re-imported but this did not solve either the presence of internal stresses nor the spontaneous crashing of the program. Numerous attempts were made to resolve this conflict but none have been successful to date. As the program had become unworkable with this geometry, a new model with no skin layer was created and further development of the waist belt and shoulder straps continued with this simplified model. This appears to have resolved all program crashes. The entire upper torso was then given the material properties of skin and meshed. This results in a much larger finite element model (>38,000 elements) than would have otherwise been necessary. Increasing the number of elements results in increased computation time. The program provides a single choice of element type, a linear element. Typically, higher mesh densities are necessary with linear elements to accurately solve areas of high strain rate. VN4D provides a highly automated mesh generation feature. Although highly automated and able to handle uncomplicated geometries well, the mesh generation feature permits minimal user control. These restrictions may limit the results of the stress analyses to very approximate values. Other FEA programs available at Queens through the Mechanical Engineering department offer complete formulation function and can interface with the DBM model should the limitations of the VN4D prove too restrictive.

4.8.2 Stress in Torso due to Shoulder Straps

The upper left torso was meshed for the linear finite element analysis with elements having a typical dimension of 15 mm. This resulted in a model having 33,800 linear elements and Figure 21 shows the resultant mesh density. Figure 22 shows some initial results for a static analysis, with the pack resting in equilibrium. Sigma Y, shown in Figure 22, is the stress in the fore/aft direction and is generally aligned with the direction of the shoulder reaction force. The deep blue area under the shoulder pad in the axilla region, indicated by the arrow in Figure 22 reflects an area of compressive stress.

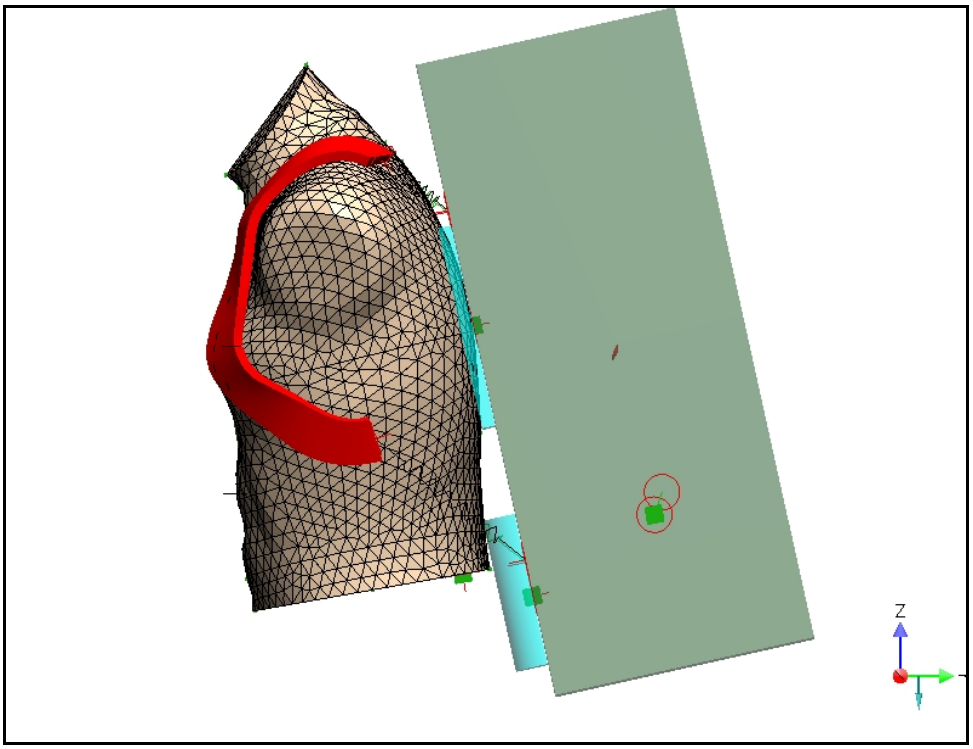

Figure 21: Upper torso finite element mesh definition; typical element dimension is 15mm.

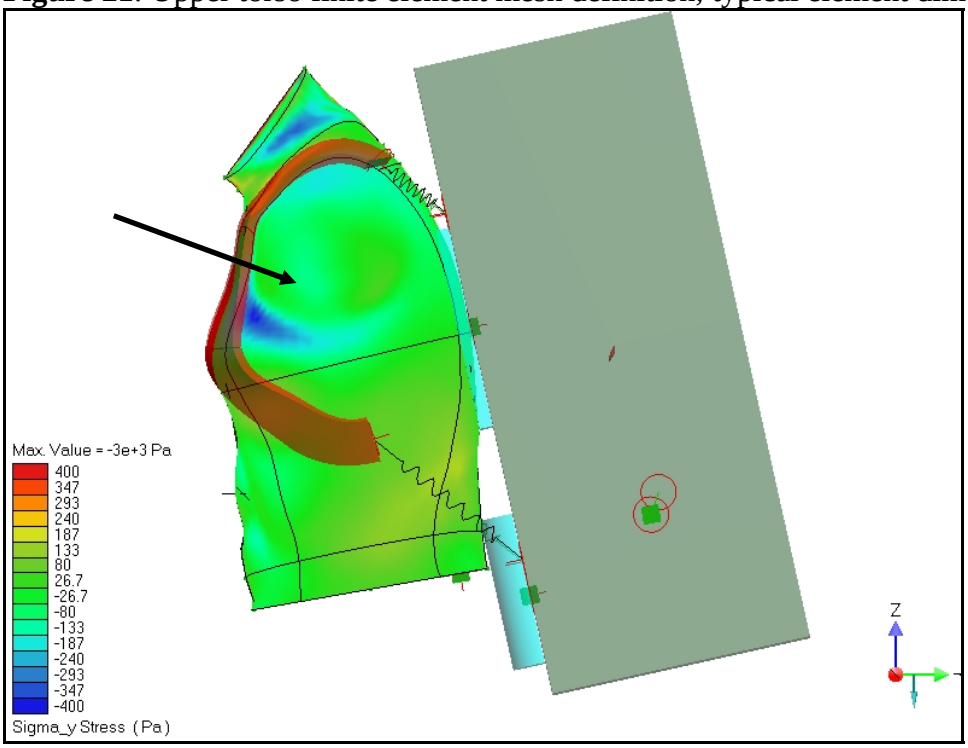

Figure 22: Plot of sigma Y (horizontal) stress in torso.
Compression of the chest/axilla region, shown by a deep blue colour (-400 Pa), is indicated by the arrow.

4.8.3 Stress in Torso due to Waist belt

The lower torso was meshed with elements having a typical dimension of 35 mm. This rather coarse mesh still creates a model with 2500 linear elements and Figure 23 shows the resultant mesh density. The waist belt is shown for reference. Von Mises stress results for a static analysis of the lower torso with a waist belt tightened to a tension of 100 N are shown in Figure 24. Von Mises stress reflects the triaxial stress state of the material; locations having the highest distortion energy are indicated by red in figure. These areas occur under several of the hip belt pads indicating that these pads are in contact at multiple points on the waist belt.

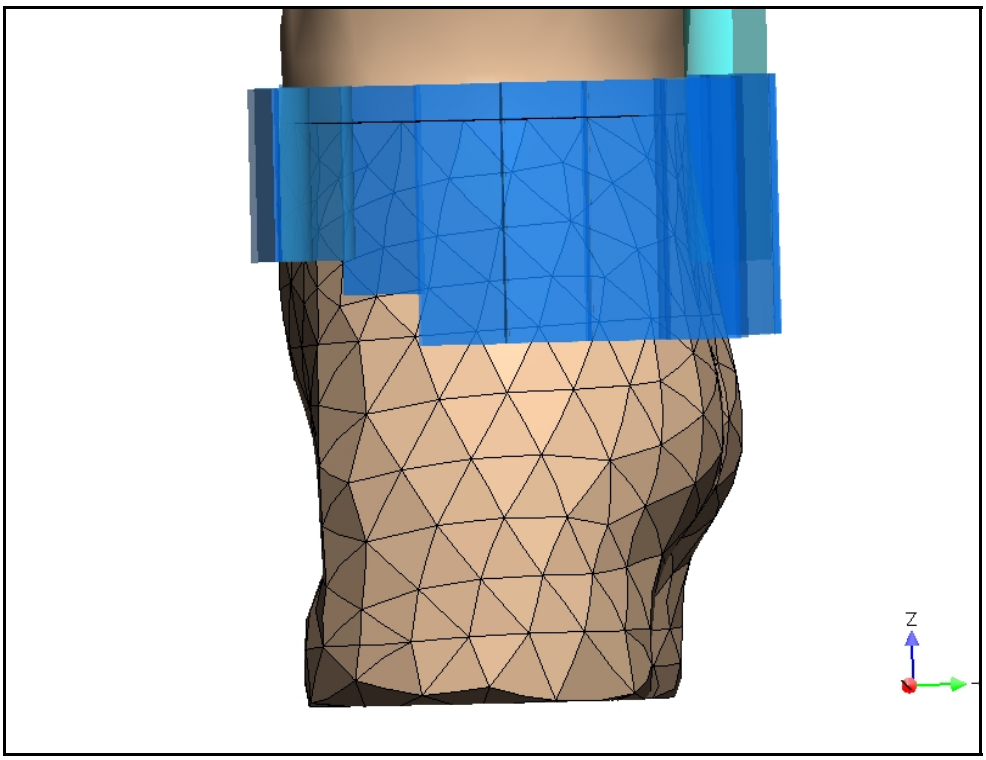

Figure 23: Lower torso finite element mesh definition; typical element dimension is 35mm.

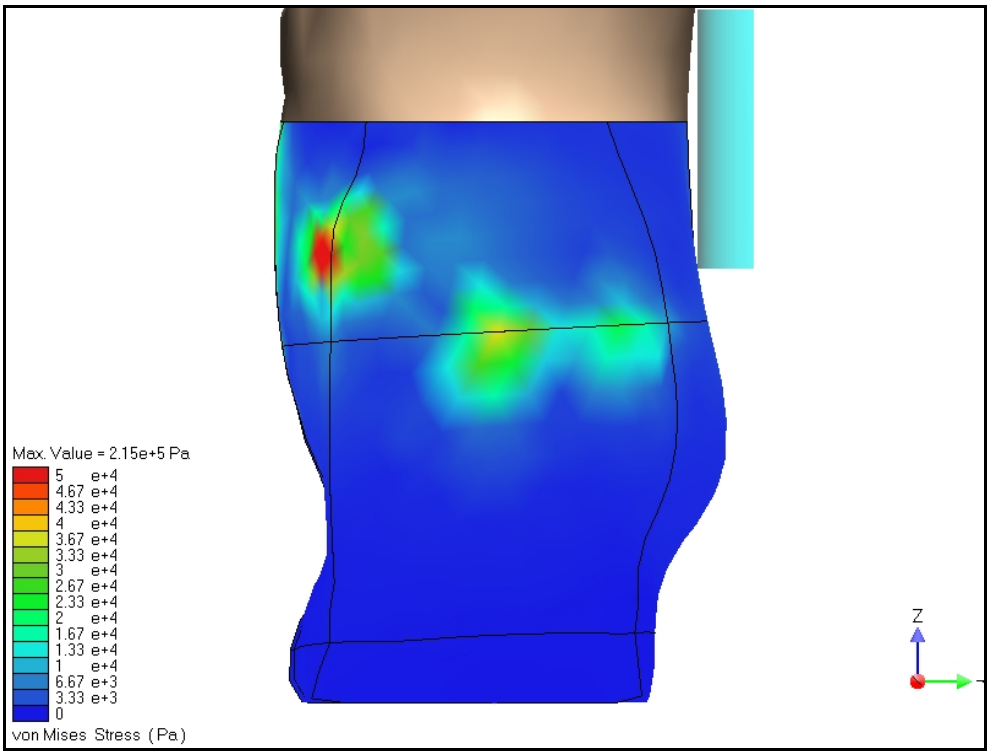

Figure 24: Von Mises stress under a waist belt tightened to 100N.
Areas of higher stress indicate contact locations of hip belt pads.

5 Conclusions and Recommendations

5.1 The Physiological Factor of the Load Carriage Limit Equation

In this report, it has been shown that the energy cost of treadmill walking increases with increasing speed, increasing incline, and increasing load carried in a backpack. Also, there is an interaction effect between load and speed, and load and incline, such that when speed or incline is increased, the metabolic cost increases at a higher rate when a load is carried. Thus, load, incline and speed are determinants of the physiological factor (PF) and must be included in the PF equation.

It has also been reported here that upper body accelerations reflect metabolic energy cost for treadmill walking. The acceleration parameters investigated (rms value, spectral power and the fundamental frequency of the vertical accelerations) are sensitive to changing speed, but less so to changing incline and changing load carried. A model to predict energy cost using the acceleration parameters and load explained 72.3% of the variance in the data. In order to reliably

estimate the PF using acceleration data, a better predictive equation is required. It would also be preferable to predict PF from acceleration parameters alone, so that the exact load carried does not have to be known. Using other acceleration parameters, for example, body lean angle which is related to load carried in a backpack, may

In the experimental study, data were also recorded using the Xsens[19] motion sensor, which measures 3-D accelerations and angular velocities and the earth's magnetic field. The Xsens was mounted under the accelerometer on the subject's sternum, and thus should provide equivalent acceleration information. The other information provided – angular velocity and orientation within the earth's magnetic field – may provide extra information that can be used in the energy cost model.

The final stage of development of the PF equation will focus on the use of acceleration parameters, and/or parameters derived from the Xsens data as independent variables used for the prediction of metabolic energy cost.

5.2 The Pack-Person Interface

The original objective of this work was to examine the dynamic contact pressures experienced by a bearer carrying a loaded backpack and to examine the relationship between these pressures and the relative motion of the pack and the body. To this end, contact pressures were measured using two Xsensor pressure pads – one under the right shoulder strap and the other on the underside of the pack, making contact with the back of the subject. However, as documented in Appendix E, the pressure readings were unreliable and it is not possible to identify the relationship. The first part of this objective – identifying the transfer function between the motion (or acceleration) of the body and the motion (or acceleration) of the pack – is being done as an M.Sc. thesis project. Future development of the transfer function between the dynamic contact pressures and the relative pack-person motion will depend on the availability of an acceptable pressure measurement system.

[19] Xsens Technologies, www.xsens.com

5.3 The Dynamic Biomechanical Model

The completion of the modeling of all relevant pack components that form the person-to-pack interface has been documented in this report. A library of material properties for biological (skin on the back, skin toughened, skin over bone) and pack materials, both individually and in combination, has been compiled. These materials have been added to the built-in material selection menu that automatically presents as part of the Properties window. Stress distribution analyses under the shoulder straps, waist belt and back area have been done.

The final stage of the model development will concentrate on:

- validating the motion and stress response of the DBM against existing test data
- improving the user interface
- adding an output format that provides the BF results, from the model, for input into the LCL equation.

6 References

Bossi L.L., Stevenson, J.M., Bryant, J.T., Pelot R.P., Reid, S.A., Morin, E.L. Development of a suite of objective biomechanical measurement tools for personal load carriage system assessment. *Soldier Mobility: Innovations in Load Carriage System Design and Evaluation* NATO-RTO Meeting Proceedings: MP-056, (Neuilly-sur-Seine: NATO), 14;1-7, 2001.

Bouten C.V., Koekkoek K.T., Verduin M., Kodde R. and Janssen J.D., "A triaxial accelerometer and portable data processing unit for the assessment of daily physical activity", *IEEE Trans. Biomed. Eng*., vol. 44, pp.136-147, 1997a.

Bouten, C.V.C., Sauren, A.A.H.J., Verduin, M. and Janssen, J.D., "Effects of placement and orientation of body-fixed accelerometers on the assessment of energy expenditure during walking," *Med. Biol. Eng. Comput.*, vol. 35, pp. 50-56, 1997b.

Bryant, J.T., Doan, J.B., Stevenson J.M., Pelot, R.P. and Reid, S.R., "Validation of objective measures and development of a Performance based ranking method for load carriage systems", *Soldier Mobility: Innovations in Load Carriage System Design and Evaluation* NATO-RTO Meeting Proceedings: MP-056, (Neuilly-sur-Seine: NATO), 15:1-20, 2001.

Duck, F.A. *Physical Properties of Tissue,* Academic Press Inc. San Diego, CA, USA, 1990.

Fewster J.B. and Eng T.J., "Calibration and Analysis Methods for the F-Scan System", *International Society of Biomechanics*, 1997.

Hadcock L. *Factors Affecting Force Distribution on a Load Carriage System Waistbelt.* M.Sc. thesis, Queens University, Kingston, Ont., 2002.

Hadcock L.J., Bryant J.T. and Stevenson J.M., *Pressure and Force Distribution Measurement for the Design of Waist belts in Personal Load Carriage Systems*. PWGSC Contract # W7711-0-7632-02/A (DRDC- Toronto) 1-140, 2002.

Hendelman, D., Miller, K., Baggett, C., Debold, E. and Freedson, P., "Vailidity of accelerometry for the assessment of moderate intensity physical activity in the field," *Med. Sci. Sports Exerc*., vol. 32, suppl. 9, pp. S442-S449, 2000.

Herren, R., Sparti, A., Aminian, K. and Schutz, Y., "The prediction of speed and incline in outdoor running in humans using accelerometry," *Med. Sci. Sports Exerc*., vol. 31, pp. 1053-1059, 1999.

Holewijn, M., and Meeuwsen, T., "Physiological strain during load carrying; effects of mass and type of backpack", *Soldier Mobility: Innovations in Load Carriage System Design and Evaluation* NATO-RTO Meeting Proceedings: MP-056, (Neuilly-sur-Seine: NATO)1: 1-12, 2000.

Johnson, R.C., Pelot, R.P., Doan, J.B. and Stevenson, J.M., "The effect of load position on biomechanical and physiological measures during a short duration march", *Soldier Mobility: Innovations in Load Carriage System Design and Evaluation,* NATO-RTO Meeting Proceedings: MP-056, (Neuilly-sur-Seine: NATO), 4:1-6, 2001.

MacNeil, S.M., *Biomechanical Assessment of Strap Forces and Pressures During Load Carriage*, M.Sc. Thesis, Queen's University, Kingston, Ont., 1996.

McGill, S.M., *Biomechanics and Motor Control of Human Movement*, 2nd edition, John Wiley and Sons Inc., Canada, 1990.

Morin, E., Reid, S.A. and Bryant, J.T., *Research and Development of an Advanced Personal Load Carriage Measurement System Phase IV: Section E Applicability of the F-scan system for human pressure assessments*, PWGSC Contract #W7711-7-7420/A, Oct. 1998.

Morin, E. and Reid, S., *Development of a Portable Data Acquisition System for Human Performance Assessment in the Field. Phase IIb: Testing and validation of module 2 – activity assessment module*, PWGSC Contract #7711-0-7632/01-TOR (7632-04), May 2003.

Naylor, P.F.D., "The skin surface and friction", *Br. J. Dermatology*, vol. 67, pp. 238-239, 1955.

Pandolf, K.B., Givonni, B., Goldman, R.F., "Predicting energy expenditure with loads while standing or walking very slowly", *J. App. Physiol.*, vol. 43, pp. 577-581, 1977.

Pelot, R.P., Rigby, A., Stevenson, J.M., and Bryant, J.T., "Static biomechanical load carriage model", *Soldier Mobility: Innovations in Load Carriage System Design and Evaluation* NATO-RTO Meeting Proceedings: MP-056, (Neuilly-sur-Seine: NATO) 25:1-12, 2001.

Rigby, A.J., *Development of a Biomechanical Model and Validation of Assessment Tools for Personal Load Carriage Systems*, M.Sc. thesis, Queen's University, Kingston, Ont., 1999.

Reid, SA, Bryant, JT, Stevenson, J.M., *Phase II Development of a Dynamic Biomechanical Model of Human Load Carriage*, DRDC Contract #W7711-0-7632-06, June 2002

Sanders, J.E., Greve, J.M., Mitchell, S.B, and Zachariah, S.G., "Material Properties of commonly used interface properties amd their static coefficients of friction with skin and socks", *J. Rehab. Res. Dev.*, vol. 35, pp. 161-176, 1988.

Schutz, Y., Weinsier, S., Terrier, P. and Durrer, D., "A new accelerometric method to assess the daily walking practice," *Int. J. Obesity*, vol. 26, pp. 111-118, 2002.

Stevenson, J.M., Bryant, J.T., Reid, S.A. and Pelot, R.P. *Validation of the Load Carriage Simulator: Research and Development of an Advanced Personal Load Carriage system: Section D (Phase 1)*, DSS Contract #W7711-4-7225/01, 1996

Stevenson, J.M., Bryant, J.T., Reid, S.A., Pelot, R.P., and Morin E.L., "Development of the Canadian Integrated Load Carriage System using Objective Measures", *Soldier Mobility: Innovations in Load Carriage System Design and Evaluation* NATO-RTO Meeting Proceedings: MP-056, (Neuilly-sur-Seine: NATO) 21:1-11, 2001.

Stevenson, J.M., Bryant, J.T., Morin, E.L., Anderson, R.A., Pelot, R.P., and Reid, S.A., *Proposed Long Range Plan for Research and Development of Dynamic load Carriage Modeling*., PWGSC Contract #W7711-0-7632-01. (DRDC: Toronto) 1-42, 2001.

Stevenson, J.M., Bryant, J. T., Pelot, R.P., and Morin, E. *Research and Development of an Advanced Personal Load Carriage System (Phase II and III)*, PWGSC Contract #W7711-5-7273/001-TOR, 1997.

Stevenson, J.M., Bryant, J.T., dePencier, R.D., Pelot, R.P., and Reid, J.G., *Research and Development of an Advanced Personal Load Carriage System (Phase I-D)*, DSS Contract # W7711-4-7225/01-XSE (DRDC: Toronto), pp. 1-350, 1995.

Stevenson, J.M., Good, J.A., Devenney, I.A., Morin, E.L., Reid, S.A. and Bryant, J.T., *Characterization of load control during a human trials circuit, Phase 3(b)*, PWGSC Contract #W7711-0-7632-06, 2002.

Waters T.R., Putz-Anderson V., Garg, A., and Fine, L.J., "Revised NIOSH equation for the design and evaluation of manual lifting tasks", *Ergonomics*, vol. 36, pp.749-776, 1993.

Woodburn J. and Helliwell P.S., "Observations on the F-scan in-shoe pressure measuring system", *Clin. Biomech.*, vol. 11, pp. 301-304, 1996.

7 Appendices

7.1 *Appendix A* - Letter of Information and Consent Form

Metabolic and Biomechanical Effects of Load Carriage under different loads, walking speeds and treadmill inclinations

Dear _____

You are being invited to participate in a research study on load carriage being conducted by the Ergonomics Research Group at Queen's University. This study is being completed for Defence Research and Development Canada - Toronto (DRDC). We will read through this consent form with you and describe the procedures in detail. You will be given time to read it yourself and ask questions at any time.

Aims and Purposes of the Study:

The overall aim of our research program is to develop a dynamic biomechanical model for application in load carriage situations. The current phase of this model is to gather data from subjects using accelerometers, pressures sensors, metabolic measuring devices and subjective feedback so that we can prove that the model is giving the same answers as subjects. The purposes of this study are:

1) to prove/validate that we get the same energy demand whether we place an accelerometer on your waist or your chest when walking at different speeds or inclines under different loads,
2) to determine the relationship between the accelerometers and the skin contact pressure you experience under different backpack loads when walking at different speeds or inclines under different loads,
3) to investigate the relationship between early signs of discomfort and skin contact pressure under different load conditions.

Study Details:

The first session will determine if you are eligible for the study by determining your VO_2 max, which is a measure of aerobic fitness. To be eligible to participate, you must demonstrate superior fitness on the maximum oxygen uptake test. If not eligible, we will still may for your time for the fitness test. If you are eligible to participate, you will be invited to participate in ten sessions within the next three weeks. Each session will last approximately 1½ hours. The VO_2 max test is a physically demanding test that will require you to work progressively harder, either by increasing speed or by increasing the treadmill inclination.

During each subsequent session you will be asked to walk on a treadmill with accelermeters, pressures sensors and oxygen consumption equipment attached to your body. For the next four testing sessions, you will be asked to carry a backpack with four different loads ranging from 15 to 50 kg. The speeds you will be asked to walk will be 2.0 m/s, 2.5 m/s and 3.0 m/s and the inclination of the treadmill will be 0˚to 7˚ to 10˚. You will walk at these speeds (or inclines) for approximately 6 minutes/condition or until steady state is achieved. A complete test will take about 15 minutes. This will be followed by a rest of approximately 20 minutes and then the three more inclines (or speeds) for approximately 6 minutes/condition or until steady state is achieved. For the final four tests, you will be instrumented with accelerometers and pressures systems and asked to walk for one hour under different loads and report your discomfort. Regardless of the test, you are allowed to stop at any time without penalty or coercion to continue. You will receive the total funding for that session even if you stop the test.

Risks of Participation:

The risks of participating in this study include: dizziness, fatigue, muscle cramping, shortness of breath, fainting, heart attack and back and joint pain. The risk of these events should be minimal for young, healthy and physically fit individuals. If you experience dizziness, fatigue, pain muscle cramps or shortness or breath please report them to the research assistant or the principal investigator immediately.

Exclusion Criteria:

To minimize the risks and reduce variation in the subject characteristics, only young, physically fit, men will participate in this study. Therefore, you will not be considered for this study if you:

- Are not between the ages of 21 and 29 years
- Are female
- Do not pass the PAR-Q and You
- Have a VO_2 max less than 51 mL/kg·min

Confidentiality:

All information obtained during the course of this study is strictly confidential and your anonymity will be protected at all times. You will be identified by a study number, not your name. Data will be stored in a locked file and will be available only to the principal researcher and research assistants who have helped collect the data.

Voluntary Nature of the Study:

Your participation in this study is completely voluntary. You may withdraw from this study at any time without coercion to continue or penalty.

Withdrawal of subject by principal investigator:

You may be withdrawn from this study or a specific trial by the principal investigator if your heart rate indicates that you are working too hard to continue safely.

Payment:

You will receive a stipend of $10.00 for each hour you participate in this study.

Subject Statement and Signature:

I have read and understand the consent form for this study. The purposes, procedures and technical language have been explained to me. I have been given sufficient time to consider the above information and to seek advice if I chose to do so. I have had the opportunity to ask questions which have been answered to my satisfaction. I am voluntarily signing this form. I will receive a copy of this consent form for future reference.

If at any time I have further questions, problems or adverse events, I can contact:

Dr. E. Morin at (613) 533-6562
Electrical & Computing Engineering .....

Or

Dr. Janice Deakin at (613) 533-6601
School of Physical & Health Education

If I have any questions regarding my rights as a research subject I can contact

Dr. Albert Clark, Chair, Research Ethics Board at 533-6081

By signing this consent form, I am indicating that I agree to participate in this study.

Signature of Subject	Date
Signature of Witness	Date

Statement of Investigator:

I, or one of my colleagues, have carefully explained to the subject the nature of the above research study. I certify that, to the best of my knowledge, the subject understands clearly the nature of the study and demands, benefits, and risks involved to participants in this study.

Signature of Principal Investigator	Date

7.2 Appendix B - Instrumentation, Testing and Data Information

7.2.1 Calibration values for the Crossbow accelerometers

The factory calibration values provided for the Crossbow accelerometers used in this study are:

Accelerometer 1 (on sternum)			
	x-axis	*y*-axis	*z*-axis
Zero-g offset (V)	2.587	2.456	2.465
Sensitivity (V/g)	0.204	0.202	0.198
Accelerometer 2 (on lumbar spine or in backpack)			
	x-axis	*y*-axis	*z*-axis
Zero-g offset (V)	2.475	2.466	2.463
Sensitivity (V/g)	0.203	0.202	0.204

The accelerometer voltage is attenuated by a factor of 0.0447 and the polarity is reversed before sampling by the Embla data recorder. The recorded voltages are converted to g's of acceleration using the following equation:

$$\text{accel} = \left(\frac{-1 \times \text{data value}}{\text{scale factor}} - \text{zero g voltage} \right) \times \frac{1}{sensitivity}$$

7.2.2 Fitted CTS backpack sizes for the subjects

The shoulder strap, waist belt and pack sizes fitted for each subject are summarized below in Table B-I.

Table B-I: Shoulder strap and waist belt sizes for each subject.

Subject	Shoulder strap	Waist belt	Pack
SL01	Medium	Medium	Large
DK03	Medium	Medium	Medium
JD06	Medium	Medium	Medium
NS07	Large	Medium	Medium
WW08	Medium	Medium	Medium
GP09	Medium	Medium	Medium
MW10	Medium	Medium	Medium
JS12	Medium	Medium	Medium

7.2.3 $\dot{V}O_{2\max}$ *Test Protocol*

The $\dot{V}O_{2\max}$ test protocol was based on the Balke treadmill protocol[20]. Before starting the test, the subject warmed up on the treadmill for 5-10 minutes and selected a speed, which he could maintain for 30-45 minutes and feel tired afterwards. The subject was given time to stretch before the test. In order to measure the volume of O_2 inspired and CO_2 expired during the test, a mask was placed over the subject's mouth and nose. The mask was connected to airflow tubes by a high flow pneumotach, which plugged into the TEEM 100 metabolic cart. The treadmill and metabolic cart timers were synchronized with the start of the walk. Throughout the test, the subject wore a polar heart rate monitor and heart rate was recorded every 20 seconds. Encouragement to continue as long as possible was given to the subject.

The subject began the test at his selected speed and a 0° incline. After 3 minutes the incline was increased by 2°; the incline was increased a further 1° each minute thereafter. When the subject reached exhaustion, he stopped the test by pressing the stop button on the treadmill, or by signalling the researcher to stop. It was confirmed that the subject had reached his $\dot{V}O_{2\max}$ if his heart rate was at the age-predicted maximum (220-age) and his respiratory exchange ratio exceeded 1.0. If the subject failed to reach a $\dot{V}O_{2\max}$ of 44.5 ml/kg/min, he was excluded from the study, because he did not fall within the required fitness level: the top 40% fitness level for the age range 20 to 39 years (ACLS, 1998).

7.2.4 Accelerometer Data Summary

Due to instrumentation problems, complete acceleration records were not obtained for all subjects. The data records are summarized in Table B-II.

[20] The Balke protocol for active and sedentary men involves walking on a treadmill at 3.3 mph (5.3 km/h). At the start of the test the treadmill grade is 0%; at the start of the second minute, the grade is increased to 2%; after 2 minutes the grade is increased 1% and after each subsequent minute the grade is increased by 1% until the subject reaches exhaustion.

Table B-II: Summary of acceleration data records for each subject and each test.

	SUBJECT							
TEST*	**SL01**	**DK03**	**JD06**	**NS07**	**WW08**	**GP09**	**MW10**	**JS12**
A1-3.22	G	G	ND	ND-2(X)	G	G	G	G
A1-4.83	G	G	ND	ND-2(X)	G	G	G	G
A1-6.44	G	ND-2	ND	ND-S(X)	G	G	G	G
A2-3.22	G	G	G	G	G	G	G	G
A2-4.83	G	G	G	G	G	G	G	G
A2-6.44	G	G	G	G	G	ND	G	G
B1-0°	G	G	G	G	G	G	G	ND
B1-5°	G	G	G	G	G	G	G	ND
B1-10°	G	G	G	ND	G	G	ND	ND
B2-0°	G	G	G	G	G	G	G	ND-1
B2-5°	G	G	G	G	G	G	G	ND-1
B2-10°	ND	G	ND	G	G	G	G	ND-1
C1-3.22	G	ND-1	G	G	G	G	ND-1	G
C1-4.83	G	ND-1	G	G	G	G	ND-1	G
C1-6.44	G	ND-1	G	G	G	G	ND-1	G
C2-3.22	G	ND-1	G	G	G	G	ND-1	G
C2-4.83	G	ND-1	G	G	G	G	ND-1	G
C2-6.44	G	ND-1	G	G	G	G	ND-1	G
D1-0°	G	G	G	ND-1	G	G	G	G
D1-5°	G	G	G	ND-1	G	G	G	G
D1-10°	G	G	G	ND-1	ND	G	G	ND
D1-0°	G	G	G	ND-1	G	ND-1	G	G
D1-5°	G	G	G	ND-1	G	ND-1	G	G
D1-10°	G	G	G	ND-1	G	ND-1	G	G

The loads for each test are given in Table I.
G – good data; ND – no data; ND-1 – no data from accelerometer #1; ND-2 – no data from accelerometer #2; ND-2(X) – no data from accelerometer #2, *x*-axis

7.3 ***Appendix C –*** Recorded and Processed Data

7.3.1 Recorded Accelerations

Representative samples of acceleration data for five test conditions are shown below in Figures C-1 to C-5.

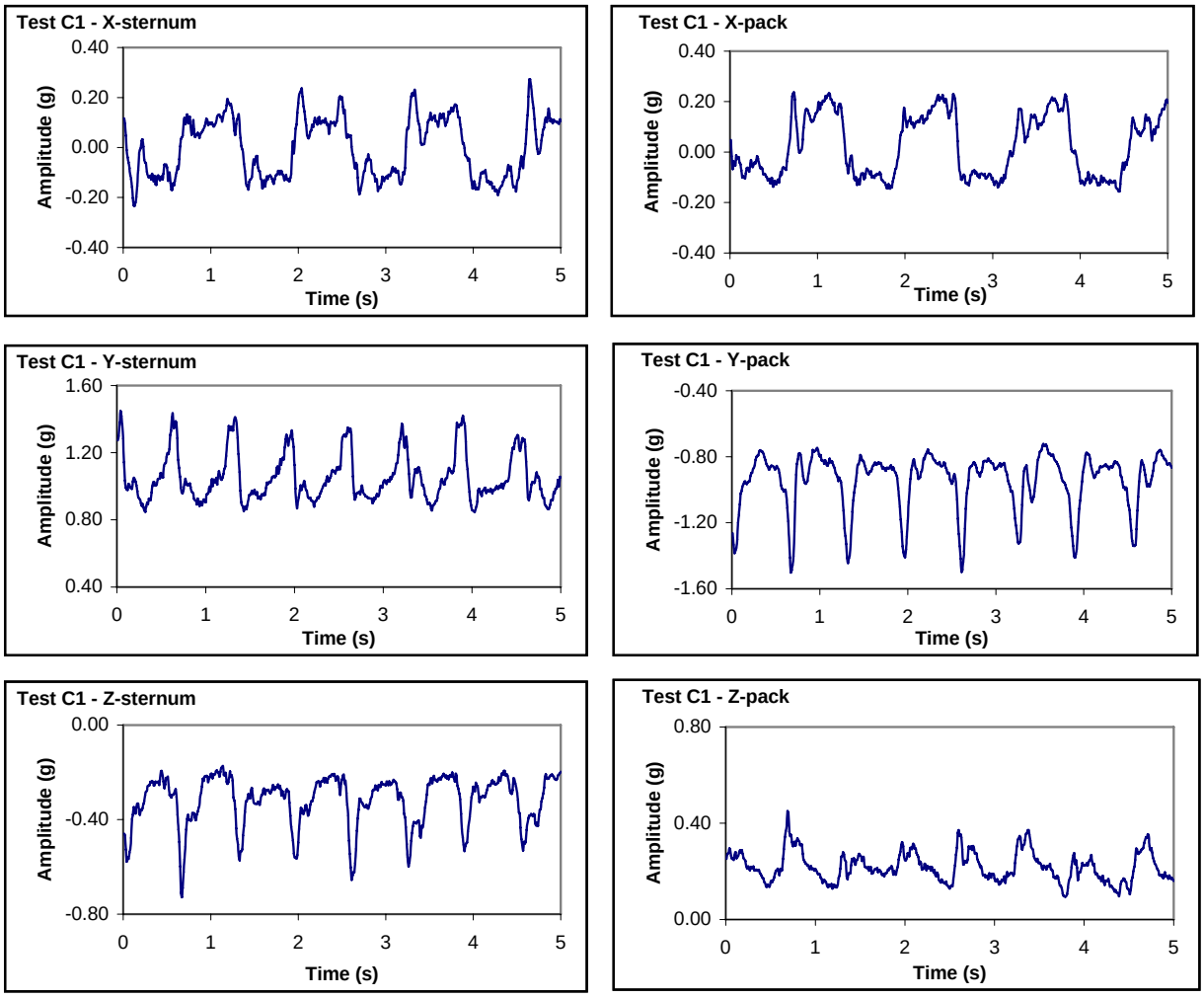

Figure C-1: Accelerations recorded in the x- (mediolateral), y- (vertical) and z- (anteroposterior) directions from the sternum (left) and pack (right) accelerometers for a subject carrying a 16.6 kg load and walking at 3.22 km/h, 0° incline.

Note, the y- and z-axis signals from the pack are inverted with respect to the sternum. For the sternum accelerometer, the +y-axis is oriented downwards, the +z-axis is oriented towards the body, pointing dorsally, and the +x-axis is oriented towards the left. For the pack accelerometer, the +y-axis is oriented upwards, the +z-axis is oriented towards the body, pointing ventrally, and the +x-axis is oriented towards the left. Acceleration due to gravity is present as non-zero average values on the y- and z- axes. Subject #01.

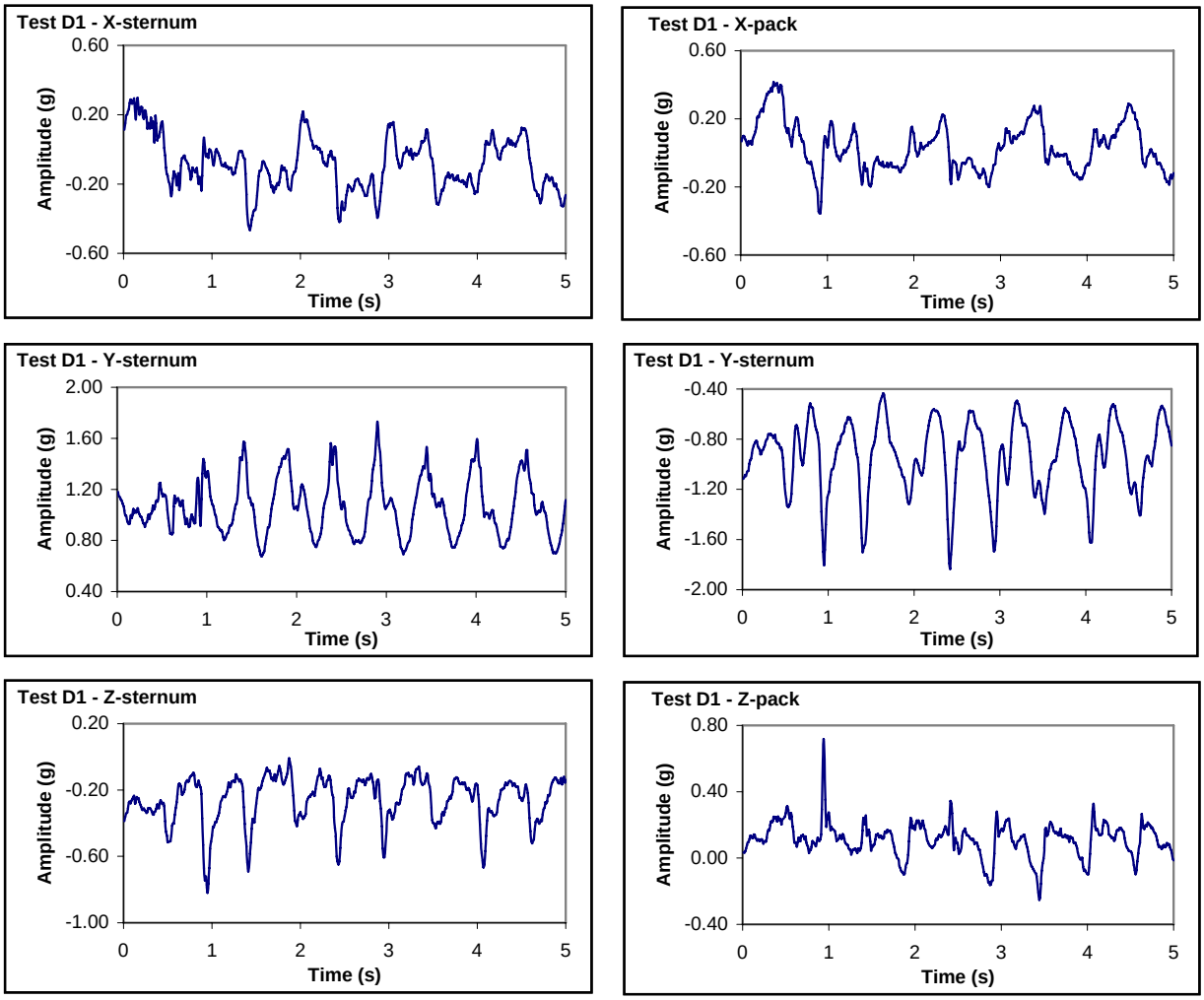

Figure C-2: Accelerations recorded from the sternum (left) and pack (right) accelerometers for a subject carrying a 16.6 kg load and walking at 4.83 km/h with 0° incline.
The accelerometer axes and the orientations of the positive axes are the same as in Fig. C-1. Again, the y- and z-axis signals from the pack are inverted with respect to the sternum. Subject #01.

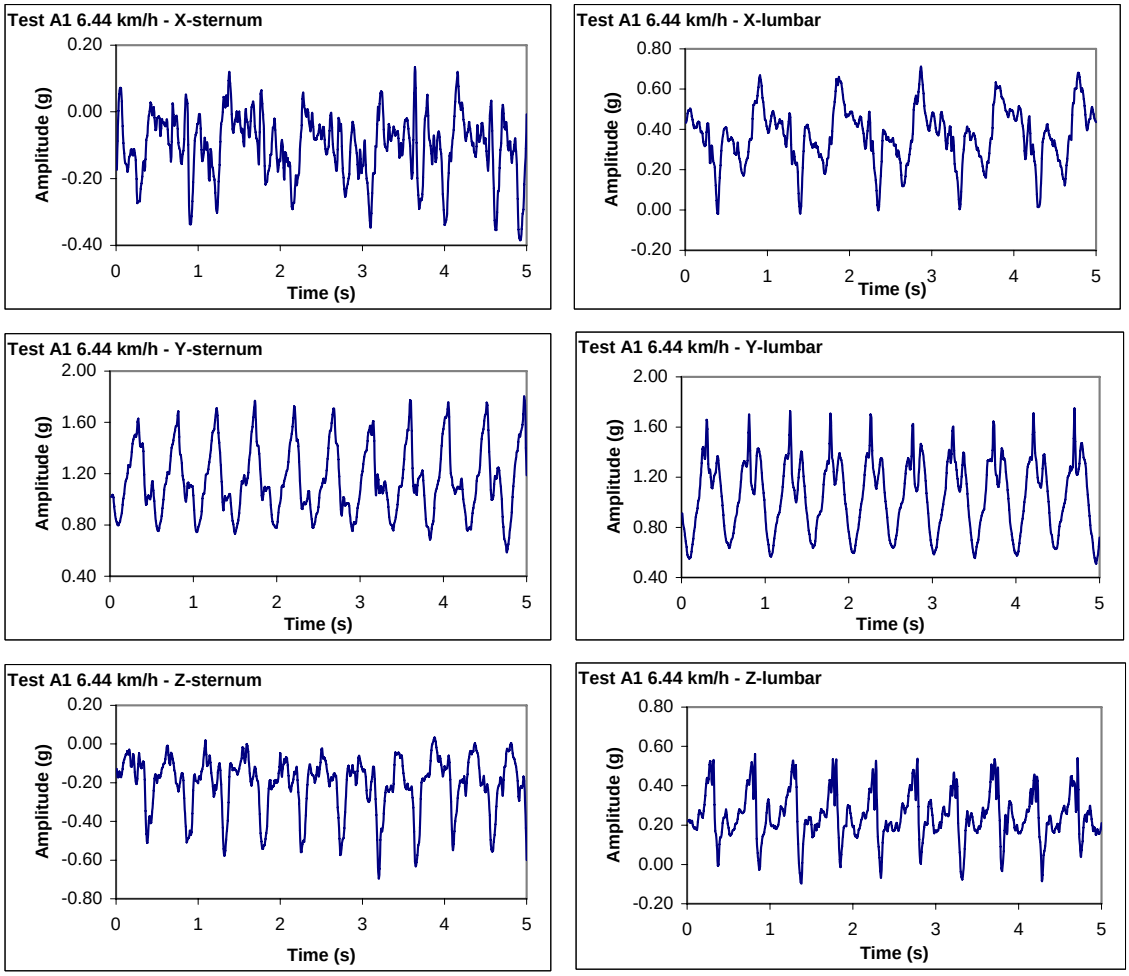

Figure C-3: Accelerations recorded from the sternum (left) and lumbar (right) accelerometers for a subject carrying no load and walking at 6.44 km/h and 0° incline.
Accelerometer axes are as given in Fig. C-1. For the sternum accelerometer, the +y-axis is oriented downwards; the +x- and +z-axes are oriented as in Fig. C-1. For the pack accelerometer, the +y-axis is also oriented downwards, the +z-axis is oriented towards the body, pointing ventrally, and the +x-axis is oriented towards the right. Subject #12.

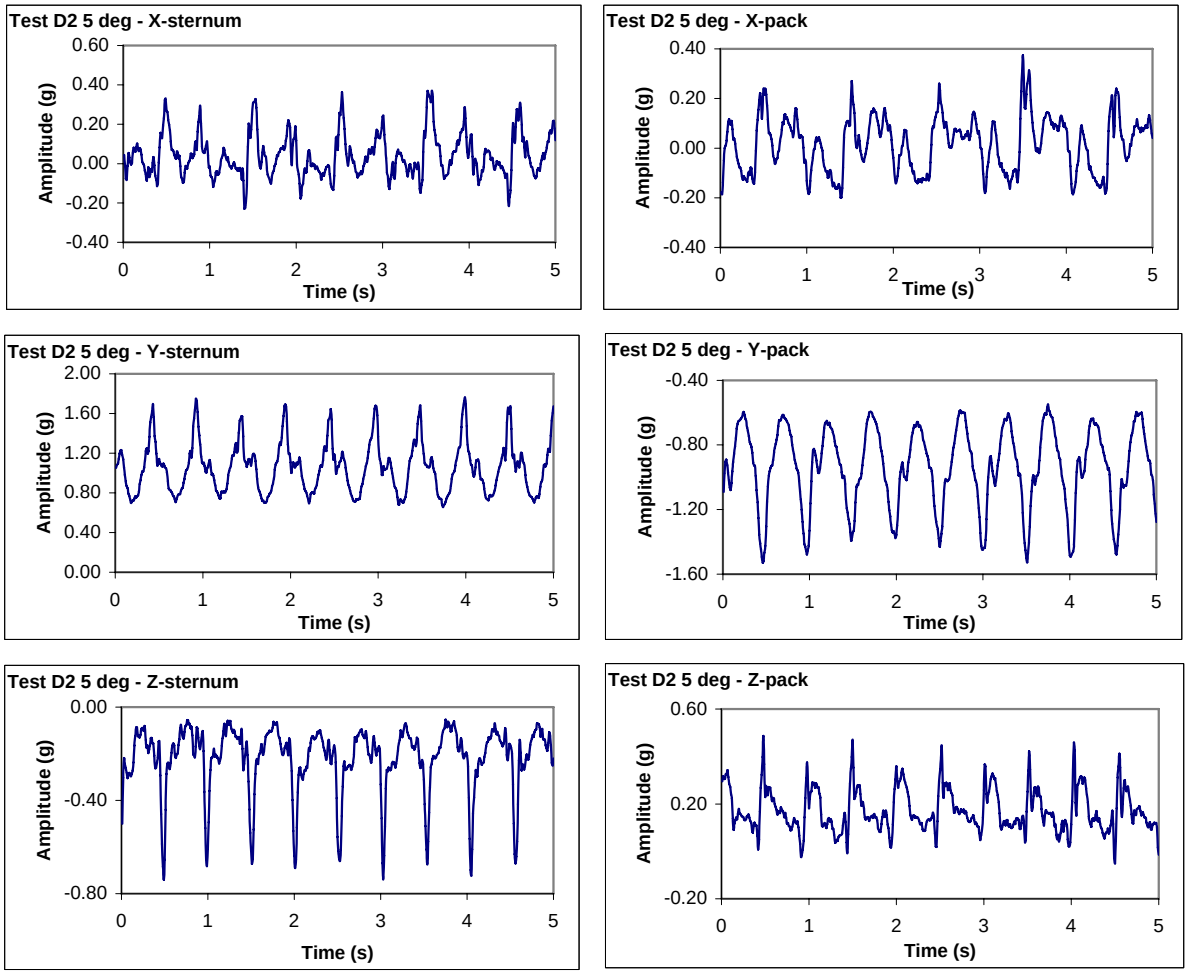

Figure C-4: Accelerations recorded from the sternum (left) and pack (right) accelerometers for a subject carrying a 25.9 kg load and walking at 4.83 km/h and 5° incline.
Accelerometer axes and orientations are as given in Fig. C-1. Subject #08.

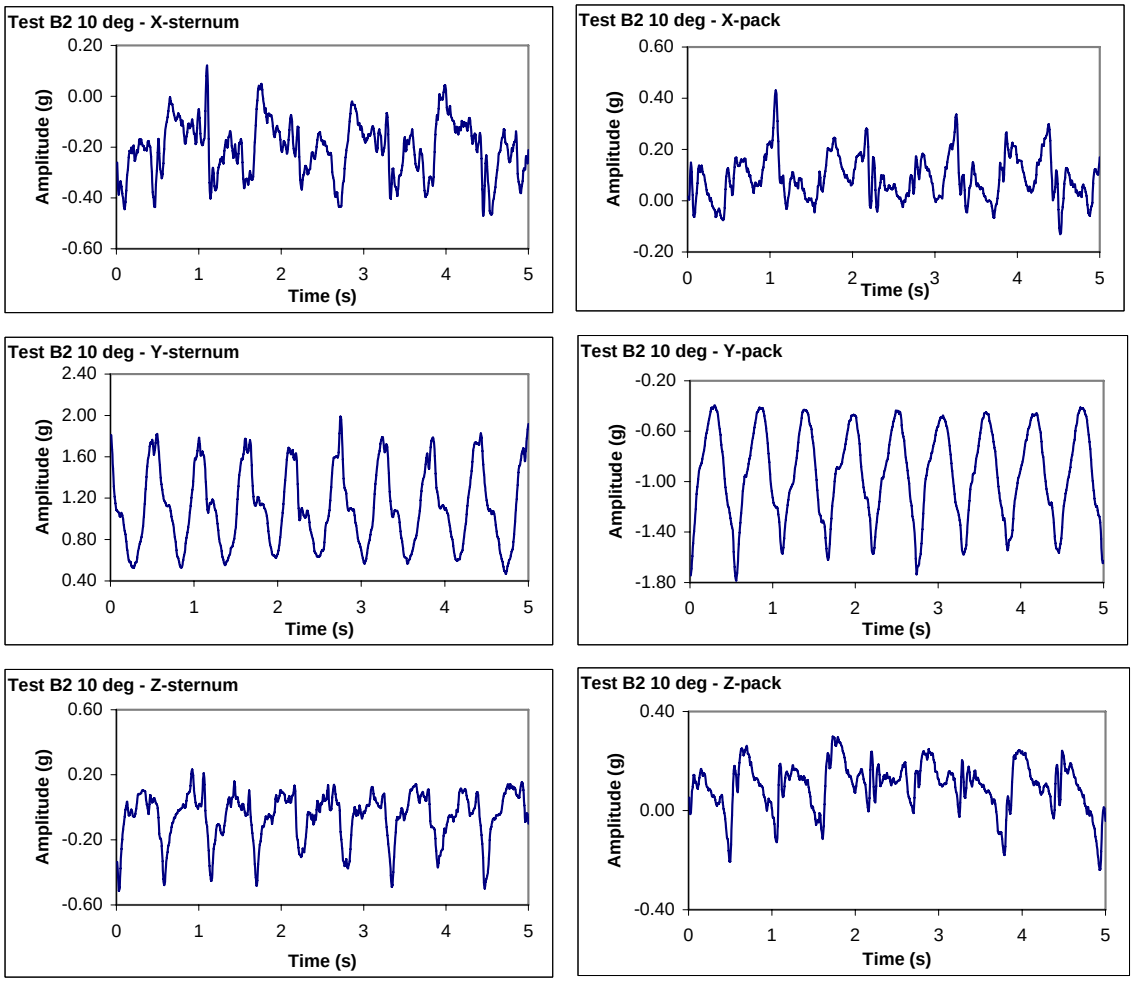

Figure C-5: Accelerations recorded from the sternum (left) and pack (right) accelerometers for a subject carrying a 38.7 kg load and walking at 4.83 km/h and 10° incline.
Accelerometer axes and orientations are as given in Fig. C-1. Subject #03.

7.3.2 Recorded $\dot{V}O_2$ Values

Average $\dot{V}O_2$ values obtained for each test condition are summarized in Tables C-I and C-II.

Table C-I: Average $\dot{V}O_2$ values for changing speed tests.

LOAD	VO_2	
	Mean	Std dev
Speed = 3.22 km/h		
0	8.202	1.055
16.6	9.115	1.098
25.9	10.752	1.928
38.7	12.334	1.338
Speed = 4.83 km/h		
0	10.343	1.453
16.6	11.954	1.345
25.9	13.949	2.577
38.7	16.208	1.783
Speed = 6.44 km/h		
0	15.838	1.667
16.6	18.672	2.292
25.9	22.552	4.054
38.7	26.649	3.506

Table C-II: Average $\dot{V}O_2$ values for changing incline tests.

LOAD	VO_2	
	Mean	Std dev
Incline = 0 deg		
0	10.884	2.730
16.6	12.320	0.816
25.9	14.085	1.486
38.7	15.649	2.009
Incline = 5 deg		
0	14.094	1.989
16.6	16.318	0.753
25.9	18.887	2.012
38.7	19.952	3.013
Incline = 10 deg		
0	19.119	1.636
16.6	23.658	3.026
25.9	27.494	3.161
38.7	29.185	5.400

7.3.3 RMS Analysis of Acceleration Data

The recorded accelerations were processed to the root mean square (RMS) values of the signals on each axis and the magnitude of the RMS values. The average values of these parameters are summarized in Tables C-III and C-IV.

Table C-III: Average RMS values on the x-, y- and z-axes and the average RMS magnitude for the changing speed tests.

LOAD	X-RMS		Y-RMS		Z-RMS		RMS-mag	
	Mean	Std dev	Mean	Std dev	Mean	Std dev	Mean	Std dev
Speed = 3.22 km/h								
0	1.117	0.156	1.492	0.208	1.020	0.193	2.142	0.142
16.6	0.812	0.133	1.500	0.111	0.902	0.197	1.939	0.162
25.9	0.771	0.144	1.492	0.163	0.781	0.101	1.857	0.192
38.7	0.923	0.168	1.416	0.161	1.005	0.292	1.988	0.201
Speed = 4.83 km/h								
0	1.542	0.394	2.581	0.403	1.355	0.368	3.333	0.427
16.6	1.029	0.233	2.394	0.264	1.421	0.375	2.989	0.342
25.9	0.997	0.115	2.580	0.288	1.328	0.240	3.078	0.291
38.7	1.174	0.385	2.569	0.350	1.823	1.083	3.433	0.945
Speed = 6.44 km/h								
0	2.207	0.836	4.199	0.688	1.962	0.522	5.212	0.701
16.6	1.465	0.344	3.864	0.598	2.251	0.519	4.748	0.510
25.9	1.402	0.141	3.928	0.487	2.334	0.543	4.809	0.457
38.7	1.655	0.569	3.417	0.558	2.774	0.223	4.733	0.587

Table C-IV: Average RMS values on the x-, y- and z-axes and average RMS magnitude for the changing incline tests.

LOAD	X-RMS		Y-RMS		Z-RMS		RMS-mag	
	Mean	Std dev	Mean	Std dev	Mean	Std dev	Mean	Std dev
Incline = 0 deg								
0	1.289	0.309	2.756	0.345	1.410	0.270	3.369	0.411
16.6	1.074	0.286	2.219	0.535	1.273	0.197	2.792	0.543
25.9	1.035	0.178	2.324	0.402	1.439	0.445	2.931	0.575
38.7	1.034	0.222	2.411	0.445	1.674	0.433	3.148	0.413
Incline = 5 deg								
0	1.295	0.276	2.921	0.491	1.646	0.224	3.607	0.503
16.6	1.106	0.311	2.700	0.359	1.423	0.152	3.260	0.379
25.9	1.089	0.156	2.910	0.398	1.720	0.707	3.581	0.647
38.7	1.085	0.247	2.762	0.649	1.756	0.602	3.486	0.730
Incline = 10 deg								
0	1.361	0.230	3.423	0.690	2.010	0.399	4.215	0.701
16.6	1.179	0.160	3.816	0.338	1.982	0.151	4.462	0.349
25.9	1.335	0.298	3.774	0.708	2.249	0.808	4.631	0.888
38.7	1.118	0.167	3.353	0.970	2.307	0.799	4.299	0.880

7.3.4 Spectral Analysis of Acceleration Data

Power spectral densities (PSD's) for the recorded accelerations were computed in Matlab. The total signal spectral power was obtained by integrating the PSD's and the fundamental frequencies were defined to be the lowest frequency at which a significant peak occurred in the PSD. Representative spectra from one subject are shown in Fig. C-6.

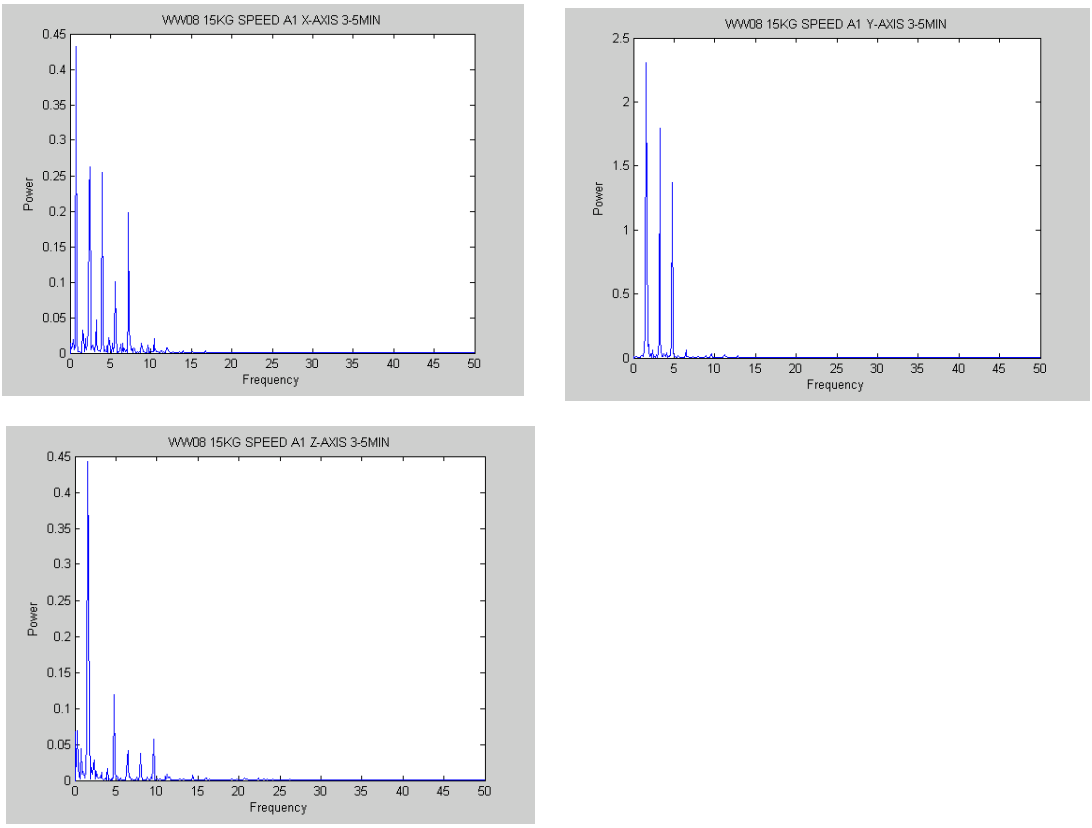

Figure C-6: Power spectral densities for x-axis (top left), y-axis (top right) and z-axis (bottom) sternum accelerations.
The subject was carrying 16.6 kg and walking at 3.22 km/h. The fundamental frequency of the x-axis signal (~0.8 Hz) is at approximately half the fundamental frequency of the y- and z-axis signals (~1.7 Hz).

Spectral power and fundamental frequency for each test was averaged across subjects; values are given in Tables C-V and C-VI.

Table C-V: Spectral power averaged across all subjects for all trials.

Test and Conditions A1 – accelerometer 1 A2 – accelerometer 2	Average X-axis Power	X-axis Power Std Dev	Average Y-axis Power	Y-axis Power Std Dev	Average Z-axis Power	Z-axis Power Std Dev
(A1) 0 kg load - 3.22 km/h	6.516	2.114	11.430	3.440	5.292	2.352
(A1) 0 kg load - 4.83 km/h	12.440	6.342	35.593	11.486	10.114	6.087
(A1) 0 kg load - 6.44 km/h	27.360	18.888	94.108	31.874	20.715	10.597
(A2) 0 kg load - 3.22 km/h	12.851	5.306	13.645	3.013	9.036	1.926
(A2) 0 kg load - 4.83 km/h	22.965	7.652	42.416	13.948	20.230	6.518
(A2) 0 kg load - 6.44 km/h	57.886	20.419	124.661	43.646	41.831	14.484
(A1) 16.6 kg load - 3.22 km/h	2.855	1.230	11.319	2.634	3.433	1.417
(A1) 16.6 kg load - 4.83 km/h	5.431	2.330	30.402	6.457	9.486	3.738
(A1) 16.6 kg load - 6.44 km/h	11.305	5.327	79.687	22.232	23.832	7.276
(A2) 16.6 kg load - 3.22 km/h	3.267	1.079	11.481	3.957	2.624	0.707
(A2) 16.6 kg load - 4.83 km/h	4.580	1.781	38.081	8.464	5.019	2.231
(A2) 16.6 kg load - 6.44 km/h	10.504	1.997	114.514	27.583	11.760	5.090
(A1) 25.9 kg load - 3.22 km/h	3.096	1.233	11.305	2.942	2.981	0.789
(A1) 25.9 kg load - 4.83 km/h	5.034	1.335	34.648	9.920	9.132	3.974
(A1) 25.9 kg load - 6.44 km/h	8.809	1.265	77.941	23.388	32.057	15.689
(A2) 25.9 kg load - 3.22 km/h	3.362	1.036	10.842	3.142	2.454	0.918
(A2) 25.9 kg load - 4.83 km/h	5.069	1.393	42.419	8.206	4.495	1.703
(A2) 25.9 kg load - 6.44 km/h	13.001	3.131	123.534	30.997	14.474	5.626
(A1) 38.7 kg load - 3.22 km/h	4.089	1.231	9.838	2.510	4.803	1.958
(A1) 38.7 kg load - 4.83 km/h	7.101	5.553	31.158	7.042	13.773	9.868
(A1) 38.7 kg load - 6.44 km/h	14.614	12.698	62.454	11.826	42.507	24.922
(A2) 38.7 kg load - 3.22 km/h	3.700	1.464	10.887	0.647	2.305	0.779
(A2) 38.7 kg load - 4.83 km/h	4.942	1.558	42.820	11.889	5.810	2.846
(A2) 38.7 kg load - 6.44 km/h	13.564	3.785	105.435	18.632	27.169	15.427
(A1) 0 kg load – 0°	9.132	3.998	35.661	4.288	9.671	1.727
(A1) 0 kg load – 5°	9.648	4.240	40.773	6.730	12.972	1.963
(A1) 0 kg load - 10°	10.579	3.941	52.207	13.329	18.011	3.202
(A2) 0 kg load – 0°	15.466	9.008	34.285	11.941	15.061	7.092
(A2) 0 kg load – 5°	10.451	3.627	41.130	9.539	14.843	5.261
(A2) 0 kg load - 10°	11.626	3.090	62.801	41.326	21.482	7.238
(A1) 16.6 kg load - 0°	6.454	2.818	30.648	6.338	9.013	1.614
(A1) 16.6 kg load - 5°	7.209	3.753	41.606	7.984	11.252	1.216
(A1) 16.6 kg load - 10°	7.059	1.897	76.076	10.038	18.800	5.792
(A2) 16.6 kg load - 0°	4.300	1.341	37.294	7.089	4.700	1.188
(A2) 16.6 kg load - 5°	4.562	1.877	42.515	10.535	6.113	1.494
(A2) 16.6 kg load - 10°	5.162	2.825	61.986	25.126	7.543	1.884
(A1) 25.9 kg load - 0°	5.792	0.775	32.319	4.546	11.349	6.003

(A1) 25.9 kg load - 5°	6.622	1.231	43.863	11.439	17.259	14.836
(A1) 25.9 kg load - 10°	8.787	3.614	68.609	16.834	24.508	17.226
(A2) 25.9 kg load - 0°	4.490	1.581	40.211	11.563	4.207	1.302
(A2) 25.9 kg load - 5°	4.603	2.029	46.413	21.160	5.581	2.784
(A2) 25.9 kg load - 10°	5.751	2.083	68.339	29.733	8.436	3.687
(A1) 38.7 kg load - 0°	5.713	2.955	29.451	10.145	14.345	6.864
(A1) 38.7 kg load - 5°	6.008	3.150	37.952	15.401	15.992	12.096
(A1) 38.7 kg load - 10°	6.156	2.021	61.283	34.771	28.564	21.088
(A2) 38.7 kg load - 0°	4.743	1.483	39.149	8.964	4.183	1.476
(A2) 38.7 kg load - 5°	5.495	3.095	42.837	19.118	4.735	1.529
(A2) 38.7 kg load - 10°	6.121	3.492	63.914	32.415	7.630	1.660

- Accelerometer 1 was on the sternum; Accelerometer 2 was on the lumbar spine (0 load) or in the backpack (16.6, 25.9 and 38.7 kg load)

Table C-VI: Fundamental frequency averaged across all subjects for all trials

Test and Conditions A1 – accelerometer 1 A2 – accelerometer 2	**Average X-axis Fund Freq**	**X-axis Fund Freq Std Dev**	**Average Y-axis Fund Freq**	**Y-axis Fund Freq Std Dev**	**Average Z-axis Fund Freq**	**Z-axis Fund Freq Std Dev**
(A1) 0 kg load - 3.22 km/h	1.131	0.406	1.703	0.098	1.689	0.095
(A1) 0 kg load - 4.83 km/h	2.231	0.680	1.980	0.093	1.980	0.093
(A1) 0 kg load - 6.44 km/h	2.594	0.620	2.233	0.117	2.191	0.148
(A2) 0 kg load - 3.22 km/h	1.174	0.603	1.703	0.098	1.703	0.098
(A2) 0 kg load - 4.83 km/h	2.558	0.896	1.980	0.093	1.980	0.093
(A2) 0 kg load - 6.44 km/h	3.073	0.168	2.262	0.111	2.345	0.260
(A1) 16.6 kg load - 3.22 km/h	0.895	0.095	1.658	0.206	1.658	0.206
(A1) 16.6 kg load - 4.83 km/h	2.260	0.966	1.987	0.133	1.987	0.133
(A1) 16.6 kg load - 6.44 km/h	2.765	0.925	2.215	0.117	2.215	0.117
(A2) 16.6 kg load - 3.22 km/h	0.868	0.035	1.610	0.076	1.610	0.076
(A2) 16.6 kg load - 4.83 km/h	1.490	0.920	1.941	0.121	1.941	0.121
(A2) 16.6 kg load - 6.44 km/h	3.006	0.738	2.235	0.131	2.210	0.146
(A1) 25.9 kg load - 3.22 km/h	0.847	0.052	1.643	0.075	1.627	0.052
(A1) 25.9 kg load - 4.83 km/h	2.060	0.905	1.970	0.113	1.970	0.113
(A1) 25.9 kg load - 6.44 km/h	3.396	0.200	2.306	0.129	2.306	0.129
(A2) 25.9 kg load - 3.22 km/h	0.843	0.052	1.635	0.071	1.440	0.503
(A2) 25.9 kg load - 4.83 km/h	1.611	0.895	1.941	0.121	1.941	0.121
(A2) 25.9 kg load - 6.44 km/h	3.331	0.199	2.261	0.130	2.233	0.173
(A1) 38.7 kg load - 3.22 km/h	0.965	0.288	1.673	0.099	1.673	0.099
(A1) 38.7 kg load - 4.83 km/h	1.734	0.845	1.976	0.087	1.976	0.087
(A1) 38.7 kg load - 6.44 km/h	2.804	0.898	2.317	0.090	2.317	0.090
(A2) 38.7 kg load - 3.22 km/h	0.844	0.116	1.673	0.099	1.673	0.099
(A2) 38.7 kg load - 4.83 km/h	1.501	0.914	1.976	0.087	1.976	0.087
(A2) 38.7 kg load - 6.44 km/h	3.097	0.818	2.317	0.090	2.317	0.090
(A1) 0 kg load - 0°	1.963	0.937	1.967	0.103	1.981	0.135
(A1) 0 kg load - 5°	2.193	0.849	1.884	0.107	1.884	0.107

(A1) 0 kg load - 10°	2.266	0.787	1.896	0.109	1.896	0.109
(A2) 0 kg load - 0°	2.578	0.960	1.926	0.156	1.913	0.157
(A2) 0 kg load - 5°	2.563	0.795	1.897	0.109	1.897	0.109
(A2) 0 kg load - 10°	3.040	0.205	1.974	0.188	1.974	0.188
(A1) 16.6 kg load – 0°	1.562	0.887	2.002	0.102	2.002	0.102
(A1) 16.6 kg load – 5°	1.532	0.908	1.970	0.113	1.970	0.113
(A1) 16.6 kg load - 10°	1.540	1.120	1.928	0.045	1.928	0.045
(A2) 16.6 kg load – 0°	1.025	0.048	1.978	0.100	1.978	0.100
(A2) 16.6 kg load – 5°	1.259	0.753	1.943	0.108	1.943	0.108
(A2) 16.6 kg load - 10°	1.303	0.749	1.905	0.049	1.905	0.049
(A1) 25.9 kg load – 0°	1.547	0.898	1.987	0.159	1.985	0.147
(A1) 25.9 kg load – 5°	1.517	0.877	1.953	0.137	1.953	0.137
(A1) 25.9 kg load - 10°	1.887	0.969	2.002	0.161	2.002	0.161
(A2) 25.9 kg load – 0°	1.989	1.060	1.964	0.110	1.976	0.114
(A2) 25.9 kg load – 5°	1.966	1.044	1.929	0.135	1.929	0.135
(A2) 25.9 kg load - 10°	2.246	1.039	1.990	0.147	2.003	0.157
(A1) 38.7 kg load – 0°	1.841	0.959	1.966	0.088	1.966	0.088
(A1) 38.7 kg load – 5°	1.701	0.941	1.953	0.078	1.953	0.078
(A1) 38.7 kg load - 10°	2.266	1.188	1.990	0.055	1.990	0.055
(A2) 38.7 kg load – 0°	1.515	0.966	1.976	0.087	1.976	0.087
(A2) 38.7 kg load – 5°	1.513	0.907	1.978	0.100	1.965	0.096
(A2) 38.7 kg load - 10°	2.017	1.045	2.017	0.082	2.017	0.082

7.4 ***Appendix D –*** Body Lean Angles

7.4.1 The Relationship between Forward Lean Angle and Load Carried

During upright standing, a person's line of gravity falls through the ear, shoulder, hips, knees and slightly in front of the ankles (Stevenson et al., 2002). If the person dons a loaded backpack, there is a backward pull on the upper body and, to compensate, the individual leans forward to bring the loaded trunk in line with the body's centre of gravity. In a previous study (Stevenson et al., 2002), subjects were photographed, in a standing posture, from the side under four load conditions: a balanced load (on the front and back) of 5.46 kg, and backpack loads of 15.7, 25.5 and 34.3 kg. The upper body lean angle, calculated as the angle subtended by the ear, hip and vertical plane, was found to increase with backpack load.

The forward lean angle is also affected by the position of the load's centre of gravity, i.e. whether the bulk of the load is positioned near the bottom, in the middle or near the top of a backpack. Johnson et al. (2001) reported that forward body lean was greater for a 36 kg load placed near the lower back (low centre of gravity), than for the same load placed near the shoulders (high centre of gravity) when subjects walked on a treadmill at 5.6 km/h and 0° incline.

In this study, the forward upper body lean of subjects walking on a treadmill under the different experimental conditions was estimated from the recorded accelerations, as described below. The relationships between forward body lean, load carried, and speed and incline of locomotion were examined.

7.4.2 Computing Body Lean Angles from Measured Accelerations

Similar to the LCSim mannequin (see Sec. 3.3.1), the sternum is not vertical when an individual is standing upright (i.e. with 0° rotation about the hips) but is tilted such that the bottom of the sternum is further away from the centre line (along the coronal plane) of the body[21]. For the purposes of this work, the angle of the sternum is denoted a backwards tilt and the tilt angle, ϕ, (see Fig. D-1) is defined as positive. If the trunk is rotated forward, the accelerometer rotates in space with respect to the gravity vector; the magnitude of ϕ decreases and with sufficient forward lean, ϕ will become negative, as shown in Fig. D-1.

[21] For a description of the anatomy of the sternum see: http://education.yahoo.com/reference/gray/27.html#i117

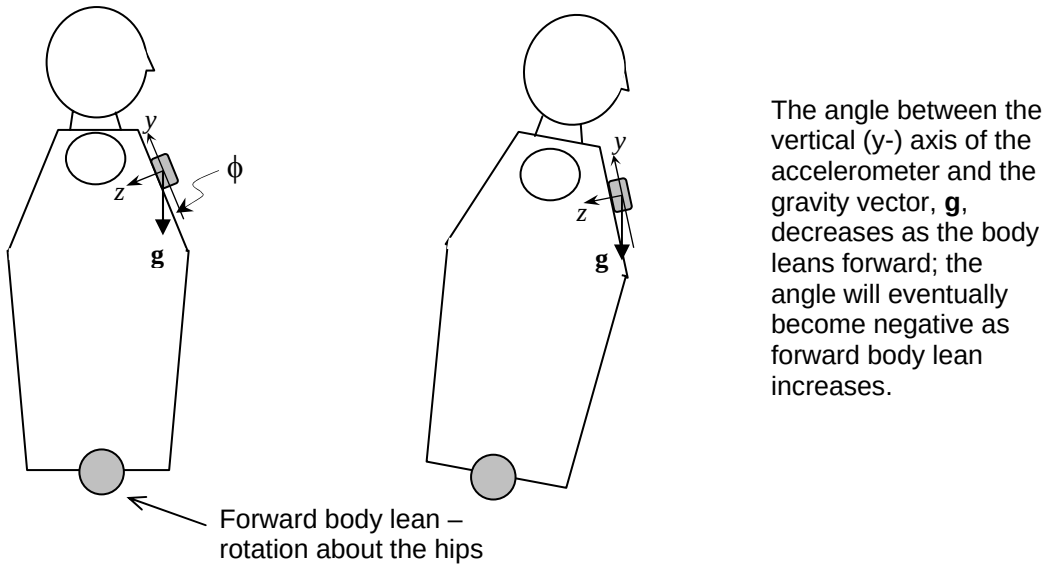

Figure D-1: Change in accelerometer angle with forward body lean.

7.4.2.1 Static Lean Angles

In the human trial, subjects were asked to stand for 10 seconds prior to beginning each treadmill walk, i.e. prior to each test (A1, A2, B1, B2, C1, C2, D1 and D2). From the recorded accelerations the tilt of the accelerometer was computed for each load: 0 kg (A1 and B1), 16.6 kg (C1 and D1), 25.9 kg (C2 and D2) and 38.7 kg (A2 and B2).

The Crossbow accelerometer was positioned on the sternum such that the y-axis was oriented vertically, the z-axis was oriented dorsally and the x-axis was oriented laterally. As noted, the accelerometer was tilted in the coronal plane, due to the tilt of the sternum. As well, there may also have been some rotation about the z-axis, such that the x-axis was not strictly horizontal. To compute the forward lean angle, the *xy*-axes are first rotated so that the *x*-axis is horizontal, i.e. reports 0g due to gravity. Two seconds of acceleration data from each axis were extracted from the standing record. The data values were converted to g's of acceleration and averaged. These averaged values were then divided by the vector magnitude to get the unit vector due to acceleration: $\mathbf{g} = \alpha\hat{\mathbf{x}} + \beta\hat{\mathbf{y}} + \gamma\hat{\mathbf{z}}$, where $\hat{\mathbf{x}}, \hat{\mathbf{y}}$ and $\hat{\mathbf{z}}$ are the unit vectors along the accelerometer axes. The xy-component of **g** was extracted and the angle, θ between $\mathbf{g}_{xy}$ and the vertical was calculated. Using θ, $\mathbf{g}_{xy}$ was rotated to be aligned with the *xy*-plane using a rotation matrix (see Fig. D-2), as follows:

$$\mathbf{g}_{xy} = \alpha\hat{\mathbf{x}} + \beta\hat{\mathbf{y}} \quad \text{and} \quad \theta = \cos^{-1}\left(\frac{\alpha}{\sqrt{\alpha^2 + \beta^2}}\right) \tag{D.1}$$

clockwise rotation matrix:

$$\begin{bmatrix}\hat{\mathbf{x}}' \\ \hat{\mathbf{y}}'\end{bmatrix} = \begin{bmatrix}\cos\theta & -\sin\theta \\ \sin\theta & \cos\theta\end{bmatrix}\begin{bmatrix}\hat{\mathbf{x}} \\ \hat{\mathbf{y}}\end{bmatrix} \tag{D.2}$$

counterclockwise rotation matrix

$$\begin{bmatrix}\hat{\mathbf{x}}' \\ \hat{\mathbf{y}}'\end{bmatrix} = \begin{bmatrix}\cos\theta & \sin\theta \\ -\sin\theta & \cos\theta\end{bmatrix}\begin{bmatrix}\hat{\mathbf{x}} \\ \hat{\mathbf{y}}\end{bmatrix} \tag{D.3}$$

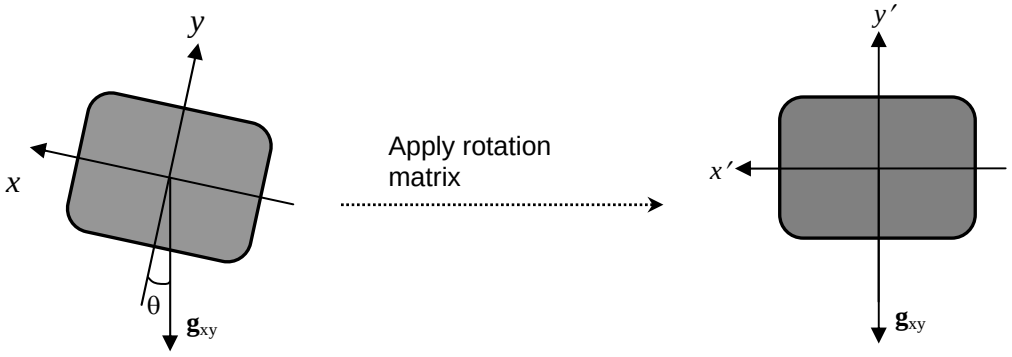

Figure D-2: The lateral tilt of the accelerometer and the equivalent horizontal orientation after rotation. Note, $\mathbf{g}_{xy}$ is rotated onto the xy-vectors, so the example shown is a clockwise rotation.

Since $\hat{\mathbf{z}}$ is orthogonal to both $\hat{\mathbf{x}}$ *and* $\hat{\mathbf{y}}$ and $\hat{\mathbf{x}}'$ *and* $\hat{\mathbf{y}}'$ then a new gravity vector is defined as $\mathbf{g}' = \alpha'\hat{\mathbf{x}}' + \beta'\hat{\mathbf{y}}' + \gamma\hat{\mathbf{z}}$ where α' and β' are the coefficients obtained after application of the rotation matrix. Using $\mathbf{g}'$, the tilt angle in the *yz*-plane is calculated using:

$$\phi = \cos^{-1}\left(\frac{\beta'}{\sqrt{\beta'^2 + \gamma^2}}\right) \tag{D.1′}$$

where ϕ is the accelerometer tilt angle in the sagittal plane; ϕ reflects the overall angle due to the backward tilt of the sternum and the forward lean of the trunk. The static lean angles computed for all subjects are given in Table D-I.

Table D-I: Computed static lean angles for all subjects at each load.

Subject #	Load (kg)	Changing speed		Changing Incline	
		Test	Lean angle (deg)	Test	Lean angle (deg)
01	0	A1	11.19	B1	9.94
	16.6	C1	-13.05	D1	-7.42
	25.9	C2	-15.16	D2	-15.92
	38.7	A2	-27.12	B2	-7.41
03	0	A1	32.54	B1	24.752
	16.6	C1	n/a	D1	10.956
	25.9	C2	n/a	D2	15.920
	38.7	A2	1.45	B2	19.188
06	0	A1	11.15	B1	3.851
	16.6	C1	37.29	D1	13.638
	25.9	C2	15.36	D2	-0.100
	38.7	A2	0.97	B2	7.974
07	0	A1	13.63	B1	16.61
	16.6	C1	2.25	D1	n/a
	25.9	C2	-1.81	D2	n/a
	38.7	A2	-14.46	B2	-30.51
08	0	A1	41.50	B1	18.573
	16.6	C1	-26.52	D1	-5.900
	25.9	C2	-20.31	D2	-14.743
	38.7	A2	-1.02	B2	-9.724
09	0	A1	16.75	B1	14.71
	16.6	C1	11.46	D1	n/a
	25.9	C2	6.28	D2	n/a
	38.7	A2	-3.52	B2	-2.50
10	0	A1	-11.63	B1	7.183
	16.6	C1	n/a	D1	-2.375
	25.9	C2	n/a	D2	-16.006
	38.7	A2	-23.92	B2	-8.197
12	0	A1	13.06	B1	n/a
	16.6	C1	2.12	D1	7.95
	25.9	C2	-6.08	D2	4.23
	38.7	A2	-1.03	B2	n/a

It is assumed that the subjects were standing upright in a comfortable posture for the zero load conditions. The accelerometer angle was found to indicate a backwards tilt in all but one case (subject #10, test A1). Disregarding subject #10, test A, the computed angle is still highly variable, ranging from a minimum of 3.9° to a maximum of 41.5°, with an average of 16.8°±10.1°. If the zero load angle is considered a reference angle and subtracted from the other angles, a relative rotation is obtained. This was done for all complete data sets (11 sets) and the data were grouped and the averages and standard deviations of the static angles were computed

for the three backpack loads. Data sets for subject #06 were removed because the computed angles indicated that the subject leaned farther backwards rather than forwards for one or more loads. The average relative lean angles and standard deviations were re-calculated using the remaining 9 data sets. The relative lean angle results are given in Table D-II.

Table D-II: Average relative lean angles for the three backpack loads.

Load (kg)	All complete data sets		Selected data sets	
	Average	Std dev	Average	Std dev
0.0	Reference angle		Reference angle	
16.6	-8.73	14.87	-14.67	6.47
25.9	-16.68	11.06	-20.42	7.90
38.7	-19.44	13.55	-23.09	11.59

As for the LCSim mannequin, the average forward lean angle increases with increasing load carried in the backpack.

7.4.2.2 Dynamic Lean Angles

The gravity vector will still be present as a component on the *y*- and *z*-axes during treadmill walking. To a first approximation, the gravity components can be determined from the mean value of the accelerometer data after converting from voltages to accelerations in g's and the zero-g offset of the accelerometer has been removed. Using these mean values in equations (D.1), (D.2), (D.3) and (D.1′) above, the dynamic lean angles were computed. Values were averaged across subjects for all test conditions; the average values and standard deviations are given in Table D-III.

Table D-III: Dynamic forward lean angles averaged across subjects for all test conditions.

Changing speed					Changing Incline			
Load (kg)	**Test**	**Speed**	**Average lean Angle (deg)**	**Std dev**	**Test**	**Incline**	**Average lean angle (deg)**	**Std dev**
0	A1-1	3.22	12.9	15.8	B1-1	0	10.3	11.3
	A1-2	4.83	12.5	16.6	B1-2	5	8.2	11.6
	A1-3	6.44	11.5	17.0	B1-3	10	5.5	13.5
16.6	C1-1	3.22	-5.7	15.2	D1-1	0	-3.9	8.5
	C1-2	4.83	-7.3	13.7	D1-2	5	-8.3	8.3
	C1-3	6.44	-5.8	11.3	D1-3	10	-11.2	10.6
25.9	C2-1	3.22	-10.3	10.7	D2-1	0	-11.8	11.9
	C2-2	4.83	-10.9	10.5	D2-2	5	-14.2	11.3
	C2-3	6.44	-8.9	7.2	D2-3	10	-16.4	10.4
38.7	A2-1	3.22	-16.6	15.9	D2-1	0	-14.6	16.9
	A2-2	4.83	-16.5	14.2	D2-2	5	-16.7	16.7
	A2-3	6.44	-13.8	14.0	D2-3	10	-21.3	19.1

The following observations can be made from Table D-III:

- the forward lean angle increases with increasing pack load
- for all loads, there is an increasing trend in the forward lean angle with increasing incline
- there is no trend in the forward lean angle with increasing speed

Again, the high standard deviations indicate that there is a large spread in the data values or that there are outliers in the data. Since there is no apparent trend in the forward lean angle with changing speed, the lean angles from all subjects for different speeds were grouped according to load carried and histograms of the angles were plotted. These are shown in Figure D-2.

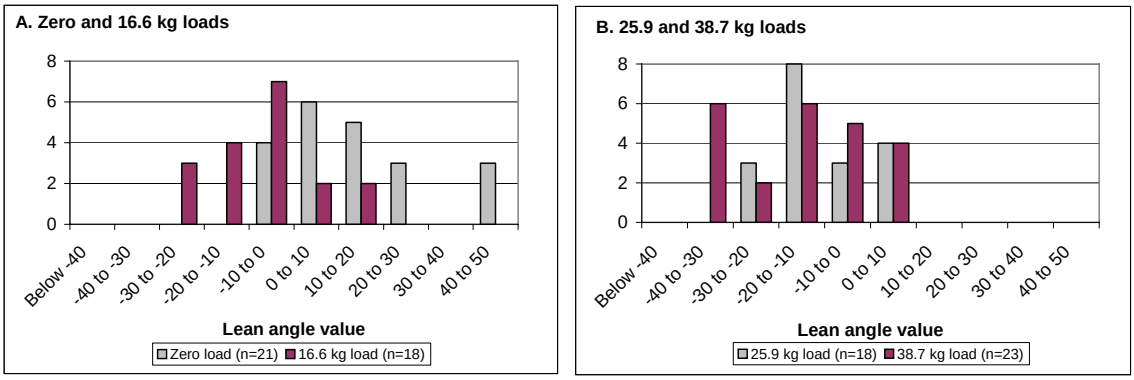

Figure D-2: Histograms of lean angles for the four loads carried.

The zero load data has the greatest spread and an outlier at a backward tilt angle greater than 40°. For the other loads, the angle values still have a substantial spread and are not normally distributed.

7.4.3 Conclusions

Both static and dynamic average forward lean angles, computed from the measured upper body accelerations, increase with load carried and the dynamic forward lean angles also increase with incline. In the dynamic case, these results indicate that there is a correlation between the mean value of the accelerometer signal and load carried and incline. However, there is a large spread in the computed angle values and the trend, versus both load and incline, is not consistent from subject to subject. The pack loads were centred in the backpack using the described packing protocol, so the effect of variation in load centre of gravity was minimized. Other possible reasons for the large spread in the data include inter-individual variation, variation in placement of the accelerometer along the sternum and differences in shoulder strap versus waist belt tension[22].

Further study is warranted to determine the following:

- the accuracy of the forward lean angle estimated from upper body accelerations; this would involve validating the estimated lean angles using a standard motion analysis system such as the Optotrak
- the distribution of the backward tilt angle of the sternum across a larger population of subjects
- the distribution of the forward lean angle for different loads across a larger population of subjects
- the effect of different shoulder strap and waist belt tensions on forward lean angle
- the interaction between the effect of load carried and incline on forward body lean

[22] Subjects were allowed to set the shoulder strap and waist belt tensions to their own comfort levels. It is likely that, whether the load is carried more on the shoulders or more on the hips would affect the forward lean angle. Shoulder strap and waist belt tensions were recorded during the treadmill sessions and the data will be examined for the variability in the adjusted tensions and correlation with computed lean angle.

7.5 Appendix E Contact Pressure Transfer Function

7.5.1 Background

One initiative of this contract was to determine if a useful transfer function could be developed that would estimate contact pressure parameters given a combination of material properties for the rucksack straps and padding combined with the acceleration histories of the pack and person.

To do this, accurate measures of contact pressures between the subjects and the equipment would be needed and correlations sought between the acceleration characteristics and the resultant pressure distributions. The FScan™ technology by Tekscan Inc. has demonstrated some particular limitations in measuring this pressure distribution accurately.[23, 24] FScan sensors themselves are not sufficiently compliant to mould to a persons' body well without inducing extraneous pressures. As well, standard available pressure ranges are insensitive below 20 kPa and FScan has been shown to typically over estimate the contact pressure magnitude. As an alternative, the Xsensor Technologies pressure sensing technology was selected for use in this study based on the excellent conformability of the sensors, sensitivity at low pressures and initial good accuracy results, as reported in PWGSC W7711-0-7632-06 Part C.

7.5.2 Initial Testing

Initial pilot studies in late July, 2003, indicated that the medical sensors the company had loaned us was topping out when loads exceeded 25 kg and we purchased industrial sensors with a higher pressure range on the advice of company. Calibration files for 0-15 psi range were provided by the manufacturer. Several subjects were then tested using the industrial sensors and the higher calibration ranges. When these results were reviewed, it was found that the sum of the body forces (recorded pressure × recorded contact area) on the shoulders and back appeared suspiciously high and a series of simple static load tests were then performed. These indicated

[23] Fewster J.B. and Eng T.J., Calibration and Analysis Methods for the F-Scan System, International Society of Biomechanics (1997).

[24] Hadcock L. *Factors affecting force distribution on a load carriage system waistbelt.* Masters thesis. Queens University, Canada (2002)

that the industrial pads were recording correct areas but pressure values were greater than the applied pressures. The manufacturer was contacted and the data was provided to them for their review. They informed us at that time that the calibration files they had provided contained two potential sources of error. First was the fact that their calibration device could only be pressurized to 10 psi and the pressure response from 10 – 15 psi had been extrapolated from lower pressure data. Second, they had only calibrated a subset of the complete 1296 sensor array, using a technique they termed "sub-sampling" to speed up the calibration process. They had used this technique with success on their medical sensors. These industrial sensors use an elastomeric substrate they had less experience with to permit the higher pressure range. Apparently this technique was not adequate with this sensor. In discussions with the manufacturer, they indicated they were confident that they would be able to work with us after testing to take recorded pressure data, apply a correction to the data post hoc, and achieve their typical accuracy specifications of +/- 10%. This assurance and the reality that test subjects, research assistants and the testing area and equipment were all only available in August supported the decision to continue the testing.

Upon completion of the testing, the sensors were shipped to the manufacturer for recalibration and for the creation of the conversion factors that would need to be applied to the subjects' data. In the interim, Xsensor had acquired a calibration device capable of applying pressures up to 20 psi. As a result of their recalibration, they provided Queens with a brief report on the existing calibration error (up to 62.25% error in some sensing elements) and provided files summarizing the correction factors that would have to be applied to the pressure data. Correction factors were provided in two forms: an average correction factor for each sensing element, and correction factors for each sensing element at each pressure level in 1psi increments. The Xsensor report appears at the end of this Appendix and a sample of the detailed factors appears below in Figure E-1. This information was provided to Queens in January, 2004. In the interest of achieving the most accurate pressure estimates, the detailed correction factors were used for correction of the pressure data. Xsensor had also provided two new calibration files: a 0-10 psi and a 0-15 psi calibration file using the whole 0 - 15 psi range and including the response of all sensing elements.

Correction matrix (mmHg to psi)				0.2 psi	Pressure (psi) = CF * Xsensor reading (mmHg)				
	Col 1	Col 2	Col 3	Col 4	Col 5	Col 6	Col 7	Col 8	Col 9
R1	0.001735	0.001646	0.001945	0.001646	0.001783	0.001646	0.001783	0.001689	0.001783
R2	0.001689	0.001605	0.001646	0.001605	0.001605	0.001566	0.001646	0.001605	0.001689
R3	0.001783	0.001646	0.001646	0.001646	0.001646	0.001605	0.001646	0.001605	0.001735
R4	0.001735	0.001605	0.001689	0.001646	0.001605	0.001566	0.001566	0.001493	0.001605
R5	0.001689	0.001646	0.001735	0.001605	0.001689	0.001646	0.001566	0.001529	0.001646
R6	0.001735	0.001605	0.001689	0.001566	0.001605	0.001605	0.001735	0.001605	0.001646
R7	0.001783	0.001605	0.001735	0.001646	0.001646	0.001646	0.001566	0.001529	0.001605
R8	0.001735	0.001646	0.001689	0.001646	0.001689	0.001605	0.001689	0.001605	0.001646
R9	0.001783	0.001689	0.001783	0.001735	0.001735	0.001689	0.001783	0.001605	0.001605
R10	0.001646	0.001529	0.001646	0.001566	0.001605	0.001566	0.001529	0.001529	0.001646

Figure E-1: Sample of Detailed Correction Factors

7.5.3 Creation of the Correction Factor Postprocessor

Using the detailed correction factor files supplied by Xsensor, a post processing program was developed. The steps were:

1. Read in the 36 row by 36 column pressure versus time data.
2. For each sensing element, at each time stamp, determine the reported pressure value
3. For each reported pressure, P_{report}, interpolate a correction factor for this pressure. For example, P_{report} = 4.27 psi, falls between the correction factors for 4 psi and 5 psi. A linear interpolation between the two correction factors was calculated.
4. Multiply the P_{report} by the interpolated correction factor to determine the final pressure

7.5.4 Correction Factor Results

A representative sample of the summer testing was processed in this way and summaries of the peak pressures, average pressures and contact areas were generated. Upon examination, this data appeared inconsistent with the physics of the testing. It was expected that average and peak pressures as well as contact areas would tend to increase with increased loads for the same subject but this was not apparent in the corrected data. At this point, a decision was made not to invest further effort in this data set.

7.5.5 Xsensor Inc. report on Correction Factors for Queens University

Correction Factors

An analysis was done in order to determine the accuracy of the existing calibration files. The results can be found under the correction factor file. The files were off as much as 62.25% of full scale below the actual value. Each pressure range and pad has an average correction factor file and a detailed correction factor file. This results in a total of 4 detailed correction factor files and 4 average correction factor files. The detail correction factor file gives a value for each cell that is to be multiplied by the original Xsensor file reading to give the true pressure reading. There are correction factors for converting both Psi and mmHg Xsensor readings into a true psi reading. The average correction factor files also contain an error analysis of the existing calibration files. In the detailed correction factor file the upper left of one matrix corresponds to cell (1,1) on the pressure pad and the lower right corresponds to cell (36,36). In the lower pressures the correction factor matrices contain some cells with values of 0. This occurred since these cells read a value of 0 at the lower pressures. Values will have to be interpolated or assumed for them.

Queen's University Seat Pad Recalibration Report

Calibration Files

New calibration files were completed and verified. The largest error observed, using the new calibration files, was 7.09% FS. The new calibration files also used dielectric profiles specifically made for the foam used in the Queens university seat pads. These new profiles are being sent as well. However they must replace the existing files in the Xsensor program directory before the new calibration files can be used. They are named exactly the same as the existing files however contain different data. The Xsensor program will have to be used with units of mmHg and dividing the reading by 10 will give a reading in units of psi. Three calibration files were made for each pad. Each calibration file is used for a pressure range. Pressure ranges that the pads were calibrated for were 0.5 to 5 psi, 0.5 to 10 psi, and 0.5 to 15 psi. The pads were verified by loading the pad with a uniform pressure then waiting three minutes and taking a reading. It was also observed that if the pad is wrinkled or folded it would give inaccurate

readings. The pad needs to be as flat, and stretched out, as possible in order to give the most accurate readings.

Locations of files

Correction factors
Pad X236N030001 (10 psi)
Average – Correction Factors/X236N030001 0-10 psi/corfacavg1.xls
Detailed – Correction Factors/X236N030001 0-10 psi/corfac1.xls
Pad X236N030001 (15 psi)
Average – Correction Factors/X236N03001 0-15 psi/corfacavg1B.xls
Detailed – Correction Factors/X236N03001 0-15 psi/corfac1B.xls
Pad X236N030002 (10 psi)
Average – Correction Factors/X236N030002 0-10 psi/corfacavg.xls
Detailed – Correction Factors/X236N030002 0-10 psi/corfac.xls
Pad X236N030002 (15 psi)
Average – Correction Factors/X236N030002 0-15 psi/corfacavg2B.xls
Detailed – Correction Factors/X236N030002 0-15 psi/corfac2B.xls

Profiles
x2thresh00.xsp
x2attrib00.xsp
x2thresh01.xsp
x2attrib01.xsp
x2thresh02.xsp
x2attrib02.xsp

Verification File
Queensverify.xls

New Calibration files
Pad X236N030002
15 psi – pad2/X236N030002DL15psi2.xsc
10 psi – pad2/X236N030002DL10psi2.xsc
5 psi – pad2/X236N030002DL5psi2.xsc
Pad X236N030001
15 psi – pad1/X236N030001DL15psi2.xsc
10 psi – pad1/X236N030001DL10psi2.xsc
5 psi – pad1/X236N030001DL5psi2.xsc

DOCUMENT CONTROL DATA
(Security classification of the title, body of abstract and indexing annotation must be entered when the overall document is classified)

1. ORIGINATOR (The name and address of the organization preparing the document, Organizations for whom the document was prepared, e.g. Centre sponsoring a contractor's document, or tasking agency, are entered in section 8.)

Publishing: DRDC Toronto

Performing: Ergonomics Research Group − Human Mobility Research Centre, Queen's University, Kingston, Ontario K7L 3N6

Monitoring:

Contracting: DRDC Toronto

2. SECURITY CLASSIFICATION
(Overall security classification of the document including special warning terms if applicable.)

UNCLASSIFIED

3. TITLE (The complete document title as indicated on the title page. Its classification is indicated by the appropriate abbreviation (S, C, R, or U) in parenthesis at the end of the title)

Development of a Dynamic Biomechanical Model for Load Carriage: Phase V: Development of the Biomechanical Model by Means of the Portable Measurement System (U)

4. AUTHORS (First name, middle initial and last name. If military, show rank, e.g. Maj. John E. Doe.)

E.L. Morin; J.M. Stevenson; S.A. Reid; J.T. Bryant

5. DATE OF PUBLICATION
(Month and year of publication of document.)

August 2005

6a NO. OF PAGES
(Total containing information, including Annexes, Appendices, etc.)

98

6b. NO. OF REFS
(Total cited in document.)

32

7. DESCRIPTIVE NOTES (The category of the document, e.g. technical report, technical note or memorandum. If appropriate, enter the type of document, e.g. interim, progress, summary, annual or final. Give the inclusive dates when a specific reporting period is covered.)

Contract Report

8. SPONSORING ACTIVITY (The names of the department project office or laboratory sponsoring the research and development − include address.)

Sponsoring:

Tasking:

9a. PROJECT OR GRANT NO. (If appropriate, the applicable research and development project or grant under which the document was written. Please specify whether project or grant.)

12CM03

9b. CONTRACT NO. (If appropriate, the applicable number under which the document was written.)

W7711−03−7863−01

10a. ORIGINATOR'S DOCUMENT NUMBER (The official document number by which the document is identified by the originating activity. This number must be unique to this document)

DRDC Toronto CR 2005−128

10b. OTHER DOCUMENT NO(s). (Any other numbers under which may be assigned this document either by the originator or by the sponsor.)

11. DOCUMENT AVAILABILITY (Any limitations on the dissemination of the document, other than those imposed by security classification.)

Unlimited distribution

12. DOCUMENT ANNOUNCEMENT (Any limitation to the bibliographic announcement of this document. This will normally correspond to the Document Availability (11), However, when further distribution (beyond the audience specified in (11) is possible, a wider announcement audience may be selected.))

Unlimited announcement

DOCUMENT CONTROL DATA
(Security classification of the title, body of abstract and indexing annotation must be entered when the overall document is classified)

13. ABSTRACT (A brief and factual summary of the document. It may also appear elsewhere in the body of the document itself. It is highly desirable that the abstract of classified documents be unclassified. Each paragraph of the abstract shall begin with an indication of the security classification of the information in the paragraph (unless the document itself is unclassified) represented as (S), (C), (R), or (U). It is not necessary to include here abstracts in both official languages unless the text is bilingual.)

(U) Soldier operational performance is impacted by a number of factors including physiological workload, the biomechanical effects of equipment used in the field, demographics and soldier readiness. The specific objectives of the work reported here are to identify components of a load carriage limit (LCL) equation specifically related to the physiological workload and biomechanical effects, and to further the development of a dynamic biomechanical model (DBM) for load carriage. The ultimate goal of this research program is to develop and fully validate an LCL equation, which includes all relevant factors and which can be used to predict the operational effectiveness of soldiers in the field.

Data were collected in a previous contract (W7711−03−7632−08) on 10 physically fit male subjects. A maximal oxygen consumption test was performed. This was followed by four experimental sessions during which oxygen consumption, accelerations at the sternum and on the framesheet of a loaded backpack, and contact pressures under the backpack were measured during a treadmill test for the conditions of: different backpack loads (0kg, 15 kg, 25 kg, 38 kg); different walking speeds (3.22, 4.83 and 6.44 km/h); and different inclines (0º, 5º, 10º). For the zero load condition, the second accelerometer was mounted on the lumbar spine of the subject, in order to compare the sternum and lumbar locations for predicting energy consumption. It was found that metabolic energy cost increased with increasing load, speed and incline and an interactive effect between load and speed, and load and incline was present. For the zero load tests, it was found that increasing energy cost due to increasing speed was well correlated with the rms magnitude of the acceleration signals (R2 = 0.96 for both recording locations). Accelerations were less well correlated with energy cost for increasing incline; however, accelerations recorded at the sternum location were better correlated (R2 = 0.79) than for the lumbar location (R2 = 0.27). A statistical model using several acceleration parameters was derived for the case in which the subjects carried loaded backpacks during the treadmill tests. An R2 = 0.60 was obtained for a model involving only acceleration parameters; R2 = 0.72 was obtained for a model involving acceleration parameters and load.

In the DBM development, a skin layer with appropriate properties was created for the torso model and the modeling of all relevant pack components that form the person−to−pack interface has been completed. Stress analyses, in the equilibrium state, for the skin layer, and the shoulder strap and waist belt contact regions were done. A library of material properties for biological (skin on the back, skin toughened, skin over bone) and pack materials, both individually and in combination, has been compiled. Completion of the DBM will entail validating the motion and stress response of the DBM against existing test data, improving the user interface, and adding an output format that will provide the biomechanical factor for input into the LCL equation.

14. KEYWORDS, DESCRIPTORS or IDENTIFIERS (Technically meaningful terms or short phrases that characterize a document and could be helpful in cataloguing the document. They should be selected so that no security classification is required. Identifiers, such as equipment model designation, trade name, military project code name, geographic location may also be included. If possible keywords should be selected from a published thesaurus, e.g. Thesaurus of Engineering and Scientific Terms (TEST) and that thesaurus identified. If it is not possible to select indexing terms which are Unclassified, the classification of each should be indicated as with the title.)

(U) Load carriage; Dynamic Biomechanical Model; Portable measurement system; load carriage limit; LCL; metabolic energy; pack−person interface; contact pressure